Investigation of Hot Deformation Behavior of C60800 Aluminum Bronze Alloy through Multi-Profile Die Extrusion with Parametric Optimization

TEKESTE AMAN NEGAWO

A Thesis Submitted to Department of Mechanical Engineering School of Mechanical, Chemical and Materials Engineering

Presented in Partial Fulfillment of the Requirement for the Degree of Master's in Manufacturing Engineering

Office of Graduate Studies

Adama Science and Technology University

May -2024

Adama, Ethiopia

Investigation of Hot Deformation Behavior of C60800 Aluminum Bronze Alloy through Multi-Profile Die Extrusion with Parametric Optimization

TEKESTE AMAN NEGAWO

Thesis Supervisor:

Dr. HABTAMU BERI (associate professor)

A Thesis Submitted to Department of Mechanical Engineering School of Mechanical, Chemical and Materials Engineering

Presented in Partial Fulfillment of the Requirement for the Degree of Master's in Manufacturing Engineering

Office of Graduate Studies
Adama Science and Technology University

May -2024
Adama, Ethiopia

DECLARATION

I hereby declare that this Master Thesis entitled "**Investigation of Hot Deformation Behavior of C60800 Aluminum Bronze Alloy through Multi-Profile Die Extrusion with Parametric Optimization**" is my original work. That is, it has not been submitted for the award of any academic degree, diploma or certificate in any other university. All sources of materials that are used for this thesis have been duly acknowledged through citation.

Tekeste Aman Negawo ______________ __________

Name Signature Date

RECOMMENDATION

We, the advisors of this thesis, hereby certify that we have read the final version of the thesis entitled "**Investigation of Hot Deformation Behavior of C60800 Aluminum Bronze Alloy through Multi-Profile Die Extrusion with Parametric Optimization**" Prepared under our guidance by Tekeste Aman Negawo submitted in partial fulfillment of the requirements for the degree of Master's of Science in Manufacturing Engineering. Therefore, we recommend the submission of the final revised version of the thesis to the department following the applicable procedures.

______________________	____________________	_____________
Advisor	**Signature**	**Date**
______________________	____________________	_____________
Co-advisor	**Signature**	**Date**

APPROVAL SHEET

I, the advisors of the thesis entitled "**Investigation of Hot Deformation Behavior of C60800 Aluminum Bronze Alloy through Multi-Profile Die Extrusion with Parametric Optimization**" and developed by **Tekeste Aman Negawo**, hereby certify that the recommendation and suggestions made by the board of examiners are appropriately incorporated into the final version of the thesis.

____________________	____________________	____________________
Major Advisor/Supervisor	Signature	Date

We, the undersigned, members of the Board of Examiners of the thesis by **Tekeste Aman** have read and evaluated the thesis entitled "**Investigation of Hot Deformation Behavior of C60800 Aluminum Bronze Alloy through Multi-Profile Die Extrusion with Parametric Optimization**" and examined the candidate during open defense. This is, therefore, to certify that the thesis is accepted for partial fulfillment of the requirement of the degree of Master of Science in **Manufacturing Engineering.**

____________________	____________________	____________________
Chairperson	Signature	Date
____________________	____________________	____________________
Internal Examiner	Signature	Date
____________________	____________________	____________________
External Examiner	Signature	Date

Finally, approval and acceptance of the thesis is contingent upon the submission of its final copy to the Office of Postgraduate Studies (OPGS) through the Department Graduate Council (DGC) and School Graduate Committee (SGC).

____________________	____________________	____________________
Department Head	Signature	Date
____________________	____________________	____________________
School Dean	Signature	Date
____________________	____________________	____________________
Office of Postgraduate Studies, Dean	Signature	Date

ACKNOWLEDGEMENT

First of all, I would like to thank Almighty God for his blessings and patience in allowing me to successfully complete this thesis. I would like to thank my advisor, Dr. Habtamu Beri, for his direction, support, encouragement, and patience throughout my studies at Adama Science and Technology University. I would also like to thank Dr. Davendra Kumahar Sihna and Dr. G.M.seyeed Ahmed for their support, and suggestions. I am also grateful to my friend, Mr. Mokonen Girma, for his tremendous support, recommendations, and remarks. I would like to express my heartfelt gratitude to the mechanical engineering department head, Mr. Sintayehu Legesse, for his endless support.

I'd like to offer my deepest thanks and gratitude to everyone who assisted me in many ways during my MSc. studies at Adama Science and Technology University. My heartfelt apologies if I accidentally left out a few names.

TABLE OF CONTENTS

DECLARATION I

RECOMMENDATION II

APPROVAL SHEET III

ACKNOWLEDGEMENT IV

ABSTRACT XIV

LIST OF ACRONYMS XV

CHAPTER I 1

INTRODUCTION 1

1.1 Background 1

1.1.2 Extrusion 2

1.1.3 Finite Element Method 3

1.1.4 Optimization of process parameter 3

1.2 Motivation of Research 4

1.3 Problem Statement 4

1.4 Research Question 5

1.5 Objective 5

1.5.1 General Objective 5

1.5.2 Specific Objective 5

1.6 Significance of Study 6

1.7 Scope of Study 6

1.8 Thesis Organization 6

CHAPTER II 7

LITERATURE REVIEW 7

2.1 Introduction to Extrusion of Copper Alloys 7

2.1.1 Classification of extrusion....7
2.1.2 Effect of extrusion parameter....8
2.1.3 Strengthening of copper alloy....9
2.1.4 Corrosion behavior and oxidation resistance....11
2.1.5 Finite element method....12
2.1.6 Die profile design and optimization....14
2.1.7 Die length and extrusion ratio....14
2.1.8 Optimization of extrusion parameters....15
2.1.9 Multi response optimization by Genetic Algorithm....15
2.2 Literature Summary....16
2.3 Research Gap....17
CHAPTER -III....18
MATERIALS AND METHODOLOGY....18
3.1 Introduction....18
3.2 Materials....18
3.2.1 Copper- aluminum alloy (aluminum bronze)....18
3.2.2 Die material....19
3.3 Methodology....20
3.4 Analysis Extrusion....21
3.5 Finite Element Analysis....22
3.6 Tools and Equipment....27
3.7 Numerical Simulation....28
3.7.1 Pre processor....28
3.7.2 Define materials....30
3.7.3 Object definition....31

3.7.4 Inter-object relation 31

3.7.5 Boundary condition 32

3.7.6 Simulation engine 33

3.7.7 Post processor 34

3.8 Optimization of Process Parameter by Taguchi Based Genetic Algorithm 35

3.8.1 Taguchi's Orthogonal Array 36

3.8.2 Signal-Noise Ratio Analysis 37

3.8.3 Analysis of Variance (ANOVA) 37

3.8.4 Regression analysis model 38

3.8.5 Multi response optimization of Genetic Algorithm 39

3.9 Experimental Investigation 41

3.9.1 Fabrication die, container, holder and ram for extrusion process 42

3.9.2 Hot extrusion 43

3.9.3 Specimen preparation for test 44

3.9.4 Microstructural characterization of aluminum bronze alloy 45

3.9.5 Hardness test 46

3.9.6 Compression test 47

3.9.7 Corrosion test 48

CHAPTER IV 50

RESULT AND DISCUSSION 50

4.1 Introduction 50

4.2 Analysis of Extrusion 50

4.2.1 Determination of extrusion strain 51

4.2.2 Determination average flow stress 51

4.2.3 Determination of ram pressure and force 52

4.3 Analysis of Numerical Simulation and Optimization for Cosine Die Profile 52
4.3.1 Numerical simulation result for cosine die profile..53
4.3.2 Analysis of extrusion load..54
4.3.3 Analysis of effective strain...56
4.3.4 Analysis of damage 59
4.3.5 Mathematical model for cosine die profile 62
4.4 Analysis of Numerical Simulation and Optimization for Linear Convergent Die Profile 64
4.4.1 Numerical simulation result for linear convergent die profile 64
4.4.2 Analysis of extrusion load..64
4.4.3 Analysis of effective strain...67
4.4.4 Analysis of damage 70
4.4.5 Mathematical model for linear convergent die 73
4.5 Analysis of Numerical Simulation and Optimization for Streamline Die Profile 74
4.5.1 Numerical simulation result for streamline die profile 75
4.5.2 Analysis of extrusion load..75
4.5.3 Analysis of effective strain...78
4.5.4 Analysis of damage 81
4.5.5 Mathematical model for streamline die profile...84
4.6 Multi-Response Optimization by Using Taguchi Based GA method.............................85
4.6.1 GA multi response optimization of cosine die profile 88
4.6.2 Confirmation analysis of GA optimum value for cosine die 89
4.6.3 GA multi response optimization of linear convergent die profile............................90
4.6.4 Confirmation analysis of GA optimum value for linear convergent die...................90
4.6.5 GA multi response optimization of streamline die profile.......................................91

4.6.6 Confirmation analysis of GA optimum value for streamline die 92
4.7 Experimental Investigation 93
4.7.1 Microstructure observation 94
4.7.2 Hardness test 95
4.7.3 Compression test 97
4.7.4 Analysis of corrosion rate 98
4.8 Validation the Result with the Required Application 100
CHAPTER-V 101
CONCLUSION AND RECOMMENDATION 101
5.1 Conclusion 101
5.2 Recommendation 102
Reference 103
Appendix I: Micro-Hardness for Deformed Product (From Vickers Hardness) 109
Appendix II: Calculation of Current Density from Tafel Plot 111
Appendix III: Spectroscopy Result of C60800 Aluminum Bronze Alloy 113

LIST OF FIGURES

Figure 1-1: a) Direct extrusion b) Indirect extrusion 2

Figure 3-1 Flow chart of research methodology 20

Figure 3-2 Schematic diagram of die profile 25

Figure 3-3 Assembled die profile and component 26

Figure 3-4 Simulation setup meshed model 29

Figure 3-5 Flow stress data of C60800 30

Figure 3-6 Materials defination 30

Figure 3-7 Inter-object relation ship 32

Figure 3-8 Boundary condition 33

Figure 3-9 Simulation engine when deform running the processor 34

Figure 3-10 Post processor extracted data 35

Figure 3-11 Flow chart of genetic algorithm 41

Figure 3-12 Part of extrusion design 42

Figure 3-13 a) Conventional lathe b) CNC lathe c) Fabrication die and container 43

Figure 3-14 Extruded samples of cosine, linear convergent and streamline respectively 44

Figure 3-15 Sample preparation for microstructure 46

Figure 3-16 Vickers hardness testing machine set up 47

Figure 3-17 Universal testing machine (UTM) setup for compression test 48

Figure 3-18 Corrosion test set up 49

Figure 4-1: stress-strain curve of C60800 aluminium bronze alloy 50

Figure 4-2 Main effect plot for SN ratios for extrusion load parameters 54

Figure 4-3 Extrusion load distribution over surface of C60800 at die length of 10mm 56

Figure 4-4 Main effect plot of for SN ratio for effective strain 57

Figure 4-5 Effective strain distribution over surface of C60800 at die length of 20mm 59

Figure 4-6 Main effect plot of for SN ratio for damage 60

Figure 4-7 Damage distribution over surface of C60800 at ram speed of 3mm/s.....................62

Figure 4-8 Main effect plot of for SN ratio for load..65

Figure 4-9 Extrusion load distribution over surface of C60800 at extrusion ratio of 3 67

Figure 4-10 Main effect plot of for SN ratio for effective strain..68

Figure 4-11 Effective strain distribution over surface of C60800 at ram speed of 2mm/s 70

Figure 4-12 Main effect plot of for SN ratio for damage 71

Figure 4-13 Damage distribution over surface of C60800 at die length of 20mm....................73

Figure 4-14 Main effect plot of for SN ratio for load..76

Figure 4-15 Extrusion load distribution over surface of C60800 at extrusion ratio 2..............78

Figure 4-16 Main effect plot of for SN ratio for effective strain..79

Figure 4-17 Effective strain distribution over surface of C60800 at die length of 10mm 81

Figure 4-18 Main effect plot of for SN ratio for damage 82

Figure 4-19 Damage distribution over surface of C60800 at die length of 30mm....................84

Figure 4-20 GA optimization multi response graph of cosine dies..88

Figure 4-21 GA optimum value cosine die profile response...89

Figure 4-22 GA optimization multi response graph of linear convergent die...........................90

Figure 4-23 GA optimum value linear convergent die profile response 91

Figure 4-24 GA optimization multi response graph of streamline die 92

Figure 4-25 GA optimum value streamline die profile response 93

Figure 4-26 Optical microscope image 95

Figure 4-27 Hardness value...96

Figure 4-28 Compression strength value...97

Figure 4-29 Tafel plot of aluminum bronze alloy specimens in 3.5%NaCl solution................99

LIST OF TABLES

Table 3-1 Chemical composition C60800 (weight %) 18

Table 3-2 Property of C60800 material 19

Table 3-3 Composition of H13 tool steel 19

Table 3-4 Properties of H13 tool steel 19

Table 3-5 List of equipment and tools used in research 27

Table 4-1 L9 cosine simulation result for (load, effective strain, damage) 53

Table 4-2 Signal to Noise Ratios for the load percentage (smaller the better) 54

Table 4-3 Analysis of Variance of extrusion load of aluminum bronze alloy 55

Table 4-4 Signal to Noise Ratios for the effective strain percentage (smaller the better) 57

Table 4-5 Analysis of Variance effective strain of aluminum bronze alloy 58

Table 4-6 Signal to Noise Ratios for the damage percentage (smaller the better) 60

Table 4-7 Analysis of Variance for damage of aluminum bronze alloy 61

Table 4-8 Verification analysis 63

Table 4-9 L9 linear convergent simulation result for (load, effective strain, damage) 64

Table 4-10 Signal to Noise Ratios for the load percentage (smaller the better) 65

Table 4-11 Analysis of Variance of extrusion load of aluminum bronze alloy 66

Table 4-12 Signal to Noise Ratios for the effective strain percentage (smaller the better) 68

Table 4-13 Analysis of Variance effective strain of aluminum bronze alloy 69

Table 4-14 Signal to Noise Ratios for the damage percentage (smaller the better) 71

Table 4-15 Analysis of Variance for damage of aluminum bronze alloy 72

Table 4-16 Verification analysis linear convergent die profile 74

Table 4-17 L9 Streamline simulation result for (load, effective strain, damage) 75

Table 4-18 Signal to Noise Ratios for the load percentage (smaller the better) 76

Table 4-19 Analysis of Variance for effective strain response 77

Table 4-20 Signal to Noise Ratios for the effective strain percentage (smaller the better).......79

Table 4-21 Analysis of Variance for effective strain response 80

Table 4-22 Signal to Noise Ratios for the damage percentage (smaller the better) 81

Table 4-23 Analysis of Variance for damage response 83

Table 4-24 Verification analysis of streamline die profile 85

Table 4-25 GA setting 87

Table 4-26 GA predicted best individual of multi response optimization results for cosine die profile 88

Table 4-27 GA predicted best individual of multi response optimization results for linear convergent die...90

Table 4-28 GA predicted best individual of multi response optimization results for streamline die 92

Table 4-29 List of components...94

Table 4-30 Surface hardness of commercially available C60800 aluminum bronze alloy and deformed in the die 96

Table 4-31 Compression strength of commercially available C60800 aluminum bronze alloy and deformed in the die 97

Table 4-32 Electrochemical corrosion for extruded and commercial alloys specimens in 3.5% NaCl solution...98

ABSTRACT

Aluminum bronze alloy is one of the most promising engineering materials for marine, automotive and aerospace application. Due to its corrosion resistance, good hardness and compression strength. However, there is still a need for various strength enhancements to meet specific and general application. Among different metal forming technique: extrusion is the easiest and most promising technique for enhancement of mechanical property. This study aimed to investigate and obtain enhanced mechanical properties C60800 aluminum bronze alloy by determined the required load analytically and optimizing process parameters of numerical analysis of hot extrusion with a multi-profile die (cosine, linear convergent and streamline) in order to determine hot deformation behaviour (damage, Z load, effective strain) and experimental investigation with optimum parameters. Numerical simulation of hot extrusion was conducted by finite element analysis tool (DEFORM 3D) in Taguchi L9 orthogonal array with three factors and levels at different extrusion ratios (2, 3, and 4), ram speeds (1, 2, and 3 mm/s), and die length (10,20, and 30mm). Extrusion load, damage and effective strain percentage were assessed and analyzed characteristics of single response using Taguchi's S/N ratio and ANOVA. Based on mathematical modelling, multi response optimization of process parameters for optimal value of output were carried out by genetic algorithm. The fabrication of extrusion dies and container carried out at optimized parameters. At optimized process parameters the billet material of C60800 extruded in all types of die profile by using a hydraulic press machine. Testing and characterization of both commercial material and extruded product was conducted using mechanical and metallurgical testing machines. Finding obtained after extrusion shows that hardness values were improved by 18%, 17.5% & 16% and compression strength also increased by 11%,9.5% & 8% for cosine, streamline and linear convergent die profile respectively. Results obtained from an optical microscope showed that refined grain microstructure for extruded samples. Corrosion rate of linear convergent and streamline die extruded sample are higher than cosine die profile but much lower than commercial sample. This research work is expected to help all industries and researchers working in this area of focus

. ***Keywords:*** *finite element analysis, extrusion, die profile, optimization and genetic algorithm*

LIST OF ACRONYMS

Al	Aluminum
ANOVA	Analysis of Variance
ASTM	American Society for Testing and Materials
Cu	Copper
FE	Iron
FEA	Finite element analysis
FEM	Finite Element Method
GA	Genetic Algorithm
NAB	Nickel Aluminum Bronze
Ni	Nickel
Stl	Standard Tessellation Language
UNS	Unified Numbering System

CHAPTER I

INTRODUCTION

1.1 Background

Copper is an elemental metal that occurs naturally. Fortunately, pure copper. is commonly used in electrical conductivity material, it also easily mixes with a variety of metals to make alloys that improve strength, corrosion resistance, and antibacterial qualities. Copper alloys are alloys based on copper, in which the main alloying elements are Zn, Sn, Si, Al, Ni. Despite the fact that pure copper has a high thermal conductivity, it weakens in high temperatures. Different copper-based alloys have been developed and used extensively in industrial applications where there are various electrical connections between cables, circuit breaker parts, wires, and electrical outlets, such as heat exchangers, high-speed rail contact lines buses, welding electrodes, lead frame structures, and nuclear reactor components because of their high strength and electrical conductivity. Copper alloys made using various strengthening techniques, have great electrical and thermal conductivity, as well as excellent strength and plasticity, excellent thermal processing properties (Guo et al., 2017).

Aluminum bronzes are copper-based alloys with up to 14% Aluminum as the fundamental alloying constituent. Smaller amounts of iron, nickel, manganese, and silicon are added to form various alloys with qualities designed to suit specific requirements for strength, ductility, corrosion resistance, and magnetic permeability(Gao & Cheng, 2008). In addition (Xu et al., 2022) stated that Aluminum bronze alloys are commonly used in maritime engineering, high-speed railways, and precision parts because they have good resistant to seawater corrosion, high mechanical strength, and high fracture toughness. But still, it has limitations in specific applications like marine, automotive and aerospace. Metal forming is one among the most cost effective and promising techniques to improve those situations. To limit the number of experimental works, it is necessary to use finite element simulation and modeling techniques to predict the impact of variables on the metal-forming procedure before manufacturing begins (Sun & Yang, 2023).

1.1.1 Metal forming

Metal forming is a generic term that denotes different manufacturing processes, used in order to reshape the metal workpiece or components starting from raw materials to fabricated products. In this procedure, forces like tension, compression, shear, and other force applications to the material cause deformation. There are several metal forming processes available to shape metals into the desired shape. The following are the basic metal forming processes such as: Bending, Extrusion, Squeezing, Drawing, Wire Drawing, Powder Metal Forming, Deep Drawing, Hot Forming, Warm Forming, & Cold Forming (Venkatesh & Venkatesan, 2014).

1.1.2 Extrusion

Extrusion is a very easy and effective way for increasing alloy strength by grain refinement. Grain refinement is considered to be the sole method for an attractive combination of high strength and good ductility. The only cost-effective method for manufacturing an item such as a long, straight, and ductile one is extrusion. For improved production, an extrusion process with various state variables that increase the process's complexity should be examined (Francis, 2020).

Extrusion can be split into four groups. There are four methods: indirect extrusion, direct extrusion, hydrostatic extrusion, and impact extrusion. When it comes to direct extrusion, a powerful ram pushes the entire billet into its die, and additional power is necessary to overcome the resistance caused by friction between the next bill and the shield.

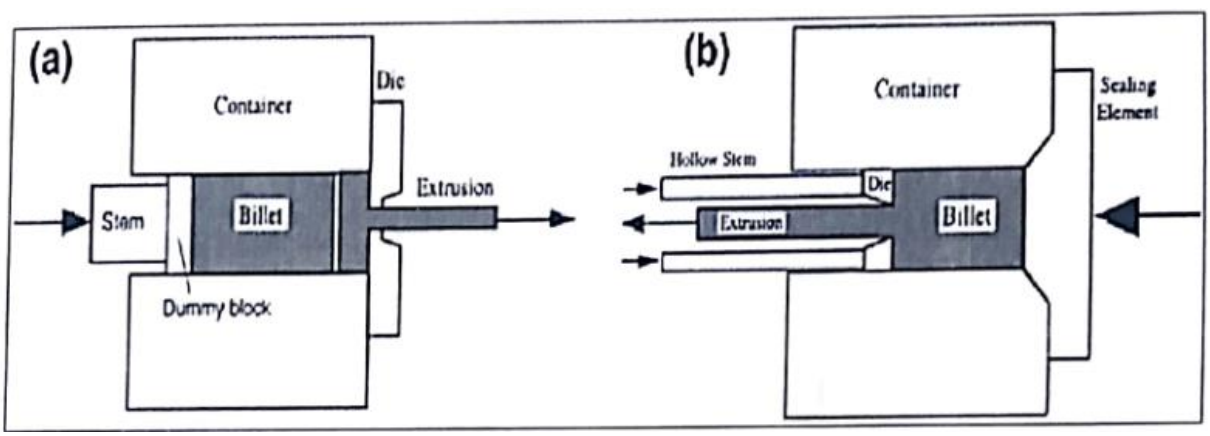

Figure 1-1: a) Direct extrusion b) Indirect extrusion (Yadav et al., 2018)

The hollow ram is driven back through a stationary, limited billet in indirect operation. The conflict between the billet and the container is resolved because there is no relative movement or required power. Because the extruded object sticks to the punch during impact extrusion, it is removed using a stripper plate. In hydrostatic extrusion, a high-pressure fluid is forced through a die into the workpiece. The loaded fluid works as a lubricant between the billet and the die, keeping the billet chambers from colliding (Yadav et al., 2018).

1.1.3 Finite Element Method

Finite element software is used to predict the properties of materials following deformation before conducting the actual experiment, which reduces time and cost. There is different simulation software for the simulation extrusion process like ANSYS, ABACUS, DEFORM and PAM-STAMP. Among that software DEFORM is a software tool for finite element analysis (FEA) that is utilized to model a variety of engineering applications, including extrusion. DEFORM includes meshing, material modeling, contact modeling, heat transfer modeling, and fluid flow modeling among its features and capabilities for simulating the extrusion process (Chen et al., 2007).

1.1.4 Optimization of process parameter

(Nag et al., 2020) stated that the optimization technique is a powerful tool for determining the best set of operating conditions and ideal design parameters. This would reduce the risk and expense of design and operation by acting as a guide for the experimental work. (Balali et al., 2018) investigated the effects of several extrusion parameters, including operating temperature, friction condition, die length, die profile, and ram speed, on both hot and cold extrusion.

The Taguchi method is a conventional technique for robust experimental design that aims to satisfy customer objectives with the most effective combination of elements and levels at the lowest societal cost. The Taguchi design process takes into account both controllable design parameters and uncontrollable noise variables that affect product quality, such as environmental influences. The Taguchi design method aims to identify design parameters that do not impact product or process performance due to noise. Parameter adjustments should aim to minimize variation and keep the product response close to the desired target (Jeyapaul et al., 2006).

In recent years, many industrial firms have paid increased attention to the optimization of multiple responses. The Taguchi approach has primarily been used for single-response situations, with minimal focus on multi-response problems. Taguchi practitioners often rely on previous experience, engineering expertise, or judgement when dealing with multiple responses. The Taguchi method and genetic algorithm provide a reliable and practical approach to optimizing multiple response issues. So, this powerful integrated strategy has the ability to address numerous response optimization concerns. The study includes a variance analysis to identify key and statistically important parameters(Senthilkumar et al., 2017).

1.2 Motivation of Research

Aluminum-bronze alloys are a promising choice for marine shafts because they can combine better mechanical qualities with superior corrosion resistance. However, traditional casting methods can limit their mechanical performance. Extrusion is a process that forces molten metal through a die for a uniform structure and aims to unlock the full potential of aluminum bronze alloys for marine applications. Extrusion can potentially improve the strength and hardness of these alloys while offering precise control over the microstructure for consistent performance, Due to their extraordinary resistance to seawater corrosion. Additionally, extrusion might provide a more efficient and productive manufacturing process.

1.3 Problem Statement

Aluminum bronze alloy is widely used in the maritime, automotive, aerospace, and electronics industries, with applications including high-rail contact wires, shafts, welding electrodes, heat exchangers, and electrical contact materials. As a result, aluminum bronze alloy is considered one of the most adaptable engineering materials. The strength of aluminum bronze alloy is moderate at casting condition which are a major limitation when it is used in marine shaft application. Due to limitations in hardness and strength, numerous types of shaft failures occur. Among the various grades of aluminum bronze alloys UNS C60800 is getting much attention in marine and automotive due to its high corrosion resistance, good strength, high wear resistance and erosion resistance in salty water and acidic environment. However, Low strength, hardness and poor wear resistance under high and varying load C60800 restricted. So, there is still a gap, it needs enhancement of various strengths by extrusion for specific applications like marine, aerospace and automotive. This thesis was aimed to fill those requirement properties for application in marine and automotive by optimizing numerical simulation of extrusion process parameters to investigate the mechanical and metallurgical properties by using different types of die profile extrusion to enhance mechanical property.

1.4 Research Question

Following research question are raised in relation to all the data presented above regarding C60800 aluminum bronze alloy and from problem description

- What were the most important parameters in analyzing the hot extrusion of C60800 aluminum bronze alloy simulation?
- At what process parameters minimum load, effective strain and damage of C60800 aluminum bronze alloy obtained?
- At what optimum condition good mechanical properties are obtained?
- What effect of extrusion on enhancing mechanical properties after extrusion?

1.5 Objective

1.5.1 General Objective

The main objective of this thesis was to conduct numerical analysis, parametric optimization and experimental investigation of aluminum bronze alloy in case of hot extrusion using multi profile die.

1.5.2 Specific Objective

To achieve the main objective of this thesis proposal, the following specific objectives designed:

- To investigate analytical load required for direct extrusion through general forming analysis.
- To investigate the effect of extrusion process parameters: extrusion ratio, ram speed and die length on optimal load requirement, effective strain and damage computationally using DEFORM-3D tool.
- To optimize multi profile die extrusion process parameters using Taguchi based genetic algorithm methodology through Matlab 2018Rb.
- To extrude C60800 with optimized parameters in cosine, linear convergent and stream line die profiles.
- Test and characterize the extrudate mechanical property (hardness and compression strength), corrosion behavior and microstructure to compare the result with required application.

1.6 Significance of Study

Among the various grades of copper alloys, aluminum bronze alloy(C60800) is getting more attention in various applications, like marine, aerospace and automotive due to superiority in characteristics over pure copper. This thesis was focused to increase mechanical property of aluminum bronze alloy C60800 through multi-profile die extrusion process. In practical aspect it will helps researchers in determining high hardness, high wear resistance, good ductility, high strength and corrosion resistant aluminum bronze alloy for marine shaft application. This work will be used as input for next researchers as a reference and for industries to develop copper alloy extrusion for specific and general application.

1.7 Scope of Study

The scope of the present thesis was focused on numerical analysis using a FEM tool called DEFORM -3D to investigate deformation behavior of aluminum bronze alloy with different extrusion parameters. SN ratio and ANOVA was conducted to show which parameter is significant in all type die profiles while a genetic algorithm was used for multi response optimization of extrusion based on Taguchi model. Then experimental investigation of aluminum bronze alloy hot extrusion process with optimized process parameters for all type of die as well as investigation of hardness test, compression strength test, corrosion behavior and characterization alloys were conducted with an optical microscope. This study establishes numerical approach, parametric validation and experimental investigation.

1.8 Thesis Organization

This research study is organized into five chapters. The first chapter covers the introduction and background study, problem statement, objectives of the study, significance of the study, scope of the study, and thesis organization. The second chapter is about the theoretical and empirical review of the aluminum bronze alloy extrusion process, as well as a literature summary and a gap. The third chapter focuses on materials and methodologies such as numerical analysis, optimization parameters, experimental procedures, and investigations. The fourth chapter contains a full discussion and analysis based on the numerical simulation results, optimizing the optimal combination parameter, experimental work for the optimal parameter, and investigation of the mechanical properties and microstructure of the developed materials. Finally, the fifth chapter provides a conclusion and recommendations for future study.

CHAPTER II

LITERATURE REVIEW

2.1 Introduction to Extrusion of Copper Alloys

Extrusion is a significant metal forming method that can be employed in both industrial and residential settings. Extrusion is a method of forcing a block of metal throughout a die opening at high pressure to reduce its cross section. Extrusion produces a number of significant end products, including channels, tubes, I-sections, and rods with varying cross sections. Extrusion is a hot-working procedure that utilizes the good deformability of heated metallic materials for shaping them, just like forging, rolling, etc. The ability to achieve a significant change in shape in a single operation is the procedure's most crucial feature. Extrusion is a way for working with metals and alloys that cannot be shaped using other production processes due to their mechanical and metallurgical characteristics. Extrusion enables the manufacture of complicated parts that are impossible to create using conventional manufacturing processes. (Francis, 2020).

Extrusion is a simple and effective method for enhancing alloy strength. Grain refinement is regarded as the only approach for achieving an appealing combination of high strength and good ductility, and extrusion is the only cost-effective method of producing such long straight and strong ductility (Ayer, 2020). Copper alloys created utilizing various strengthening procedures, on the other hand, offer good thermal and electrical conductivity, as well as high strength and ductility. For better production, a process with many state variables that increase the difficulty of the process should be examined. The impact of parameters for both hot and cold extrusion, such as operating temperature, friction condition, die length, die profile, and ram velocity (Onuh et al., 2003).

2.1.1 Classification of extrusion

Numerous techniques can be used to carry out extrusion. The difference between direct and indirect extrusion is one that is crucial. A different division is made according to the extrusion temperature: warm, hot, or cold. Finally, extrusion might be discrete or continuous (Ma, 2016). In the process of direct extrusion, sometimes referred to as forward extrusion, a metal billet is fed into a container and compressed by a ram, forcing it to pass through one or more die openings at the other end of the container. As the ram gets closer to the die, a small amount of the billet is left behind and cannot be forced through the die aperture. The butt, or excess material, is cut out of the product by cutting it slightly past the die's exit. Indirect extrusion, alternatively referred to as reverse and backward extrusion, mounts the die to the ram rather than the opposite end of the container. As the ram is driven deeper into the work, metal is forced to flow through the clearance in a direction opposite to the ram's motion. Because there is no friction at the container walls, where the billet would otherwise be urged to move in proportion to them, the ram force is less than in direct extrusion. Indirect extrusion is limited by the hollow ram's decreased rigidity and the difficulty of sustaining the extruded product as it comes out of the die (Yadav et al., 2018).

Both hot and cold extrusion are possible, depending on the work metal and the degree of strain placed on it during deformation. (Qamar et al., 2019) Common metals that are hot extruded include aluminum, copper, magnesium, zinc, tin, and their alloys. The billet is heated to a temperature higher than its recrystallization temperature before hot extrusion. As a result, the metal becomes more ductile and loses strength, enabling the creation of intricate shapes and more drastic size reductions. A heated billet below the temperature of recrystallization is used in cold and warm extrusion operations to create discrete pieces, frequently in finished or almost finished form.

To achieve the overall research goal, it is divided into several subsequent categories.

2.1.2 Effect of extrusion parameter

Hot extrusion's impacts on a nickel-aluminum bronze (NAB) (Cu-9Al-4.5Ni-4Fe-1Mn, wt%) alloy's microstructure, mechanical characteristics, corrosion, and erosion-corrosion behaviors were studied. After hot extrusion, the microstructure improved in refinement and homogeneity. Moreover, sepheroidization and disintegration of the multilayer structures occurred. These microstructural alterations improve resistance to corrosion and erosion as well as mechanical qualities (hardness, strength, and elongation). Better corrosion resistance is a result of the hot-extruded NAB alloy's reduced potential between phases, denser and more uniform corrosion layer, and strong adherence to the substrate, especially under flow conditions. (Wang et al., 2023).

Yield strength and Young's modulus raised following extrusion as a result of dispersion strengthening, precipitate hardening, work hardening, and grain refining. On the other hand, both dropped as strain rate and extrusion increased. The maximum hardness (1305.06 MPa), compressive yield strength (367.24 MPa), and residual stress (1267.609 MPa) of the specimen extruded at 450 °C and 0.3 s-1 were measured. None of the microstructures showed any signs of porosity. Extrusion parameters, approach angle, and ratio were thus all high enough to produce fully densified products from powder compacts (Bharath et al., 2020).In addition (X. Xu et al., 2022) studied heat deformation during, the strengthening mechanism of aluminum bronze involves twin strengthening, dispersion strengthening, and grain refining strengthening, resulting in an increased activation energy of the aluminum bronze alloy.

Ayer, (2020) conducted a study to determine the impact of extrusion ratio and extrusion die angle on the microstructure and mechanical characteristics of the AZ31 magnesium alloy. at 300 °C extrusion temperature using three different extrusion ratios of 1.77, 2.68, and 3.55 and die angles of 100, 150, and 200. The microstructure was shown to be greatly refined for all extrusion ratios. There was a decrease in average size from 22.4 m to 4.1 m–13.3 m. By increasing the extrusion ratio, tensile properties were greatly improved at room temperature. After extrusion, tensile strength reached a maximum of 331 MPa, when the initial measured value was 168.28 MPa. Grain refinement, mechanical strength, and micro hardness values all rose significantly with smaller die angles. larger mechanical strength and better grain dispersion in the microstructure are the results of using a lower die angle in conjunction with a larger extrusion ratio in every trial.

2.1.3 Strengthening of copper alloy

Copper alloys strengthened by simple or traditional procedures such as solid solution alloying, strain hardening, and grain refining are insufficient to fulfill expanding industrial demands. In general, solute atoms in the copper matrix reduce the electrical conductivity of alloys. As a result, precipitation-enhanced copper alloys are being created for aging to obtain an ideal mix of strength, electrical conductivity, and wear resistance (Zhang et al., 2017).In addition to that Borodin et al., (2019) examined severe plastic deformation on Cu-Cr-Zr at ultimate grain size of material are frequently prevented from seeing a much broader range of adjustments to material defect structure. It might be argued that the reduction in material grain size is just the result of numerous separate processes associated with plastic deformation in metals. We performed constitutive experimental, FEM, and discrete complex-based studies on two copper alloys exposed to ECAP and MDF deformation processes.

Xu et al., (2022) conducted a study to investigate the flow behavior, phase change, and microstructure evolution of an aluminum bronze alloy (Cu9Al4Fe). The hot compression behavior of aluminum bronze was explored utilizing simulated isothermal hot compression experiments at strain rates of 0.01–10 s^{-1} and temperatures ranging from 500 to 800 ^{o}C.

Cackett et al., (2018) conducted a study on CuCrZr, CuCrZr was heated at various temperatures to alter the size and spacing of the Cr precipitate. The values of initial flow stress were then determined from the stress-strain curves created by spherical Nano-indentation using various tip radii for all samples. The stress required to initiate plasticity was discovered to have a significant indentation size effect (ISE), despite the fact that at greater impression strains, the flow stress became constant for tip radii, R, approximately 8 m. This shows that whereas dislocation source activation dominates the ISE at the beginning of plastic deformation, the interaction with microstructural material length-scales takes over at later stages.

Nwaeju et al., (2022) aimed at enhancing the mechanical characteristics of aluminum bronze with alloying additives and building a predictive model using response surface methods. Independent statistical analysis was performed. Because the alloying components were added individually to the Cu-10% Al alloy, five alloying elements were designated as independent variables and mechanical properties in 11 experimental runs. The experiment's response variables were ultimate tensile strength, elongation, hardness, and impact strength. The matrix of mental design the mechanical analysis findings Using RSM-Design Expert's optimal custom design software, the experiments were optimized and a predictive model for regression was constructed.

Ma et al., (2021) investigated nickel aluminum bronze (NAB) alloys with higher-density nano/ultrafine annealing twins generated using heavy hot rolling (HHR) and subsequent annealing at 800 °C for different periods. The effect of grain size on the annealing twin density of the preceding matrix phase throughout a range of 1.0 to 10 m, as well as its impact on mechanical properties, was studied. The results reveal that creating high-density annealing twins in phases improves strength-ductility combinations and work hardening significantly.

A fine-grained structure of aluminum bronze alloy was created using multi-directional forging and aging processes. Wear resistance cannot be increased by improved hardness and reduced friction coefficient after MF. Reduced work hardening reduces wear resistance in the aluminum bronze alloy's fine-grained structure. Despite a greater friction coefficient, the fine-grained structure of the aluminum bronze alloy with superior sliding wear resistance can be attributed to higher hardness, good ductility, and suitable work hardening after MF and aging (Liu et al., 2020).

Ma et al., (2020) conducted a study to explore the forming properties of a Cu-Cr-Zr alloy in SLM, a statistical approach based on the influence of processing parameters on density was created using an experimental methodology (response surface method and analysis of variance) in this paper. Furthermore, samples with nearly full density and standard tension specimens were manufactured, and their microstructures and mechanical characteristics were examined using the optimized processing parameters. X-ray diffraction data demonstrate that the as-constructed sample by SLM contains only the a-Cu phase, and the maximum peaks of the a-Cu phase in the SLM sample differ significantly from that of powders and wrought copper alloys.

Casting in a shared environment produces a new high-strength aluminum bronze alloy. The following elements influence casting alloy performance: smelting rate, deoxidization, refinement degasification, and pouring temperature. The mechanical and microstructure properties of an alloy are influenced by solid solution temperature, solid solution time, aging temperature, and aging time. The outcome demonstrates that the new aluminum bronze alloy is a good high-strength material (Xu et al., 2004).

2.1.4 Corrosion behavior and oxidation resistance

Farzam, (2008) conducted study on Carbon steel (AISI 1020), stainless steel (AISI 304 and 316), ferritic alloy steel (B1274), brass (C27000), phosphor bronze (C51000), and aluminum bronze (C60800) test pieces were made and tested in a venturie tube. Despite the fact that carbon steel was the least resistant and aluminum bronze the most resistant of these alloys, there was no statistical correlation found between cavitation resistance and the mechanical properties that were assessed. The microscopic analyses demonstrated that the misalignment of polishing lines was caused by plastic deformation brought on by cavitation. When the hydraulic settings of an

Iranian sugar cane company's centrifugal pumps were not followed exactly, cavitation was produced, and the gray cast iron's resistance was found to be insufficient, according to a field evaluation of the pumps' susceptibility. In addition to the venturi tube, other configurations were investigated, such as the building and testing of a cavitation choke valve for the oil industry.

Dilute copper-aluminum alloys were oxidized in air at temperatures ranging from 700 to 1000°C. Two unique behaviors have been found: alloys containing at least 3% aluminum displayed exceptional oxidation resistance across the entire temperature range. Alloys containing 2% or less aluminum displayed good oxidation resistance up to 800 °C; however, as the temperature was raised higher, the oxidation rate of these alloys increased and became comparable to that of pure copper. A kinetic model was developed to describe the oxidation behavior and indirectly determine the amount of dissolved oxygen in the alloys tested. The oxygen dissolved in alloys having up to 2% Al exceeded its solubility limit in copper, whereas the oxygen dissolved in alloys containing greater aluminum did not. This distinction could account for the highly varying oxidation resistance. (Plascencia & Utigard, 2005)

2.1.5 Finite element method

DEFORM-3D does the real FEM-based analysis. Based on a rigid-plastic FE formulation, this simulation engine can handle a large number of billets and dies with non-isothermal modeling capacity. This is the program that actually does the numerical calculations required to solve the problem. In this study, a rigid curved die is used to model a round billet of rigid plastic material for extrusion of triangular, square, hexagonal, heptagonal, and octagonal sections. The tetrahedral solid elements are chosen for examination. Aluminum AA6063, which is plastic in nature, is used as the work material. The mesh is automatically produced (Ajiboye & Oyinbo, 2014).

Kang et al., (2002) has studied the indirect and direct extrusion of copper-clad aluminum rod. DEFORM, to simulate the extrusion of copper-clad aluminum rod, a commercially available finite element program that can be used to simulate metal forming and welding, heat transfer, and machining procedures was employed. For varied sheath thicknesses, die exit sizes, and die temperatures, simulations were done on copper-clad aluminum rod to anticipate temperature, effective strain rate, effective stress, and mean stress distributions. The calculations found that the greater the die exit diameter and sheath material thickness, the better the results. The experimental result for lubricating material with carbon oil correlates well with the extrusion force calculated using finite element analysis.

Chen et al., (2007) studied the plastic deformation behavior of an aluminum billet during its axisymmetric extrusion via a conical die is investigated using rigid-plastic finite element DEFORM TM 3D software. The die and container are taken to be solid objects with no attention for the temperature change generated by extrusion. The current numerical analysis explores the stress-strain distribution, die load, damage factor distributions, and billet flow velocity at the exit under various extrusion settings.

Reinikainen et al., (1992) investigated the finite-element simulation of multiple copper extrusion methods. The metal motion in axisymmetric extrusion was studied first. Metal flow through flat-faced and converging dies was studied. The extrusion was assumed to be isothermal. Two distinct frictional scenarios were studied. The DEFORM finite-element program was used to simulate the extrusion process. The FEM simulation findings were discovered to agree well with the laboratory testing results.

The significance of streamlined die profiles is highlighted by comparing three different profile geometry types, such as shear facing, spline, and cosine, using the finite element approach. DEFORM 3D V6.1 software is used to analyze die profiles in FEM. ProE was used to construct a solid model of die geometry with hexagonal and cylindrical portions. The interconnection between the cylindrical and hexagonal portions was extended as a die land measuring. Die land is made up of spline curves for spline dies, cosine curves for cosine dies, and sharp edges for shear-faced dies (Venkatesh & Venkatesan, 2014).

Tolaminejad & Fakhar, (2023) simulated the ECAE process of copper billets using Deform 3D software for up to 8 passes. The die and ram were modeled as rigid bodies, and the sample as an elastic-plastic substance. The trials used the same die shape, sample size, and ram speed. Copper's material behavior was determined via tensile tests.

A plastic simulation of the billet extrusion using rigid tools is the first step in the numerical extrusion simulation. Next, multiple cycles of the same process are simulated using only the elastic 2-part container and time-dependent boundary conditions for temperature and radial stress at the inner diameter of the liner (Sommitsch et al., 2007).

Effective strain is an important factor in influencing the mechanical properties of extruded materials. By reducing effective strain, it is possible to improve the quality and performance of the extruded product, resulting in superior mechanical and structural integrity. Lower effective strain levels during extrusion can improve the quality performance of extruded parts, resulting in a smoother surface finish, more precise measurements, and overall product quality. Minimizing effective strain through numerical simulation data optimization can help disclose the forming mechanism of extruded parts, guaranteeing that the material performs the intended deformation process with less strain and better results. Lower effective strain levels help to minimize metal tearing at thin edges or sharp corners, which can happen when strain levels are too high. Minimizing effective strain can ensure dimensional accuracy, ensuring that the extruded pieces satisfy needed tolerances (Sun & Yang, 2023).

2.1.6 Die profile design and optimization

Extrusion is a crucial metal-forming technique that can be used in both home and commercial settings. Extrusion is the technique of using high pressure to force a metal block through a die opening, lowering the block's cross section. (Francis, 2020) proposed work includes experimental studies on the extrusion of copper rod. A copper circular rod with a diameter of 12.5 mm was extruded using a commercial extrusion machine. Before and after deformation (extrusion), microstructure investigations of copper extruded products were undertaken. Copper's material characteristics were determined using tensile and hardness testing. Extrusion results in more regular and homogeneous grains. The tensile strength of the extruded product improves by 6.8% after extrusion, and the braking load increases by 22.9%.

Die profile is extremely important in die design. The degree of redundant work done during deformation is influenced by the die profile; a streamline die profile avoids redundant effort, minimizing extrusion load and assuring dead metal zone free flow of material during deformation (Venkatesh & Venkatesan, 2014).

2.1.7 Die length and extrusion ratio

It was discovered that the length of the die land influenced the shape of the products, whether they were straight or curved. (Chen et al., 2007) studied that state variables such as the friction factor, extrusion ratio, and die semi-angle affected the plastic deformation of AA-602. The outer layer of the billet sustains the most damage in the die's exit zone; the effective strain of the billet rises with an increase in the extrusion ratio; the effective stress of the billet rises and the flow velocity falls with an increase in the die's semi-angle.

Badashah, (2012) conducted an experiment on Lead and aluminum extruded through multiple holes using separate dies with varying extrusion ratios and die lengths. Extrusion of result with a 10 mm die length enhances the micro hardness of the extruded products from the central hole as the extrusion ratio rises. Extruded items from 3 mm die land length dies are comparable in hardness to those from 10 mm die land length dies. The extrusion ratio has no discernible effect on the micro hardness of extruded products from dies with a 3 mm land length. Aluminum extrusion with a 15-mm die land length produces a 5% increase in average hardness over a 10-mm die land length.

2.1.8 Optimization of extrusion parameters

The hot extrusion process is enhanced by using finite element analysis to create the optimal die profile, resulting in a more uniform surface-load distribution on the die profile surface. A cubic-spline curve represents the die profile of a hot extruded product. An upgraded sequential quadratic programming (SQP) strategy is employed to accomplish the optimal computation for unstable metal formation based on the rigid-viscoelastic finite element method (FEM). The analysis for unstable metal formation was performed in order to duplicate the process using the die curve produced through optimal computation. (Lin et al., 2003)

Giarmas & Tzetzis, (2022) studied die design optimization for aluminum alloys in the 6xxx family was investigated using finite element analysis. Die design and optimization are crucial in the fabrication of 6xxx series alloys to create high-quality end products. Before using finite element analysis (FEA) in the aluminum extrusion industry, several experiments and changes are required until an acceptable product is generated. The application of finite element analysis is becoming more popular in the removal of trials and defective extrudes.

2.1.9 Multi response optimization by genetic algorithm

A genetic algorithm (GA) is an approach to global search optimization. The genetic algorithm is based on evolutionary, natural selection, and genetic ideas. In essence, the genetic algorithm outperforms most traditional optimization techniques in terms of optimal solution quality. Genetic algorithms employ scientifically based techniques such as genetic inheritance, natural selection, mutation, recombination, and crossover (Panwar et al., 2021).

The genetic algorithm was chosen for its capacity to solve multidimensional problems with many solutions. The Pareto frontier was used to balance more than two objectives(Senthil kumar et al., 2017). Multi-objective optimization. Problems in complicated manufacturing systems are difficult to solve with conventional tools. If the goal is to determine the best combination of input parameters for improved output outcomes, one of the basic random-based Evolutionary Algorithms known as the Genetic algorithm (GA) was applied. If we need to determine the most common combination of input parameters that produces the best output result, the genetic algorithm was applied as a multi-objective optimization. It is used to determine multi-objective optimization based on the weight set formula (Singh et al., 2021).

2.2 Literature Summary

Several research studies have been undertaken on extrusion copper alloys with different extrusion parameter types and Die profile design. The above literature research indicates numerous extrusion processes. Primarily effect extrusion parameter and optimization technique as well as extrusion die profile design. Extrusion is a highly effective metal forming method for strengthening copper alloy materials. Extrusion has the advantage of refining material. This increases the overall strength of the finished product. Finite element modeling and simulation approaches can reduce the number of experimental attempts by identifying the impact of variables on the metal forming process before actual manufacture. This is because they save both money and time.

The DEFORM 3D Finite Element Analysis (FEA) proved the most successful simulation for metal forming. DEFORM-3D's adaptive geometric shape and traditional application offer superior performance in forming loads, stress/strain distribution, material distortion, temperature distribution, displacement and velocity field. and is thus employed in study.

2.3 Research Gap

Many studies on copper alloys have been undertaken, but there are lack studies on multi-profile die (cosine, linear convergent and streamline) extrusion C60800. Many studies have been conducted on the multi-profile die extrusion of aluminum alloys and other copper alloys. But there is a scarcity of data on UNS C60800 aluminum bronze alloy hot extrusion. which is employed in a variety of applications across industries. Extrusion is one the simplest and economical way to improve mechanical and metallurgical properties. The other drawback in marine environments is corrosion. C60800 is excellent resistant to saltwater corrosion and extrusion improves material property which helps to prevent degradation and extends the life of the shaft.

The present thesis was aimed to improve the mechanical property and deformation behavior of UNS C60800 by utilizing a multi-profile die extrusion technique. Mechanical and metallurgical properties were improved to meet the requirements for the application of shafts for marine applications.

CHAPTER -III

MATERIALS AND METHODOLOGY

3.1 Introduction

This chapter covers the materials used for extrusion, as well as the extrusion process, parameters used for extrusion, numerical simulation analysis, experimental procedures, and testing settings. This chapter organizes the instruments, equipment, and processes for data analysis. The experiment setup and characterization are given with specific optimum parameters. The chapter covers optimization steps, formulas, and standards for experiments and tests.

3.2 Materials

To select the materials, proper understanding of aluminum bronze alloy properties required for use of shaft in marine application. It is critical to understand the characteristics of the aluminum bronze alloy used in shaft applications. All analyses relating to mechanical properties, metallurgical properties, corrosion behavior.

3.2.1 Copper- aluminum alloy (aluminum bronze)

Aluminum bronze alloy (C60800) is a copper-aluminum alloy having a composition of copper, aluminum and small amounts of arsenic used to protect the alloy against dezincification. It is a hard, strong, and corrosion-resistant alloy utilized in a wide range of applications such as, electrical contacts, bearings, shafts, springs, valves, pumps in marine and aerospace applications.

C60800 is a high-strength alloy, making it a great choice for high-strength applications such as shaft, bearings and springs. The alloy is employed in a variety of environments, including seawater, acids, and alkalis. This makes it a good choice for applications that need corrosion resistance, such as marine and chemical processing, Excellent electrical conductivity. This makes it a good choice for applications that require electrical conductivity, such as electrical contacts, wiring, and connectors.

Table 3-1 Chemical composition C60800 (weight %)

Cu	Al	As	Fe	Ni	Zn	Mn	Pb
93.78	5.808	0.0256	0.0139	0.0267	0.0173	0.0137	0.025

Table 3-2 Property of C60800 material (M Spittel &thilo spittel, 2006)

Property	**Value**
Density	8.17g/cm^3
Melting point	1050℃
Tensile strength	415MPa
Yield strength	185Mpa
Modulus of elasticity	121GPa
Poisson’s ratio	0.325
Hardness Rockwell F	77
Thermal conductivity	79.5 W/mK

3.2.2 Die material

Chromium-molybdenum hot-rolled steel Uses for H13 in hot and cold work tooling applications are widespread due to its versatility. Heat fatigue cracking happens when materials are heated and cooled repeatedly in hot work tooling applications. H13's hot hardness (hot strength) resists this phenomenon. H13 is used in more hot work tooling applications than any other tool steel due to its exceptional combination of high toughness and resistance to thermal fatigue cracking, often known as heat checking.

Table 3-3 Composition of H13 tool steel (Markforged, 2018)

Composition	Fe	Mn	Si	Cr	Mo	C	V
Weight percentage (. wt.%)	91.26	0.34	0.9	5.07	1.22	0.40	0.81

Table 3-4 Properties of H13 tool steel (Work & Steel, n.d.)

Properties	Value
Density	7.80g/cm^3
Melting point	1427℃
Tensile strength, yield	1000 - 1380 MPa
Tensile strength, ultimate	1200 - 1590 MPa
Modulus of elasticity	215 GPa
Poisson’s ratio	0.27-0.30

3.3 Methodology

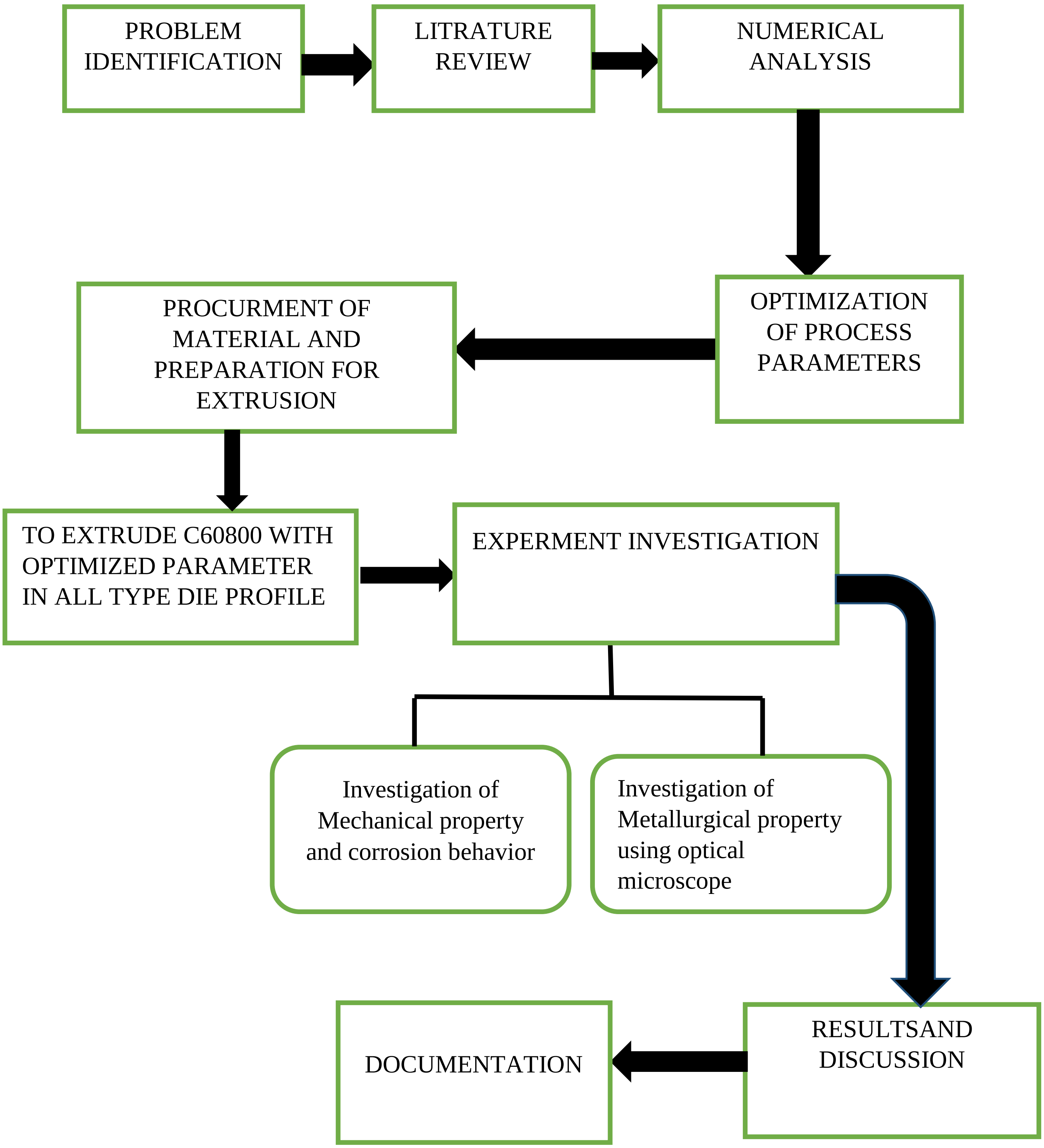

Figure 3-1 Flow chart of research methodology

This study used literature reviews to obtain data on the extrusion concept as well as DEFORM-3D software, a finite element method (FEM)-based process simulation system designed to investigate hot deformation behavior of C60800 aluminum bronze alloy. Initially, the die and work piece models are produced using SOLID WORK software. These models were imported into the DEFORM-3D software, where the extrusion operation was simulated to predict the effect of each parameter. Optimization of process parameters from simulation responses is done using Taguchi based Genetic Algorithm for all die profiles. Copper alloy of C60800 billet was used to perform experimental work for multi profile die hot extrusion of copper alloy with optimum parametric combinations to assess required properties. Finally testing and characterization is conducted for extruded products to investigate the mechanical properties of material and metallurgical behavior. The die employed for extrusion is made of H13 material, which is heat treated to increase hardness and surface finish.

3.4 Analysis Extrusion

Friction occurs in direct extrusion between the work and the die, as well as between the billet surface and the container wall. The empirical equation for determining extrusion strain (under friction condition) was proposed by Johnson.

$$\epsilon_x = a + b \ln r_x \tag{3.1}$$

Where ε_x = extrusion strain; and a and b are empirical Constants for a given die angle. Typical values of these constants are: a = 0.8 and b = 1.2 to 1.5. Values of a and b tend to increase with increasing die angle.

The ram pressure in direct extrusion is higher than in indirect extrusion due to the friction between the billet and container walls. The ram pressure in direct extrusion can be calculated using the following formula.

$$p = \bar{\sigma}\left(\varepsilon_x + \frac{2L}{D_o}\right) \tag{3.2}$$

Where the term 2L/Do accounts for the additional pressure due to friction at the container– billet interface. L is the portion of the billet length remaining to be extruded, and Do is the original diameter of the billet.

$$F = PA_o \tag{3.3}$$

Shape factor

$$K_x = 0.98 + 0.02\left(\frac{C_x}{C_c}\right)^{2.25} \tag{3.4}$$

Cx = Perimeter of extruded cross-section

Cc = perimeter of a circle with the same area

$$p = K_x \sigma_{ave.f}\left[\varepsilon_x + \frac{2L}{D}\right] \tag{3.5}$$

3.5 Finite Element Analysis

Simulation work was applied within those three types of die profile (linear convergent, cosine, streamline) and parameters (extrusion ratio, ram speed, die length). Then analyze the response (damage, effective strain and load) from simulation software, compare the response with all die profile type and extrusion parameters.

The commercial finite element tool DEFORM is used in this study to simulate the plastic deformation behavior during the aluminum bronze alloy hot extrusion process. The basic equations of rigid-plastic elements are as follows (Yang et al., 2008).

Equilibrium equation

$$\sigma_{ij,j} = 0 \tag{3.6}$$

compatibility and incompatibility equation

$$\dot{\varepsilon} = \frac{1}{2}(u_{i,j} + u_{j,i}) \qquad \varepsilon_v = u_{i,j} = 0 \tag{3.7}$$

yield criterion, $f(u_{ij}) = 0 : \sigma = \sqrt{\frac{3}{2}}(\sigma_{ij}'\sigma_{ij}')^{1/2} = \bar{\sigma}(\bar{\varepsilon}, \bar{\varepsilon})$ (3.8)

constitute equation $\sigma'_{ij} = \frac{2\bar{\sigma}}{3\dot{\bar{\varepsilon}}}\dot{\varepsilon_{ij}} \qquad \bar{\sigma} = \sqrt{\frac{3}{2}(\sigma_{ij}\sigma_{ij})}$ (3.9)

$$\bar{\varepsilon} = \sqrt{\frac{3}{2}\dot{\varepsilon_{ij}}\,\varepsilon_{ij}}$$

Boundary condition:

$$\sigma_{ij} = F_j \text{ on } S_F, \quad u_i = U_i \text{ on } S_U \tag{3.10}$$

Where σ_{ij} and $\dot{\varepsilon_{ij}}$ are the stress and strain rate, respectively, $\bar{\sigma}$ and $\dot{\varepsilon}$ effective stress and effective stress rate, respectively, F_j is the force on boundary surface of S_F and U_i is deformation velocity on the boundary surface of S_{ij} . The weak form of rigid-plastic FEM can be derived by applying the variation method to equation (3.6-3.9).

$$\int_v^{-} \varepsilon\delta\bar{\varepsilon}dV + K\int_V \varepsilon_V \delta\varepsilon_V dV - \int_{SF} F_i \delta u_i dS = 0 \tag{3.11}$$

where K is the penalty constant and V and S, are the material's volume and surface area respectively. The choice of suitable material models is the most significant and critical aspect of software simulation. Selecting the appropriate material model based on the requirements is crucial for obtaining precise results, as DEFORM-3D offers multiple models for elastic, stiff, and porous materials, each with varying appropriateness. Before the solver is run, the preprocessor must receive detailed material properties from the majority of material models, such as the strength coefficient, strain hardening exponent, and young modulus of elasticity. Preprocessors require the input of specific process parameters, such as heat transfer coefficient, friction coefficient, and extrusion wheel velocity, in addition to material properties. Von Mises yield criteria are employed in the deform-3D problem solution process.

$$\bar{\varepsilon} = \frac{\sqrt{2}}{3}\sqrt{(\varepsilon_1 - \varepsilon_2)^2 + (\varepsilon_2 - \varepsilon_3)^2 + (\varepsilon_3 - \varepsilon_1)^2} \tag{3.12}$$

$$\bar{\sigma} = \frac{1}{\sqrt{2}}\sqrt{(\sigma_1 - \sigma_2)^2 + (\sigma_2 - \sigma_3)^2 + (\sigma_3 - \sigma_1)^2} \tag{3.13}$$

Eq. (3.12) and (3.13) show effective strain and effective stress respectively.

For this simulation material was assumed as rigid-plastic workpiece whereas all dies assumed as rigid. As per guidelines of DEFORM 3D software for an isothermal forming problem with rigid dies and rigid-plastic workpiece flow stress should be determined only for workpiece. Flow stress data for selected aluminum bronze alloy is obtained from (M Spittel &thilo spittel, 2006).

DEFORM 3D provides several ways for defining flow stress. For simulation of aluminum bronze alloy power law (equation 3.14) is employed as a constitutive equation to determine flow stress developed during hot deformation.

$$\bar{\sigma} = \bar{\sigma}(\bar{\varepsilon}, \dot{\bar{\varepsilon}}, T) \quad (3.14)$$

Where $\bar{\sigma}$ is flow stress, $\bar{\varepsilon}$ is effective plastic strain, $\dot{\bar{\varepsilon}}$ is effective strain rate, T temperature.

Die profile design

Die profile is critical for guiding metal flow during extrusion. Die profile is critical for guiding metal flow during extrusion. Metal flow in extrusion is directly influenced by the die profile and friction conditions. The load requirement for deformation by using a cosine die profile is minimum at zero friction due to its geometrical fetcher zero entry and exit angle. But it is a traditional practice to use LC dies due to the ease of manufacturing. As shown in figure 3.2 and 3.3 the Streamline, linear convergent, and cosine dies, along with the container, holder, punch, and billet geometry, were designed by SolidWorks software (Mohapatra, 2016). The die profile functions for streamline, linear convergent and cosine as follows:

$$R(z) = R_1 + (R_1 - R_2)\left[2\frac{z^3}{L^3} - 3\frac{z^2}{L^2}\right] \quad (3.15)$$

$$R(z) = R_2 + (R_1 - R_2)\frac{(L-Z)}{L} \quad (3.16)$$

$$R(z) = \frac{R_1+R_2}{2} + \frac{R_1-R_2}{2}\cos\left(\frac{\pi z}{L}\right) \quad (3.17)$$

Where ‘L’ is the die length and ‘Z’ is the number of steps in between ‘0’ and ‘L’

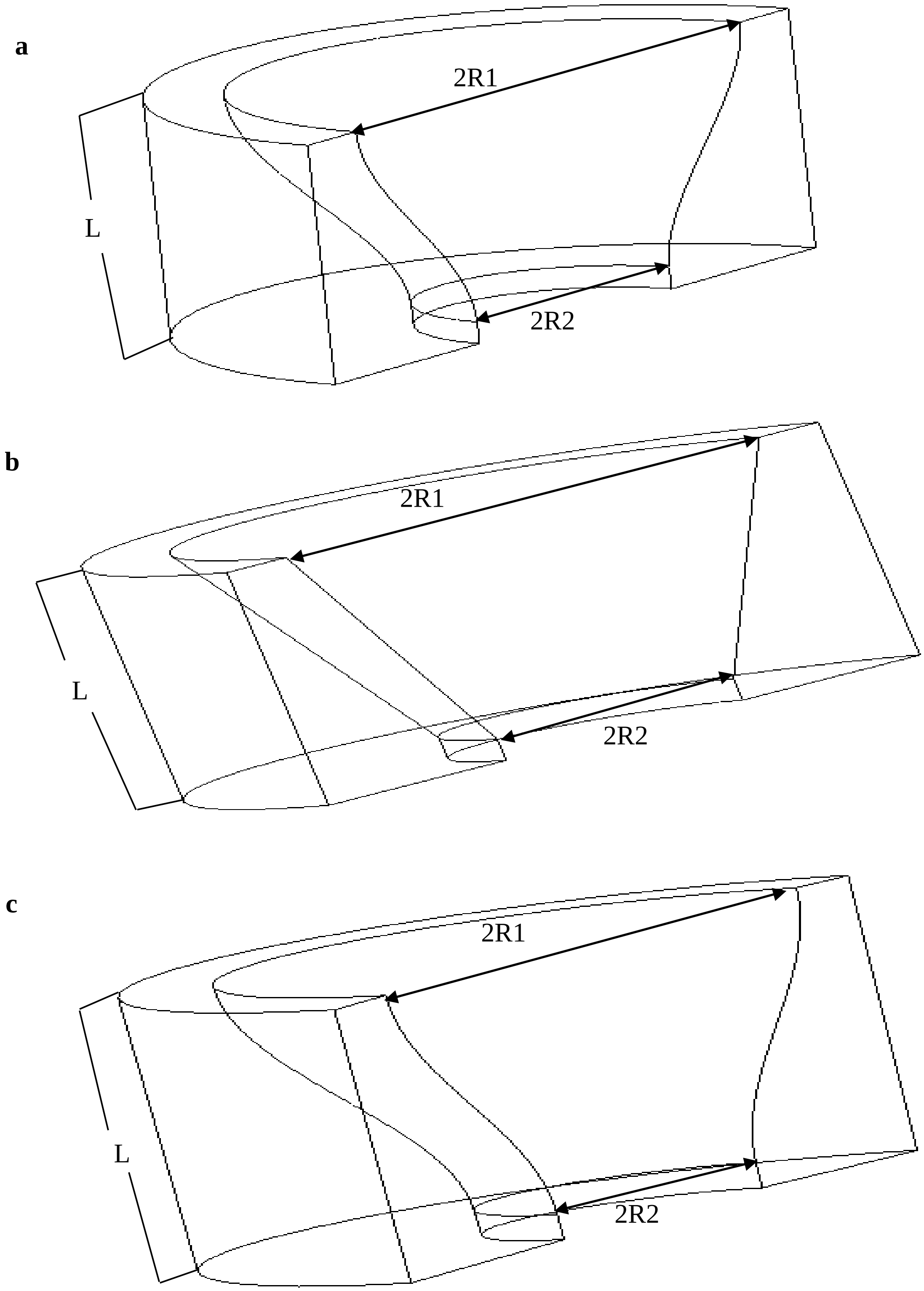

Figure 3-2 Schematic diagram of die profile a) streamline die b) linear convergent die c) cosine die

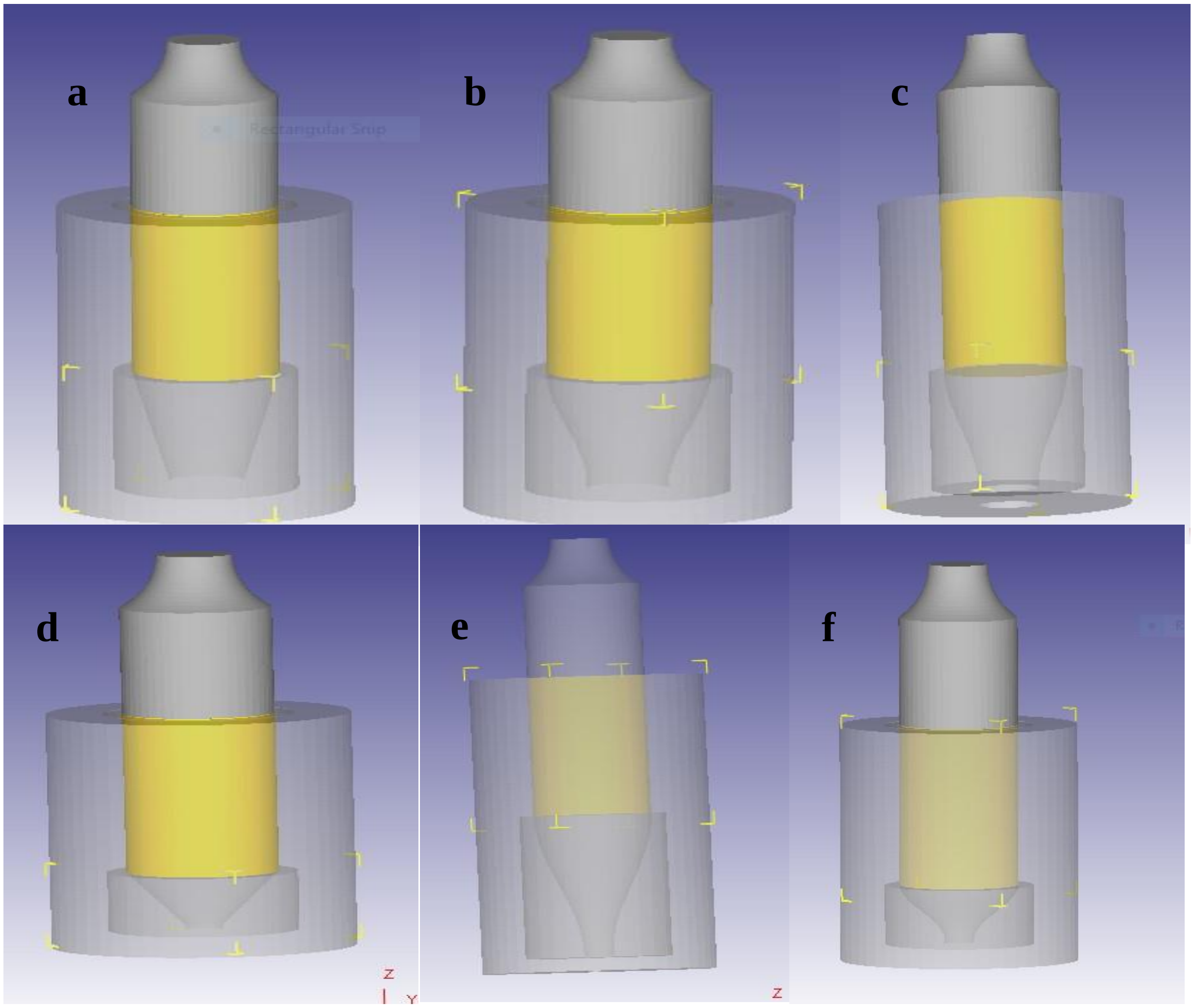

Figure 3-3 Assembled die profile and component for (a), linear convergent extrusion ratio 2 (b), cosine extrusion ratio 2 (c), streamline extrusion 3 (d), linear convergent extrusion 4 (e), cosine extrusion ratio 4 (f), streamline extrusion ratio 4

Figure 3.3 Shows the die profiles for linear convergent, cosine, and streamline dies. For die lengths of 10mm, 20mm, and 30mm, use extrusion ratios of 2, 3, and 4 for a workpiece diameter of 20mm. A solid model of dies for various extrusion ratios and die lengths of streamline, linear convergent, and cosine has been built using equations (3.15), (3.16), and (3.17). Finite element methods of computer simulation can forecast the effect of all critical parameters that influence the process. The previous research study was conducted using commercially available DEFORM-3D software. Solid geometries were imported as STL files, and simulation of extrusion of C60800 aluminum bronze alloy was carried out by lagrangian incremental type rigid-viscoplastic simulation with direct iteration method and conjugate-gradient solver at a temperature of 800℃.

3.6 Tools and Equipment

In order to complete the necessary work, this study used the machines and tools listed in the table below.

Table 3-5 List of equipment and tools used in research

S. No	**Tools**	**Function**
1	DEFORM 3D v11	It is software used for simulation of deformation behavior of materials that predict load, damage and effective strain developed
2	Minitab 21 software	Minitab is a software package used for the analysis of data and optimization using tools in it surface response (S/N ratio, ANOVA)
3	MATLAB 2018b software	MATLAB software is used for optimizing multi response data by using genetic algorithm tool.
3	CNC Lathe and milling machine	To prepare die, container, holder and punch
4	Furnace model (FXL-30-11)	To heat the billet material
5	Hydraulic press machine (50 Ton)	To extrude the billet in die
6	Abrasive cutter Model (RB 203 Abcut-M)	To sectioning sample while preparing testing specimen
7	Grinder/polisher Model (RB 204 Metpol-II)	To obtain a flat mirror-like surface
8	Chemical (Keller ‘s etchant) solution (Ammonia hydroxide, hydrogen peroxide and distilled water)	To keep away from any particles, dust, debris…. etc. from the fabricated specimen for micro structural characterization

9	Optical Microscope Model (Huvitz HR-300 series)	To investigate microstructural analysis of developed aluminum bronze alloy
10	Universal testing machine	To determine compression strength of prepared aluminum bronze alloy
11	Vickery hardness machine Model (HVS-50)	To determine hardness of aluminum bronze alloy
12	potentiator	To determine corrosion behavior of aluminum bronze alloy

Table 3.5 provides a list of all the instruments and equipment used in this study, together with details on their models and purposes. The software used to simulate the work piece and the optimization software for single and multi-response optimization are listed in this table. The machine used in the die and container fabrication process is also mentioned. List all of the instruments and apparatus needed to test corrosion behavior, metallurgical properties, and mechanical properties in the end.

3.7 Numerical Simulation

Deform 3D is a three-dimensional finite element simulation tool for investigating various forming and heat treatment conditions in the metal forming industry. Designers and engineers are authorized to minimize material costs during manufacturing, shop floor costs, tooling redesign to increase tool life, and production time for new products. The Deform 3D tool system consists of three main components: a preprocessor, a simulation engine, and a postprocessor.

3.7.1 Pre processor

The pre-processor generates and modifies data for simulation analysis and database file creation. The DEFORM pre-processor provides a graphical user interface for assembling simulation data. Input data contains object description, material data, inter-object conditions, simulation control, and inner material data. Mechanical, thermal and phase transfer problems can be simulated by deform mode. Punch was considered as the primary die for which the stepping and stopping criteria were decided. Stepping of the primary die can be controlled by either time and displacement reference. The primary die will move the stroke length per step as specified up to the completion of the total number of steps assigned.

Table 3.6 List of mesh element

S.No	Objects		Mesh elements
1	Workpiece		89114
2	Top die		73,633
3	Bottom die	Die length 10mm	43,164
		Die length 20mm	53,456
		Die length 30 mm	64,351
4	Container	For die length 10mm	92,321
		For die length 20mm	101,452
		For die length 30mm	107,954
5	Holder		46,093

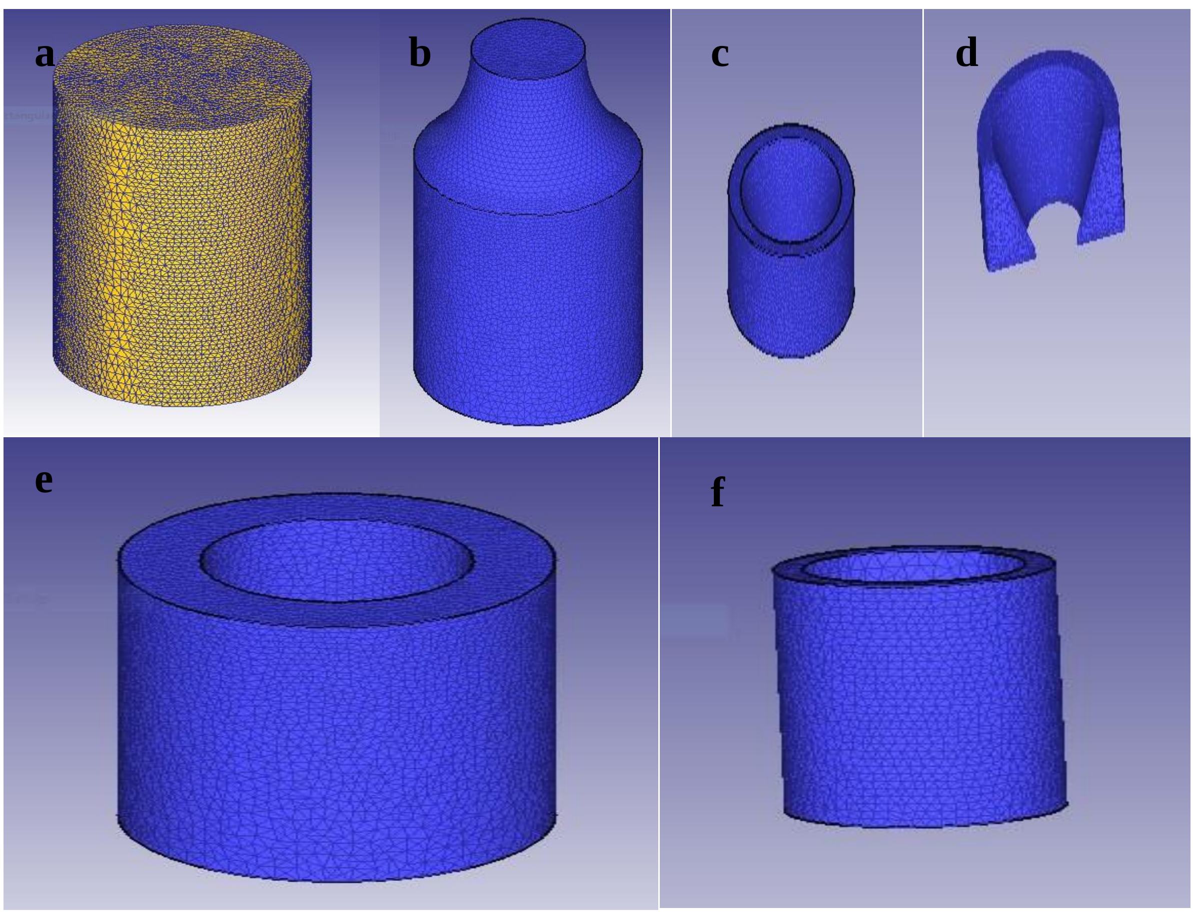

Figure 3-4 Simulation setup meshed model (a) workpiece (b) top die (c) bottom die (d) section bottom die (e) container (f) holder

Table 3.6 demonstrates that the mesh size of die and container in all die length, punch, holder and workpiece as the volume component as shown in the figure 3.4 above.

3.7.2 Define materials

If an object is defined using a mesh, it must be assigned a material. Selecting the material icon allows to allocate material data. The software database list includes the characteristics of the most common materials. The software allows to develop new material models. The material model chosen in this situation is an isotropic, rigid visco-plastic model as shown in the figure 3.5 and 3.6.

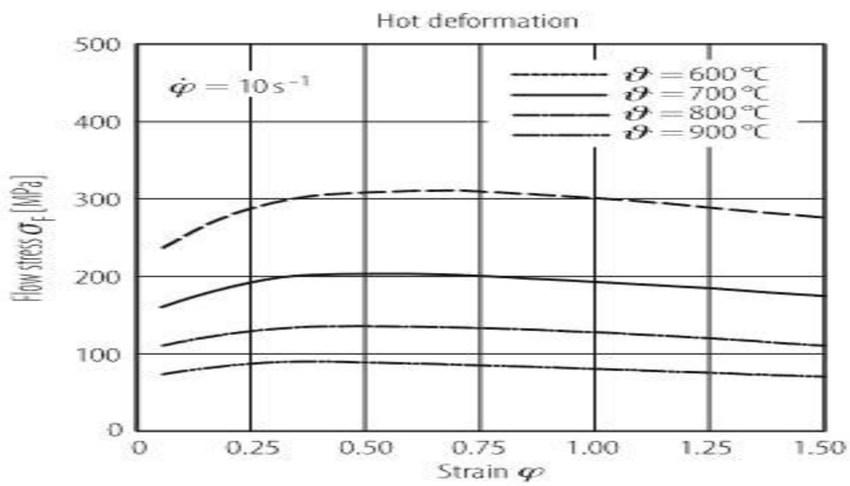

Figure 3-5 Flow stress data of C60800 taken from (M Spittel &thilo spittel, 2006)

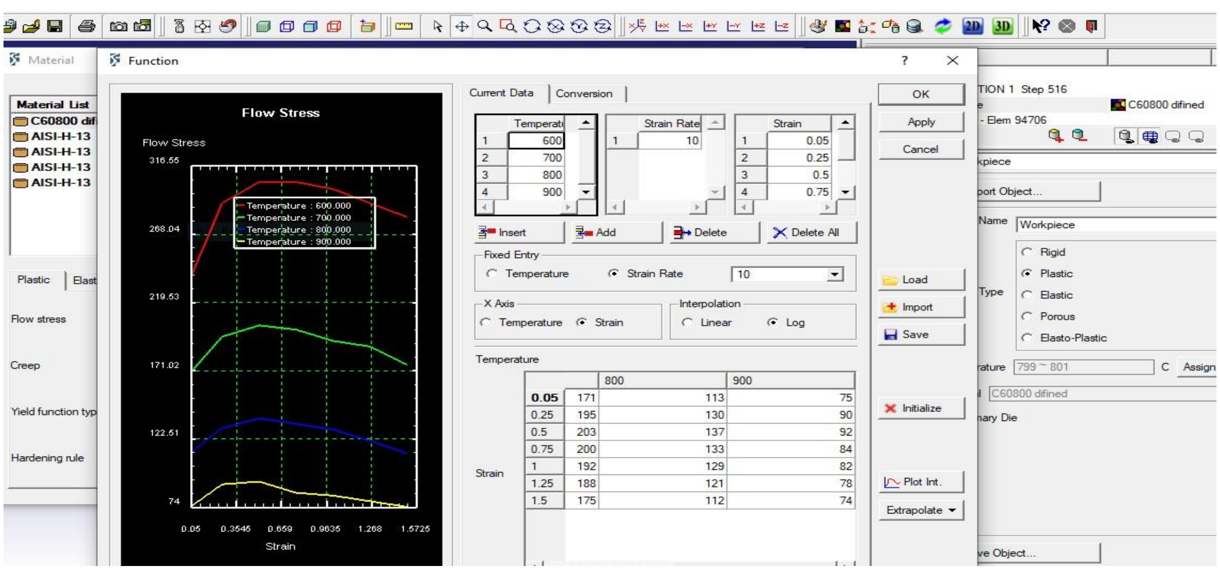

Figure 3-6 Materials are available in database and new material also defined based on stress data

3.7.3 Object definition

How the deformation is modeled for various items must be defined here. A non-deformable part can be represented as a rigid body. Specifically, the top die, bottom die, container, and holder are all represented by geometrical profiles. This type of object is capable of performing force transmission, velocity, heat transmission, and diffusion calculations. These types are used for tooling configurations. Depending on the material properties, the billet can be classified as rigid plastic or rigid visco-plastic. Plastic deformation occurs when the strain rate reaches a certain level. This material model does not consider the spring back effects. These two material models are utilized for this investigation but other models like elastic, elastic-plastic (does not consider strain rate sensitivity), and porous are also available with this software.

3.7.4 Inter-object relation

The master-sleeve relationship was established to define the inter-object relationships between various objects. The finer mesh should be given to the slave or softer item. In this scenario, there was no need to define the "no contact" relationship. The activated nodes show the contact or assignment between the nodes and the surface, which limits the master object's penetration into the sleeve. The behavior of the contacting object while in contact is described below. The problem assigns a shear friction coefficient and a conduction heat transfer coefficient across the inter material boundary. In this formulation, frictional resistance was supposed to be shear-type. The friction factor m ($0 < m < 1$) can be represented as $m = \sqrt{3}\ \tau/\sigma$ as shown in the below figure 3.7.

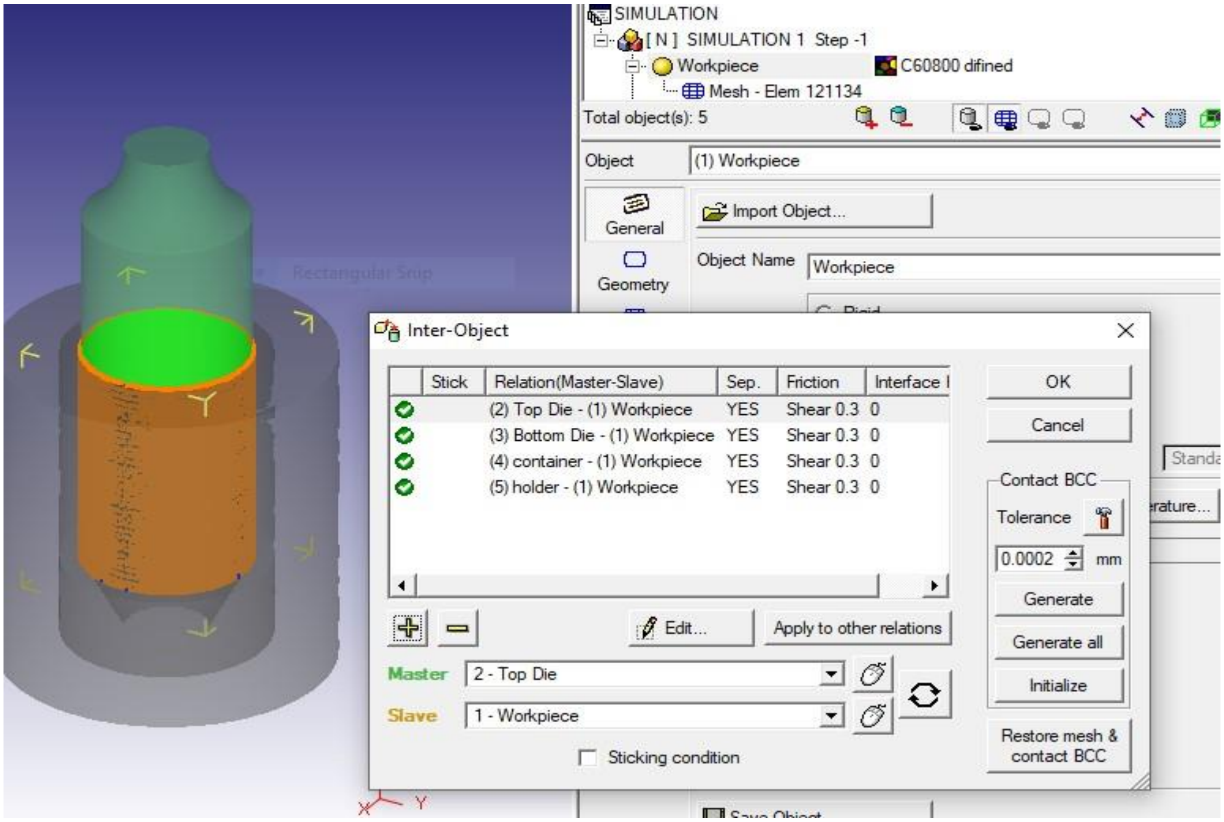

Figure 3-7 Inter-object relation ship

3.7.5 Boundary condition

The boundary condition determines how an object's boundary interacts with others and with the environment. In the majority of circumstances, the object boundary exchanges heat with the environment. The objects' movement boundary condition is defined to meet the extrusion condition. The die and container's velocity are set to zero in all directions, whereas the paunch can only move in the extrusion direction as shown in the below figure 3.8.

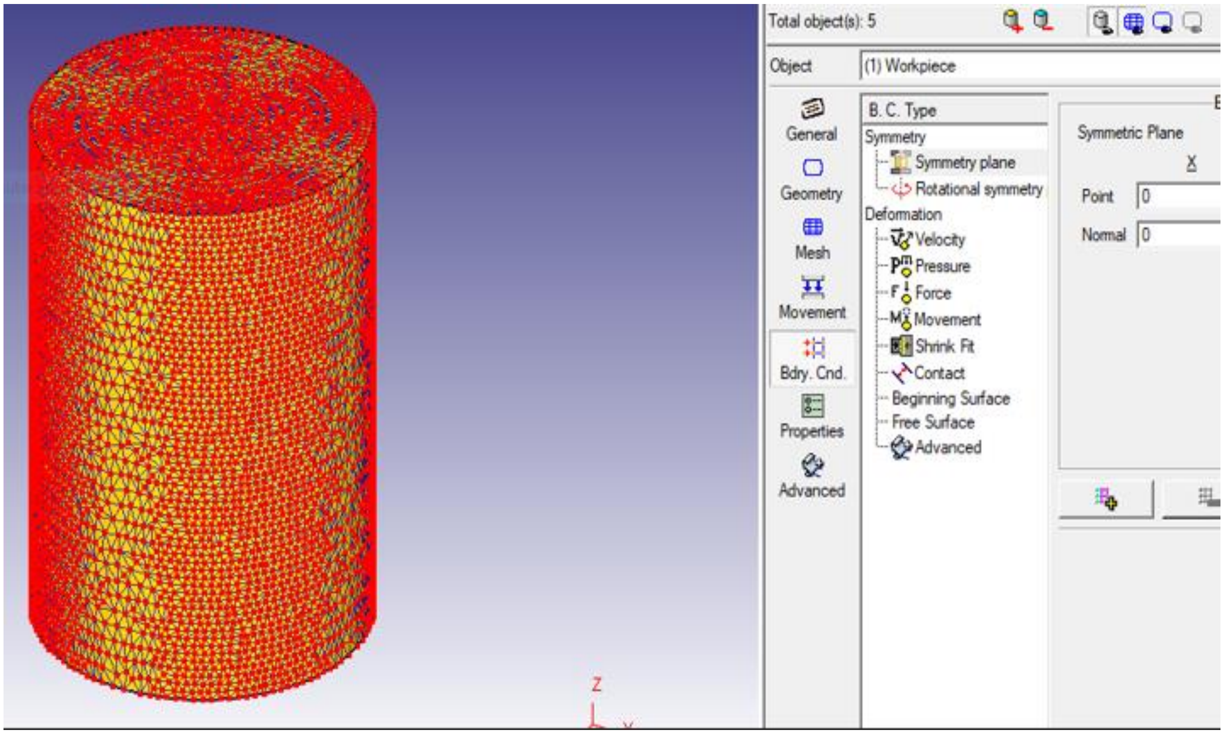

Figure 3-8 Boundary condition

3.7.6 Simulation engine

The assigned simulation or numerical work defined in the preprocessor is further processed by clicking the run icon. The simulation engine runs numerical calculations to analyze the process and store the results in a database. The simulation engine reads the database file, computes the solution, and adds it to the database file. The simulation engine interfaces with the Automatic Mesh Generation (AMG) system to create a fresh FEM mesh for the workpiece. The simulation engine stores status information, including error messages, in the message (.MSG) and log (.LOG) files while running. The simulation graphics option can be used to show the most recent step while the problem is running. Different consequences, such as effective stress, strain, temperature distribution, and damage, as shown in figure 3.9 can be seen specifically for that stage. The user can abort the problem if there is a constraint and continue until the completion messages appear.

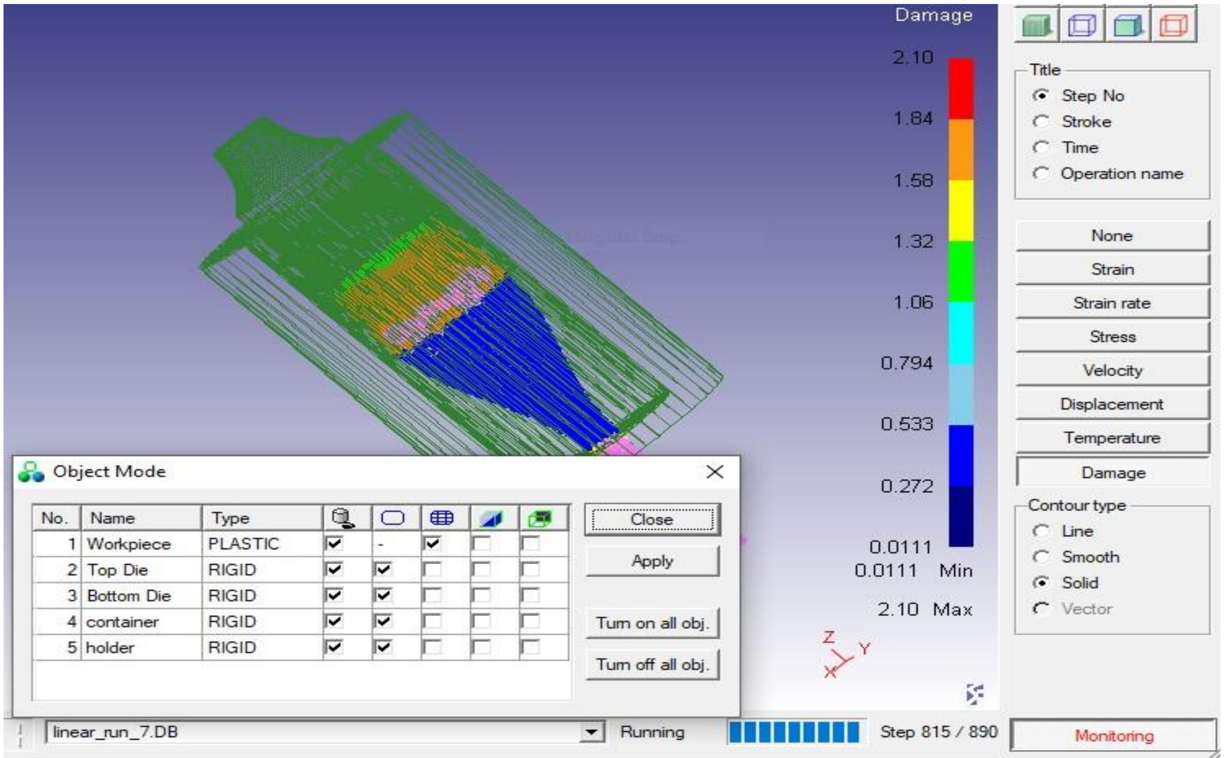

Figure 3-9 Simulation engine when deform running the processor

3.7.7 Post processor

During this stage, the outcome results were shown and can be taken from the database. The geometry follows deformation with tool movement at each stage, and multiple views can be assigned. The distribution of state variables on objects can be examined using contour plots. Contoured plots allow for the variation of distribution styles such as solid saddling distribution, line distribution, and vector distribution. Graphs of any state variable in relation to several abscissa can be drawn and retrieved. Point tracking and flow net are the two most essential tools for studying the internal behavior of a component during the deformation stage given by the postprocessor. The graphic utility window allows you to manipulate the range and vision based on the analysis results. The postprocessor is used to display simulation data. The postprocessor provides a user interface with graphics for displaying geometry, field data (such as strain, temperature, and stress), and simulation data (e.g., die loads). Additionally, the postprocessor can extract graphic or numerical data for use in different applications. Figure 3.10 shows that the extracted effective strain data.

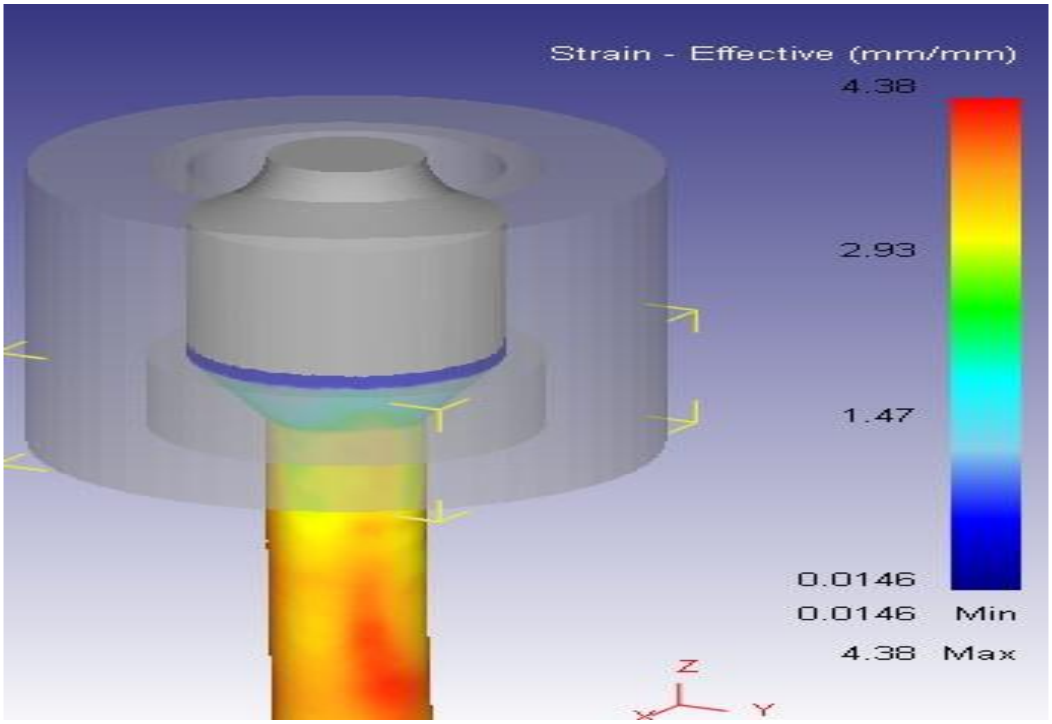

Figure 3-10 Post processor extracted data

3.8 Optimization of Process Parameter by Taguchi Based Genetic Algorithm

The Taguchi approach to experimental design is commonly used for offline quality assurance of products and processes. Most reported Taguchi implementations focus on optimizing a single response. Multiple reactions are prevalent in complicated systems, and optimization often relies on experience and engineering knowledge, leading to ambiguity during decision-making. Taguchi SN ratio with a genetic algorithm to optimize multiple responses in industrial tests. Taguchi experiments with multiple responses, discusses results from a case study on gear hobbing machining, introduces genetic algorithm-based inference, and determines weighted SN ratios (WSN) using SN ratios and GA for the same case study. Finally, an analysis of variance is performed to identify critical factors influencing the WSN (Jeyapaul et al., 2006). The hybrid Taguchi-genetic algorithm technique combines Taguchi algorithms with genetic algorithms to optimize process parameters based on multiple performance factors. The Taguchi technique is a single-response optimization strategy that is utilized in conjunction with genetic algorithms. Genetic algorithm reduces multiple Taguchi responses to a single one, by using weight sum approach technique then optimized using the genetic algorithm method. To establish the most crucial parameters during hot extrusion simulation, it's important to conduct effective experiments with a limited number of runs (Chu et al., 2020).

Table 3-7 Extrusion parameters and their levels

S.NO	Factors	Levels		
		Level 1	Level 2	Level 3
1	Extrusion ratio	2	3	4
2	Ram speed(mm/s)	1	2	3
3	Die length (mm)	10	20	30

Table 3.7 shows as the extrusion parameter and their levels were used for numerical simulation analysis for stream line, linear convergent and cosine die profile

3.8.1 Taguchi's Orthogonal Array

Taguchi's orthogonal array requires the production of a pair of parameters from all levels at two column intervals in the experimental table, with each composition having the same frequency (Hsia, 2013). The orthogonal array sacrifices experimental cost and precision, requiring fewer tests to produce acceptable statistical information. Nonetheless, orthogonal array experiments do not constitute full factorial experiments. The "bias" cannot be completely avoided, but it is acceptable because not all levels of composition are represented on the orthogonal array. As a result, the experimental group may not contain the appropriate composition.

Table 3-8 Experimental parameter distribution using Taguchi L9 orthogonal array

L9 orthogonal array			
S.No.	Extrusion ratio	Ram speed (mm/s)	Die length (mm)
1	2	1	10
2	2	2	20
3	2	3	30
4	3	1	20
5	3	2	30
6	3	3	10
7	4	1	30
8	4	2	10
9	4	3	20

3.8.2 Signal-Noise Ratio Analysis

To choose the best extrusion parameters, the Taguchi method evaluates the signal-to-noise ratio (S/N) of each extrusion parameter level for each output function. The performance feature is determined by an analysis of the S/N ratio, i.e., the lower the better, the higher the better, and the nominal the better. Based on the S/N analysis, the S/N ratio for each level of process parameters is calculated. Regardless of the performance characteristic category, a greater S/N ratio indicates a better performance characteristic. In Taguchi optimization, the S/N ratio is a measure of quality attributes that is calculated as follows (Kothasiri & Chalamalasetti, 2022).

$$\frac{S}{N} = -10\log\{\frac{1}{n}\int_{i=1}^{n} Yi^2 \tag{3.18}$$

$$\frac{S}{N} = -10\log\{\frac{1}{n}\int_{i=1}^{n} \frac{1}{Yi^2} \tag{3.19}$$

where Y = observation n = total number of observations, Y = the average of observed data and Y_i = ith response.

Eq. (3.18) is utilized for smaller the better S/N ratios, and Eq. (3.19) is appropriate for greater the better S/N ratios. To decrease extrusion force, damage, and time, the S/N ratio is estimated for damage, extrusion force, and time using the smaller-is-better criterion. To maximize displacement, the S/N ratio is determined for billet displacement using the larger-is-better criterion (Kothasiri & Chalamalasetti, 2022).

3.8.3 Analysis of Variance (ANOVA)

The analysis of variance (ANOVA) was used to identify which parameters had a significant impact on the quality characteristic. The statistical method of ANOVA is utilized to determine the influence of all control values. In the analysis of variance, the percentage contributions of each control factor are utilized to quantify the associated effects on performance attributes. This analysis employed a 5% significance level, which corresponds to a 95% level of confidence. The ANOVA results indicate whether there is a statistically significant variance in output characteristics. ANOVA analysis is performed when values less than .05 and more than .05 are not significant.

3.8.4 Regression analysis model

The processing parameters of the L9 Orthogonal table were used as the independent variables to prepare a prediction model of processing quality (extrusion load, damage and effective strain). An interactive prediction model was obtained as shown in formula

$$y = \beta_0 + \sum_{i=1}^{k} \beta_i X_i + \sum_{i=j}^{k} \sum_{j=2}^{k} \beta_{ij} x_i x_j + \varepsilon \quad (3.20)$$

y is the dependent variable; β0 is the intercept of the prediction model; k is the number of independent variables for the model; x is the independent variable; ε is the error value of the prediction model; βi and βij are the simulated parameters based on the measured value of the dependent variable for the model. In this paper the Minitab toolbox linear regression model was used to solve β0, βi, βij and ε. ANOVA was used to evaluate the precision of the prediction model(Chu et al., 2020). The degree of freedom for the analyzed ANOVA value was determined using formulas (3.21),(3.22) &(3.23)

$$D_{fB} = k - 1 \quad (3.21)$$

$$D_{fW} = N - k \quad (3.22)$$

$$D_{fT} = N - 1 \quad (3.23)$$

DfB is the model's degree of freedom, DfW is the residual degree of freedom, DfT is the total degree of freedom, k is the number of groups, and N is the number of samples. After determining the degree of freedom in ANOVA, the model's coefficient of determination can be calculated using the sum of squares. The sum of the squares analysis value of ANOVA was determined using formulas (3.24),(3.25) and (3.26).

$$SS_B = \sum_{i=1}^{n} (a_1 - \bar{a})^2 \quad (3.24)$$

$$SS_W = \sum_{i=1}^{n} (a_1 - b_i)^2 \quad (3.25)$$

$$SS_T = SS_B + SS_W \quad (3.26)$$

SSB is the sum of squares of the model; SSW is the residual sum of squares; SST is the total sum of squares; a is the value obtained by calculation using the created regression model and the independent variable; ¯a is the mean of a; b is the value of the dependent variable.

Divide the sum of squares by the corresponding degree of freedom to get the sum of mean squares, and then divide by the sum of mean squares of the model and the residual difference. The sum of mean squares for the analyzed value of ANOVA was obtained using formulas (3.27), (3.28) and (3.29).

$$MS_B = \frac{SS_B}{Df_B} \tag{3.27}$$

$$MS_W = \frac{SS_W}{Df_W} \tag{3.28}$$

$$F - value = \frac{MS_B}{MS_W} \tag{3.29}$$

MSB is the sum of mean squares of the model; MSW is the sum of mean squares of the residual difference; F − value is the data for the determination of the model. The coefficient of determination R^2 of the model and the coefficient of determination R^2(adj) after model adjustment can be found using formulas (3.30) and (3.31).

$$R^2 = 1 - \frac{SS_W}{SS_T} \tag{3.30}$$

$$R^2 = 1 - \frac{\frac{SS_W}{Df_W}}{\frac{SS_T}{Df_T}} \tag{3.31}$$

Finally, if the F − value based on ANOVA is greater than the F − value of 95% confidence, this can be used to decide the confidence level of the prediction model (Chu et al., 2020).

3.8.5 Multi response optimization of Genetic Algorithm

The genetic algorithm "imitates" biological evolution. It is commonly used in engineering due to its ability to swiftly calculate linear and nonlinear optimization problems. Before determining the number of evolutions, the environment's fitness value is assessed based on the original number of genes. Genes are selected for duplication based on their fitness level. This continues until the number of duplicates equals the beginning number. The self-defined crossover rate decides if mating happens.

The mating process involves randomly selecting two genes and rearranging them to create two new ones. The novel gene combination causes mutations and alters the proportion of genes.

The modified gene is examined to determine if it fits environmental criteria. If not, duplication, mating, and mutation occur until the required number of evolutions are reached (Chu et al., 2020).

In Genetic Algorithm, the fitness function reflects the objective function, while the fitness value relates to the performance of an individual chromosome. Population: a group of individuals. GA allows for several population size possibilities. Two crucial factors are initial population generation and population size. Fitness scaling prevents early convergence and slow finishing. There are various varieties, including rank, proportional, top quantity, and shift linear. Selection (reproduction) is the process of selecting two parents from a population to cross paths with. There are several selection procedures, including stochastic uniform, remainder, roulette wheel, random, rank, tournament, and elitism. Crossover, also known as replication, is the process of merging two individuals in order to produce new offspring for the next generation.

There are various sorts of crossovers, including dispersed, single-point, two-point, intermediate, heuristic, and mathematical. After crossover, springs undergo mutation. Mutation functions create small random changes in individuals, increasing genetic variety and allowing the genetic algorithm to search a wider range. There are several types of mutation, including constraint-dependent, uniform and adaptively feasible. Mutating a bit involves flipping it from to 1 or vice versa, with a low mutation probability. Stopping Criteria: The algorithm's stopping conditions, such as generation, duration, and fitness limits, determine when it terminates (Majumdar & Ghosh, 2015). Figure 3.11 display that flow chart every genetic algorithm optimization step from data entry up to analysis multi response optimization.

-

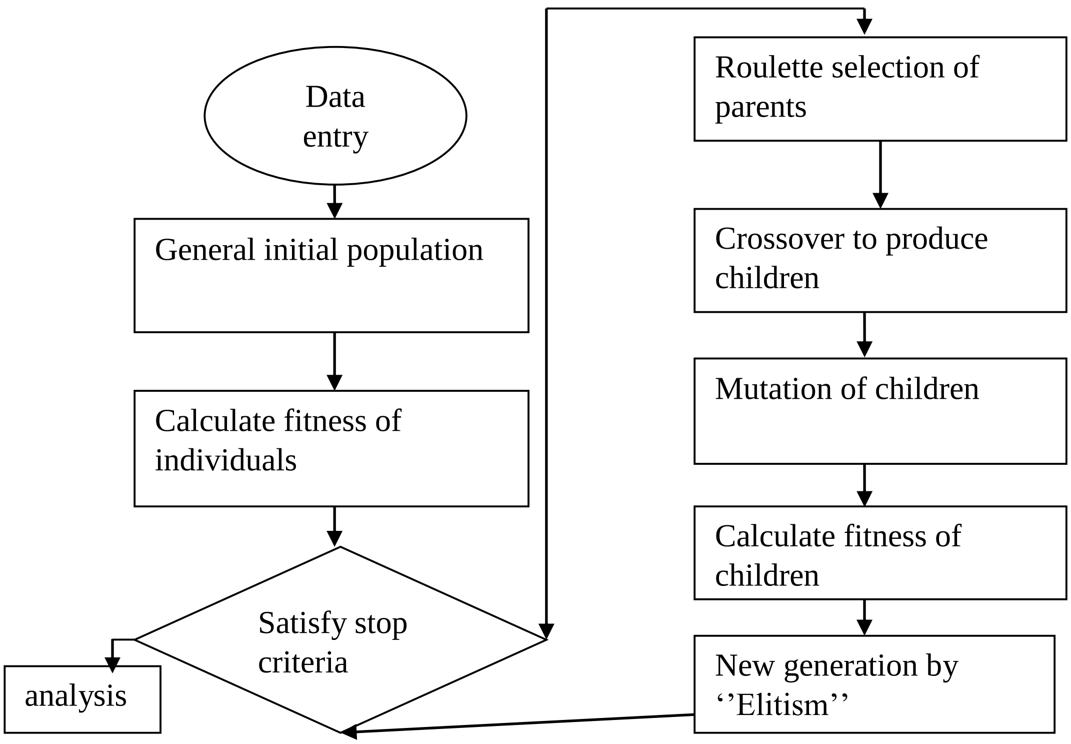

Figure 3-11 Flow chart of genetic algorithm

The overall objective function is obtained by giving weightage based on based on 'weight sum method' as follow

$$F(x) = w1*f1 + w2*f2 + w3*f3 \quad (3.\ 32)$$

Where w1, w2 and w3 is weight function

3.9 Experimental Investigation

The extrusion process was performed with optimum parameters and in all type die profiles for the investigation of mechanical properties and material characterization. The methodology for experimental investigation presented from fabrication die, container, holder and ram up to material testing and microstructure characterization.

3.9.1 Fabrication die, container, holder and ram for extrusion process

Prepare die, container, holder and ram from H13 tool steel material in CNC lathe and milling machine. Heat treatment is done for hardening tools as shows in the below figure.

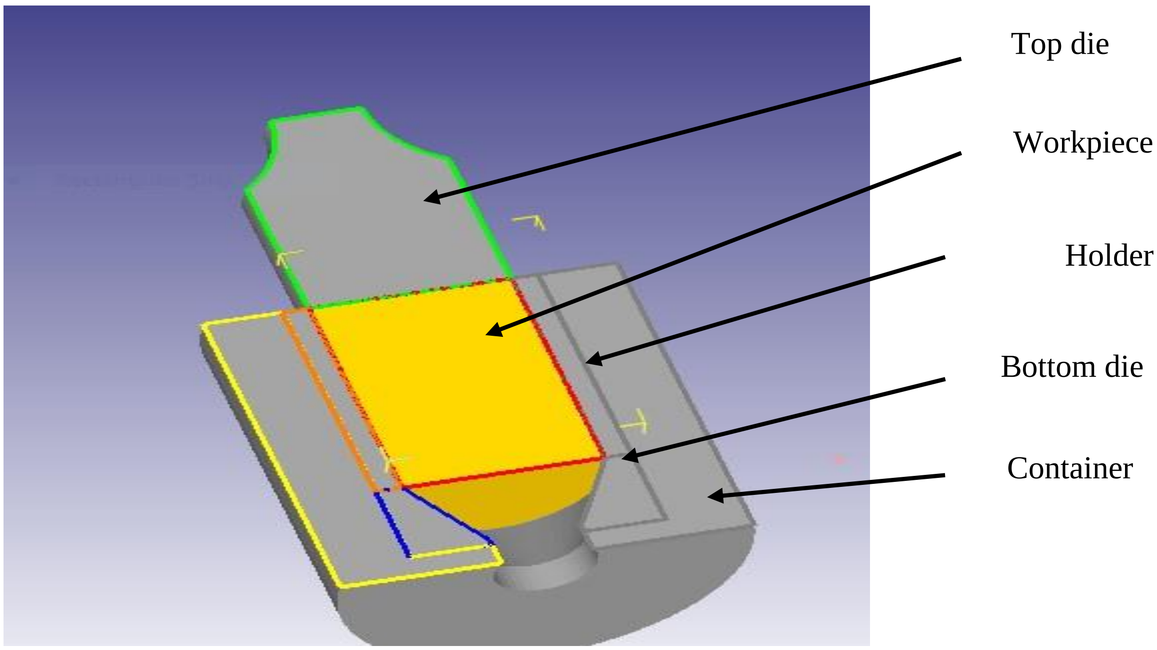

Figure 3-12 Part of extrusion design

The method uses a mathematically constructed cosine, linear convergent and streamline die for round to cylindrical extrusion. A H13 die steel stock with 100mm and 50 mm diameters was obtained from Kolfe industrial college (Addis Ababa, Ethiopia) and power hacksaw cut to the necessary size for the die chamber punch and guide plate. The die chamber and punch were pre-machined using a CNC milling and lathe, including facing, turning, drilling, and boring operations. After pre-machining, the die cylinder and punch set were heat treated in a muffle furnace in three stages: stress relief, hardening, and tempering. The stress treatment process involved heating to 650°C for an hour and then cooling slowly. To harden the die components, they were placed in a preheated furnace at 1000 °C for 25–30 minutes before being quenched in still air. The pieces were placed in the furnace for tempering. The temperature was raised to 900°C and gently cooled. Finally, die components were polished with a cylindrical grinder. Container and holder were pre-machined in conventional lathe using facing, turning drilling and boring operation as displayed in figure 3.13.

Figure 3-13 a) Conventional lathe b) CNC lathe c) Fabrication die and container

3.9.2 Hot extrusion

Direct hot extrusion is used for this study, which is accessible at the manufacturing technology & engineering industry research and development center (Addis Ababa, Ethiopia). Before beginning hot extrusion procedure, the C60800 aluminum alloy were preheated for 20 minutes at 800℃ to uniformly heat the sample volume. (Anantapong et al., 2014) investigated the deformation behavior of aluminum bronze alloy with a temperature range of 800-950 °C at a strain rate of 10 s-1 and achieved good mechanical properties at 800 °C. To reduce friction during the extrusion process, graphite powder and grease are mixed and applied to the inside surface of the die. Graphite is a popular solid lubricant due to its low cost and low friction coefficient. Graphite requires lubrication due to its decreased shear strength when exposed to humidity (e.g., air). Argon gas is used to protect the material from oxidation during extrusion process. Hot extrusion was accomplished utilizing a 500KN hydraulic press. The furnace and the hydraulic press machine was in close range to reduce heat dissipation during moving the billet from furnace to hydraulic machine. To minimize heat dissipation was used oxy acetylene flame during moving. For cosine die used extrusion ratio of 2, ram speed f 2.05mm/s and die length of 10mm, for linear convergent die profile extrusion was performed by using extrusion ratio of 2, 3 mm/s ram speed and die length of 10mm and for streamline die profile also extrusion ratio 2 (extrusion ratio = billet area/shape area), ram speed 1mm/s and die length 30mm. figure 3.14 below shows the extruded C60800 aluminum bronze alloy.

Figure 3-14 Extruded samples of cosine, linear convergent and streamline respectively

3.9.3 Specimen preparation for test

After the aluminum bronze alloy was successfully extruded using a hydraulic press, the sample was ready for microstructural examination and mechanical testing. In compliance with ASTM standards, the specimen was machined on a lathe to the required size and shape for mechanical and microstructure study testing.

Machining and cutting

Machining on a lathe was performed to achieve the required shape and size in accordance with ASTM requirements.

3.9.4 Microstructural characterization of aluminum bronze alloy

An optical microscope is used to examine the intergranular attack, the volume percentage of grain particle size, extent of decarburization and carburization and percent spheroidization of alloy.

The specimen is prepared in the following steps:

i, sectioning It has two purposes: creating a cross-section of the specimen for examination, reducing its size for placement on an optical microscope stage, and embedding it in mounting media for additional preparation steps. Abrasive cutting is used to slice synthetic aluminum bronze alloy. Specimens are sectioned using a narrow spinning disk with abrasive particles and an appropriate medium.

ii, Grinding Grinding is the process of smoothing a surface and removing damage produced by sectioning. Abrade the specimen with a graded sequence of abrasives, starting with coarse grit. Aluminum bronze alloy is grinded using 400, 800, and 2000 grit sandpapers.

iii, Polishing Polishing creates a smooth and shining surface by rubbing the sample with a diamond suspension and gradually reducing pressure to prevent plastic deformations. The RB 204 Metpol-II Model polishing technique was utilized.

iv, Etching Chemical etching creates contrast in microstructural characteristics on specimen surfaces. Etching is a controlled corrosion process that happens between surfaces with differing electrochemical potentials. To accomplish microstructural analysis, polished samples of aluminum bronze alloy were etched with a mixed etchant solution (25 ml ammonia hydroxide, 20 ml hydrogen peroxide, and 25 ml distilled water). Etching was accomplished by immersing the samples in the solution for 30 seconds.

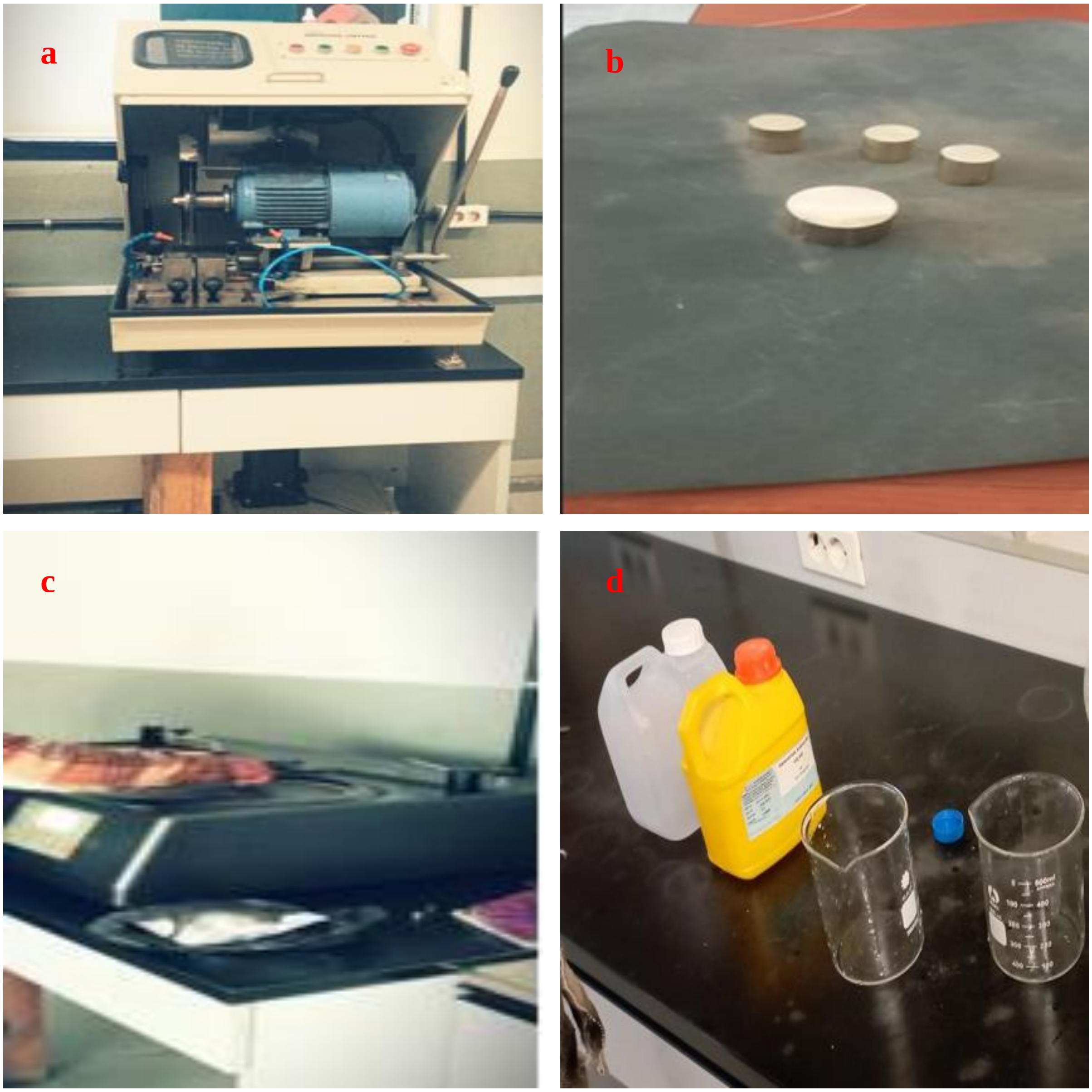

Figure 3-15 Sample preparation for microstructure (a) sectioning (b) grinding (c) polishing and (d) etching

3.9.5 Hardness test

A material's hardness typically indicates its resistance to deformation. A hardness test is designed to verify the appropriateness of a produced aluminum bronze alloy material for a specific engineering application. The Vickers hardness tester was utilized, using a square-base diamond pyramid as the indenter. The pyramid's opposed faces make a total angle of 136°. The diamond-pyramid hardness number (DPH), also known as the Vickers hardness number (VHN or VPH), is derived by dividing the force exerted by the surface area of the indentation. The

Vickers test for hardness uses a diamond indenter and a mild force to create an indentation on the subject being tested. The depth of the indentation is used to calculate the object's hardness value.

$$HV = \frac{constant\ t \times test\ force}{surface\ area\ of\ identation}$$

$$= .102 \times 2F(\sin\left(\frac{136}{2}\right))/d^2 \quad (3.\ 33)$$

Where F- is test force and d- is surface area of indentation.

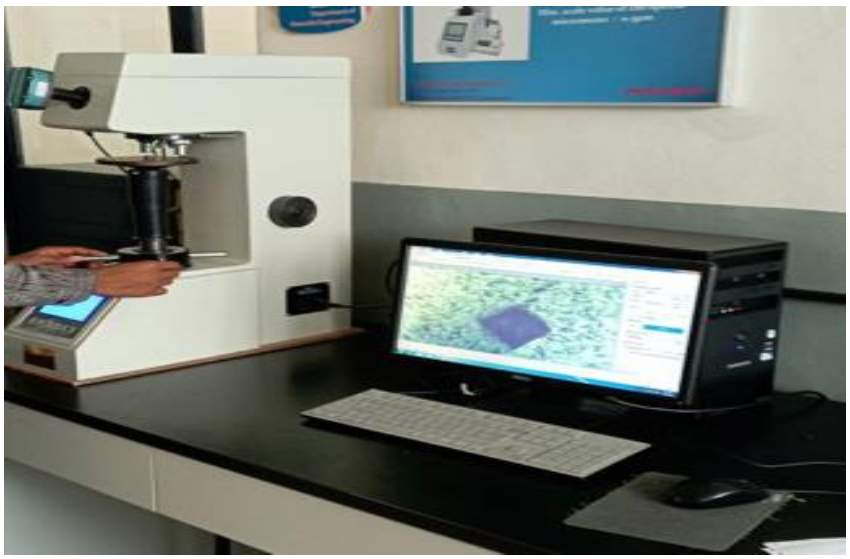

Figure 3-16 Vickers hardness testing machine set up

3.9.6 Compression test

Compression strength refers to a material's or structure's ability to endure loads that cause it to shrink. A material's ultimate tensile strength is defined as the magnitude of uniaxial compressive stress reached when it totally fails. Compressive strength is frequently determined experimentally using a compressive test and a uniaxial compressive force. The compression test cylindrical specimen was constructed in accordance with the ASTM E-9 standard with a length-to-diameter ratio of 3mm (L = 18 mm and 6 mm in diameter) and then tested using a universal testing machine (UTM) with a load capacity of 100 KN. The load was applied until the specimens fractured.

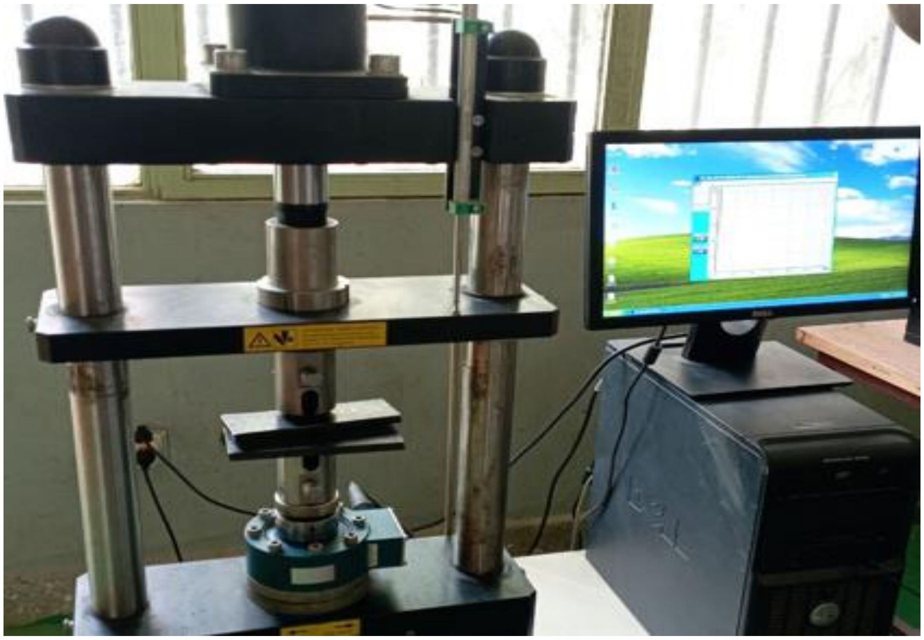

Figure 3-17 Universal testing machine (UTM) setup for compression test

3.9.7 Corrosion test

Corrosion tests are carried out by submerging the specimens in a 3.5% NaCl bath for 30 minutes. The specimens utilized in the testing measured 10mm in diameter and 7mm in length. To eliminate any stray lines from the specimen's surface and make it mirror cleaned alloy specimens were cleaned with 800 sheets of emery cleaning paper, followed by 12 meters of diamond paste on a dual disc polishing machine. The working electrodes were copper-based alloy samples with a 1 cm2 exposed area, the auxiliary (counter) electrode was graphite, and the reference electrode was either a standard calomel electrode (SCE) or mercury. Tafel curves were generated by automatically changing the electrode potential from -250 to +250 mV relative to the corrosion potential (Ecorr) at a scan rate of 1 mVs-1. Tafel polarization curves provide electrochemical data such as corrosion current density (Icorr), corrosion potential (Ecorr), and corrosion rate (Cr). The cathodic and anodic portions of Tafel plots were utilized to compute the corrosion current density (Icorr) and potential (Ecorr). Extrapolating linear sections of anodic and cathodic curves resulted in current densities (Icor) and corrosion potentials.

The corrosion rate was calculated using the conversion formula (3.34)

$$\text{Corrosion rate(mmpy)} = \frac{\text{CEwIcorr}}{\text{d}} \qquad (3.\ 34)$$

Where C is the conversion constant (0.129), Ew is the specimen's equivalent weight (g), and d is its density (g/cm3).

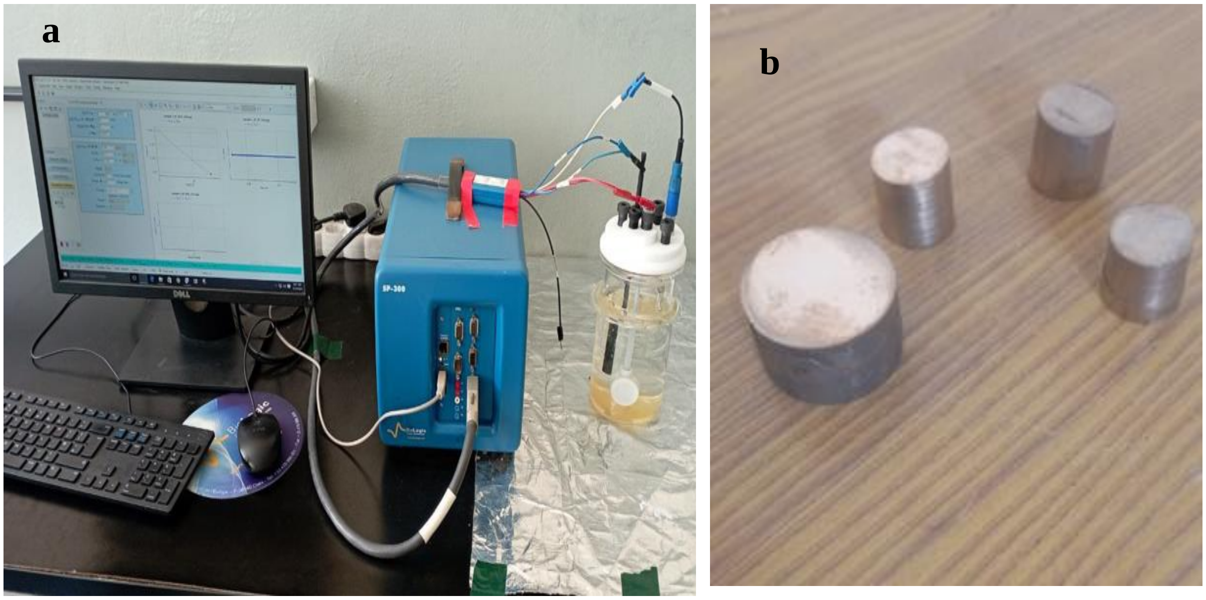

Figure 3-18 Corrosion test set up (a) potentiator setup for corrosion test and (b) sample prepared for corrosion test

CHAPTER IV

RESULT AND DISCUSSION

4.1 Introduction

This chapter includes the results and discussions on optimizing numerical simulation result of extrusion parameters and experimental investigation. DEFORM 3D used to forecast the impact of extrusion process parameters on the workpiece. The response results were examined using Taguchi's S/N ratio for damage, effective strain, and load, as well as multi response optimization using Taguchi based genetic algorithm by MATLAB software. The extrusion process was conducted using optimized parameters in all type of die and investigation of compression test, hardness test, corrosion test and material characterization test were discussed in detail.

4.2 Analysis of Extrusion

Analytic equation is done based extrusion ratio of each parameter and compare the result with the simulation data done by deform 3D. Stress-strain curve of C60800 aluminum bronze alloy under an axial tensile test from extrudate casted ingot to determine engineering stress-strain.

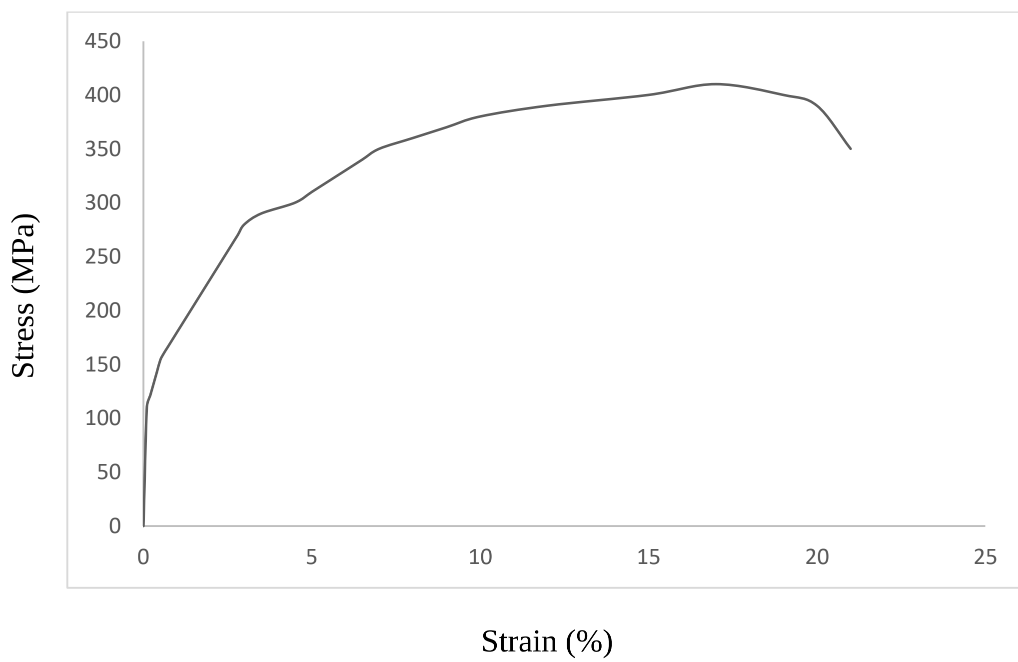

Figure 4-1: stress-strain curve of C60800 aluminium bronze alloy

4.2.1 Determination of extrusion strain

Extrusion strain is calculated based on empirical constant a and b in Johnson formula and extrusion ratio. The true strain also calculates based on the engineering strain data.

The true strain is:-

$$\varepsilon_t = \ln(1+\varepsilon)$$

= ln (1+0.21)

= .19

Extrusion strain for extrusion ratio of 2

ϵ_x = .8+1.2*ln2

=1.6317

For extrusion ratio 3

ϵ_x = .8 + 1.2*ln3

= 2.118

For extrusion ratio of 4

ϵ_x = .8 + 1.5*ln4

= 2.88

4.2.2 Determination average flow stress

Average flow stress was calculated from true stress-strain data of extrudate and ingot of C60800 aluminum bronze alloy. The true stress and true strain of both extrudate and ingot is calculated from engineering stress-strain data.

True stress of ingot:- $\sigma_t = \sigma_o(1+\varepsilon)$

= 410(1+0.21)

= 496.1MPa

True stress for extrudate: - = 520(1+0.19)

= 618.8MPa

The average flow stress:= = (496.1+618.8)/((0.21+1)+0.19))*2/2*0.157

= 125MPa

4.2.3 Determination of ram pressure and force

The ram pressure for extrusion was calculated by shape factor, average flow stress, extrusion strain , diameter and length of the billet. The applied force is the multiplication of pressure and area of the billet

$$p = K_x \sigma_{ave.f} \left[\varepsilon_x + \frac{2L}{D} \right]$$

K_x is the shape factor for round bar extrusion case is equal to one. The average stress is 125MPa at temperature of 800℃ calculated from flow stress data from (M Spittel &thilo spittel, 2006).

pressure applied in the ram is calculated for extrusion ratio of 2.

P = 125(1.6317+2(20)/20

= 453.96MPa

F = 453.96*π(20^2)/4

= 132.54KN

For extrusion ratio of 3

P = 125 (2.118+2(20)/20

= 514.75MPa

F = 514.75* π(20^2)/4

= 161.63KN

For extrusion ratio 4

P = 125 (2.118+2(20)/20

= 609.93MPa

F = 609.93* π(20^2)/4

= 191.518KN

4.3 Analysis of Numerical Simulation and Optimization for Cosine Die Profile

Finite element is the representation of a collection of sub domains of billet. which, depending on the type of element chosen, are circumscribed by a set of nodes; all the body's qualities are given to the nodes. This represents an approximate method of target estimation, and accuracy can be increased by increasing the element.

The finite element model of cosine die profile in the C60800 aluminum bronze alloy extrusion process DEFORM 3D predicts this analysis in terms of load, damage, and effective strain by taking input process parameters such as extrusion ratio, ram speed, and die length. The process also uses a constant temperature of 800℃ for all L9 Taguchi combinations.

The significant coefficient is computed using Minitab 21, a statical software, and final models including these coefficients are built to estimate the extrusion load, damage, and effective strain of the cosine die profile. Nine experiments are required for three factors and three levels of the L9 Taguchi orthogonal.

4.3.1 Numerical simulation result for cosine die profile

The extrusion load, effective strain and damage was predicted using the DEFORM 3D V11 program. Table 4.1 shows simulation results of extrusion load, effective strain, damage by setting Taguchi's L9 design of the experiment. This study examined the impact of numerous control factors, including extrusion ratio, ram speed, and die length, at various levels. To minimize material damage, extrusion load and effective strain in engineering applications, we choose smaller, higher-quality characteristics to study the impact of extrusion process parameters on material. DEFORM 3D software was used to forecast extrusion load, damage and effective strain across 9 simulation runs of cosine die using a numerical approach is shown as follows.

Table 4-1 L9 cosine simulation result for (load, effective strain, damage)

S. No	Extrusion ratio (X1)	Ram speed (X2)	Die length (X3)	Load (KN)	Strain effective	Damage
1	2	1	10	91.4	0.0415	1.79
2	2	2	20	105.29	0.0402	1.91
3	2	3	30	127.31	0.0405	2.23
4	3	1	20	215.95	0.0494	2.65
5	3	2	30	169.13	0.0432	0.93
6	3	3	10	248.58	0.0516	1.31
7	4	1	30	189.3	0.0712	2.06
8	4	2	10	317.18	0.0573	2.43
9	4	3	20	334.83	0.0512	0.429

4.3.2 Analysis of extrusion load

I. Analysis of SN ratio for extrusion load (cosine**)**

The statistical rule "smaller the better" has been used to assess and describe extrusion load. To compute the signal-noise ratio, use equation (3.18) Smaller is better.

Table 4-2 Signal to Noise Ratios for the load percentage (smaller the better)

Level	Extrusion ratio(X1)	Ram speed (X2)	Die length (X3)
1	-40.59	-43.82	-45.72
2	-46.39	-45.01	-45.88
3	-48.69	-46.83	-44.07
Delta	8.10	3.02	1.81
Rank	1	2	3

Table 4.2 displays delta statistics for extrusion load, which rank factors influencing responses based on S/N ratios obtained from the Taguchi orthogonal array. The delta statistics were computed by subtracting the highest and lowest average values for each factor. The highest delta value represents the most significant element impacting the extrusion load. The extrusion ratio has a rank of 1 and a delta value of 8.10, making it the most significant factor impacting the required load of the aluminum bronze alloy during hot extrusion. Ram speed and die length were placed second (3.02) and third (1.81), respectively.

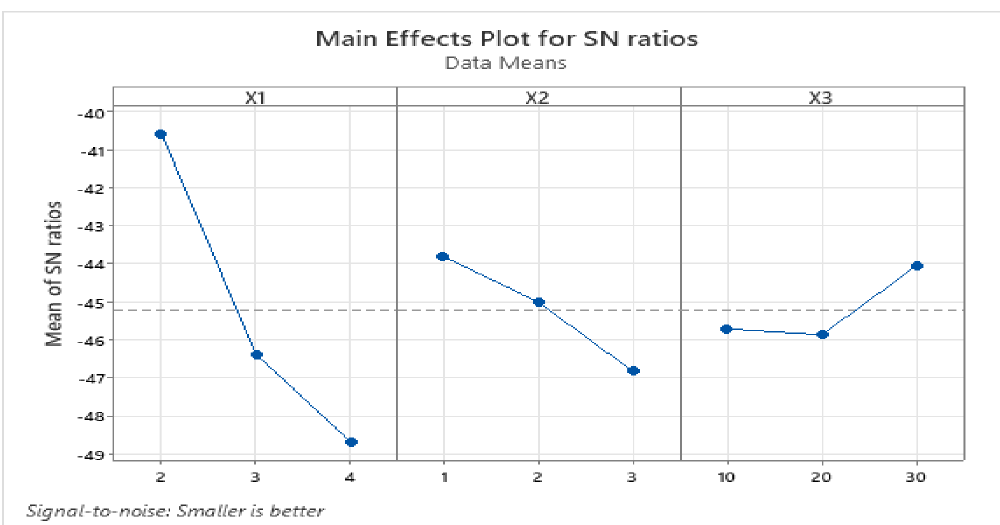

Figure 4-2 Main effect plot for SN ratios for extrusion load parameters

The best combination for extrusion load as shown in the above figure (smaller is better for extrusion load). Due to the fact that a higher SN ratio is preferable, it was chosen for investigation. The optimum possible combination of factors at that level is shown by the numerical value of the maximum point on each graph in the S/N ratio. The above figure shows the optimum value **($X_12X_21X_330$)** for extrusion ratio X1 at 2, ram speed at X2 at 1mm/s and die length X3 at 30mm.

II. Analysis of Variance for load response (cosine)

The extrusion ratio (X1), ram speed (X2), and die length (X3) of aluminum bronze alloy are determined by means of ANOVA. The following are abbreviations: F (F-ratio), DF (degree of freedom), SS (squares), and MSS (mean squares).

Table 4-3 Analysis of Variance of extrusion load of aluminum bronze alloy

Source	DF	Seq SS	Adj SS	Adj MS	F	P	Percentage of contribution
X1	2	104.545	104.545	52.272	21.01	0.045	80.8%
X2	2	13.858	13.858	6.929	2.79	0.264	10.7
X3	2	6.019	6.019	3.010	1.21	0.453	4.65
Error	2	4.976	4.976	2.488			
Total	8	129.398					

S	R-Sq	R-Sq(adj)
1.5773	96.15%	84.62%

Table 4.3 shows the ANOVA results of load. The analysis was conducted with 95% confidence and 5% significance. The table shows that the extrusion ratio is the most significant factor (80.8%) in determining the extrusion load, followed by ram speed (10.7%) and die length (4.65%). The ANOVA table uses F-values and P-values to show the significance of each factor. A parameter's effect on a response variable is considered significant if its F-value exceeds the tabulated value. Extrusion ratio ($P = .045 < .05$) significantly impacts extrusion load, while ram speed and die length do not. Increasing the extrusion ratio causes the aluminum bronze alloy extrusion load to increase. The regression model fits the data well, as indicated by a higher-than-normal R-square value of 84.62%.

The below figure 4.2 demonstrates that as the extrusion ratio of the cosine die is increased, the load required to extrude aluminum bronze alloy tends to increase. As shown in the ANOVA result, extrusion ratio was a high percentage of contribution for extrusion load. (Kothasiri & Chalamalasetti, 2022) analyzed the die angle has greater significance followed by ram speed.

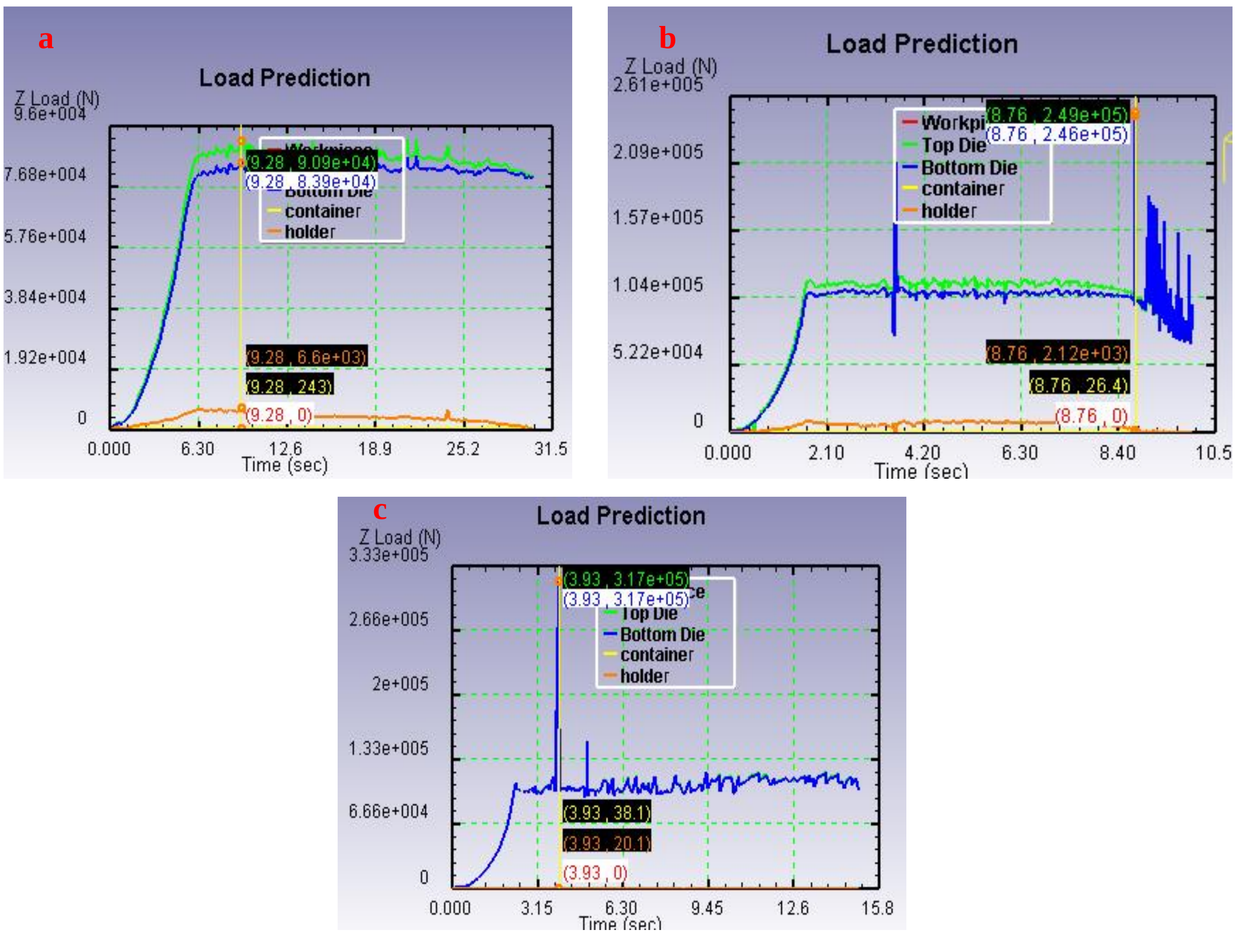

Figure 4-3 Extrusion load distribution over surface of C60800 at die length of 10mm.(a) extrusion ratio of 2 (b) extrusion ratio of 3 (c) extrusion ratio of 4

4.3.3 Analysis of effective strain

I. Analysis of SN ratio for effective strain (cosine)

The statistical rule "smaller the better" has been used to assess and describe effective strain. To compute the signal-noise ratio, use equation (3.18) Smaller is better

Table 4-4 Signal to Noise Ratios for the effective strain percentage (smaller the better)

Level	Extrusion ratio (X1)	Ram speed (X2)	Die length (X3)
1	27.80	25.57	26.07
2	26.39	26.68	26.62
3	24.53	26.47	26.03
Delta	3.27	1.11	0.59
Rank	1	2	3

The table 4.4 displays the delta statistics of the S/N ratio for effective strain based on the characteristics impacting responses ranked by the Taguchi orthogonal array. Delta data were calculated by comparing the highest and lowest average values for each factor. The factor with the greatest impact on effective strain percentage has the largest delta value and is ranked first. The analysis indicates that the extrusion ratio of extruded material, designated a rank 1 with a delta value of 3.27, was the primary factor determining the effective strain percentage of the aluminum bronze alloy. Ram speed and die length were designated as second (1.11) and third (0.59), respectively.

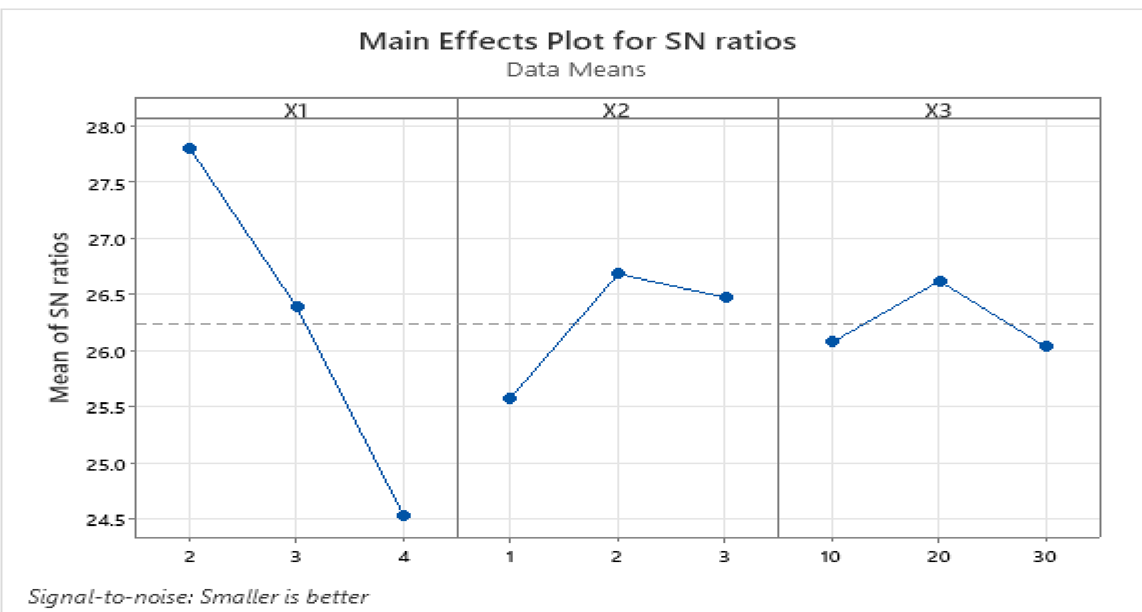

Figure 4-4 Main effect plot of for SN ratio for effective strain

Figure 4.3 indicates the best combination of extrusion parameters for minimal effective strain percentage (the smaller the better). The maximum point on each graph represents the optimal combination of parameters in the S/N ratio. The graph above shows the maximum point of SN ratio is optimum point at **($X_1 2 X_2 2 X_3 20$)** for extrusion ratio X1 at 2, ram speed X2 at 2mm/s, and die length X3 at 20mm**.**

II. Analysis of Variance for effective strain response (cosine die)

ANOVA is used to identify key factors influencing aluminum bronze alloy extrusion ratio, ram speed and die length. Abbreviations: DF (degree of freedom), SS (squares), MSS (mean squares), and F (F-ratio).

Table 4-5 Analysis of Variance effective strain of aluminum bronze alloy

Source	DF	Seq SS	Adj SS	Adj MS	F	P	Percentage of contribution
X1	2	16.1147	16.1147	8.0573	25.03	0.038	74.29
X2	2	2.8483	2.8483	1.4242	4.424	0.184	13.13
X3	2	2.0832	2.0832	1.0416	3.235	0.236	9.6
Error	2	0.6438	0.6438	0.3219			
Total	8	21.6900					

S	R-Sq	R-Sq(adj)
1.1934	97.03%	88.13%

Table 4.5 shows the ANOVA findings for the effective strain. The analysis was carried out with 95% confidence and 5% significance. The table demonstrates that the extrusion ratio is the most significant factor (74.29%) in determining effective strain, followed by ram speed (13.13%) and die length (9.6%). The ANOVA table displays each factor's importance using F-values and P-values. A parameter's effect on a response variable is regarded as significant if its F-value is greater than the tabulated value. The extrusion ratio ($P = .038 < .05$) has a substantial impact on effective strain, while ram speed and die length do not. The effective strain of the aluminum bronze alloy increases when the extrusion ratio is increased. The regression model fits the data well, as evidenced by a higher-than-normal R-squared value of 88.13%.

The below Figure 4.4 Displayed that the extrusion ratio of cosine die profile at 20mm die length increased, the effective strain required for extrusion of C60800 aluminum bronze alloy also increased. As shown in the above ANOVA table also extrusion ratio has high percentage of contribution on effective strain followed by ram speed.

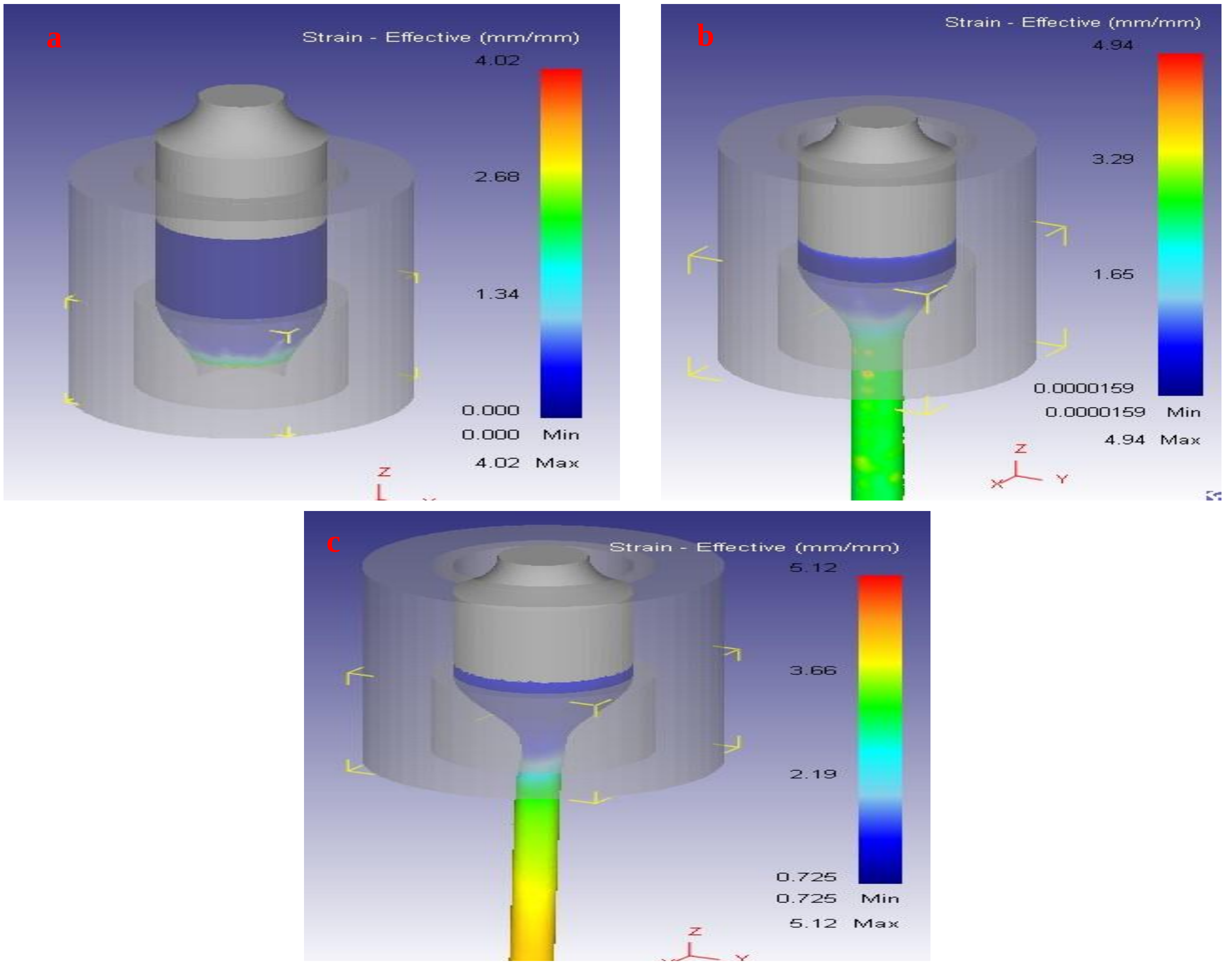

Figure 4-5 Effective strain distribution over surface of C60800 at die length of 20mm.(a) extrusion ratio of 2 (b) extrusion ratio of 3 (c) extrusion ratio of 4

4.3.4 Analysis of damage

I. Analysis of SN ratio for damage (cosine)

The statistical rule "smaller the better" has been used to assess and describe damage. To compute the signal-noise ratio, use equation (3.18). Smaller is better.

The table 4.6 shows the delta statistics of the S/N ratio for damage based on the Taguchi orthogonal array-ranked factors that influence responses. Delta values were obtained by comparing the highest and lowest average values for each factor. The factor with the greatest influence on the damage percentage has the largest delta value and is ranked first. The tables show that the extrusion ratio of extruded material, classified as rank 2 with a delta value of 3.6684, was the key factor determining the damage percentage of the aluminum bronze alloy. Ram speed is the first rank with value of 5.9462 and die length was ranked third (2.7933) .

Table 4-6 Signal to Noise Ratios for the damage percentage (smaller the better)

Level	Extrusion ratio (X1)	Ram speed (X2)	Die length (X3)
1	-5.8813	-6.5998	-5.0382
2	-3.3933	-4.2342	-2.2449
3	-2.2129	-0.6536	-4.2044
Delta	3.6684	5.9462	2.7933
Rank	2	1	3

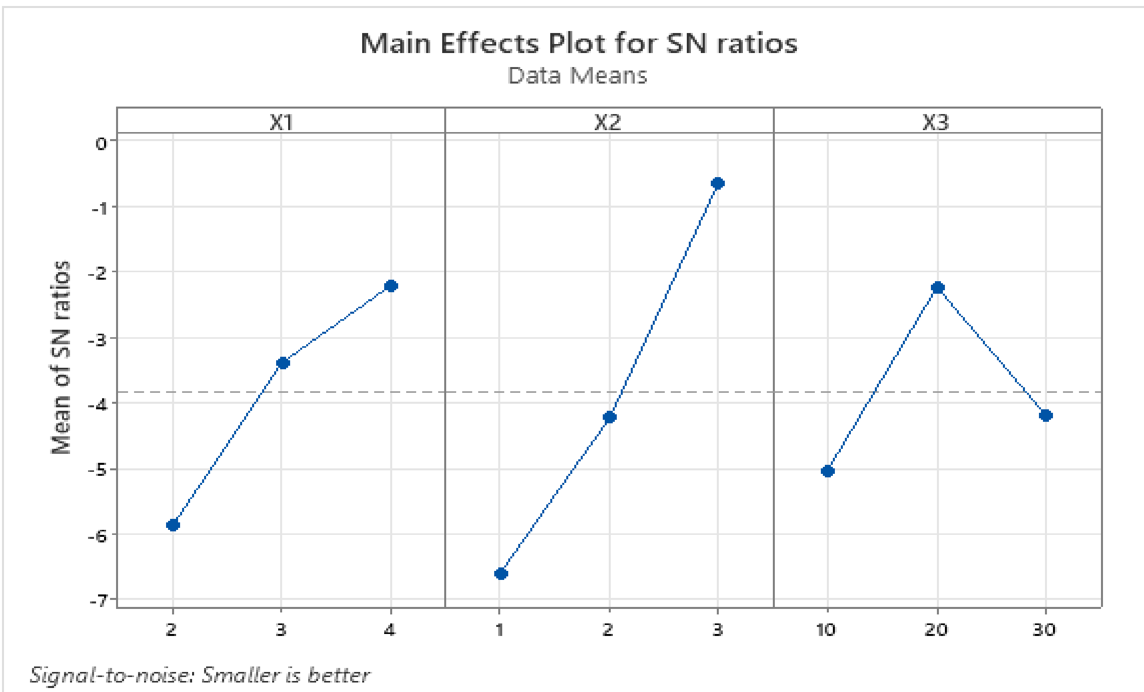

Figure 4-6 Main effect plot of for SN ratio for damage

Figure 4.5 shows the optimal combination of extrusion parameters for the lowest damage percentage (smaller is the better). Each graph's maximum point represents the best parameter combination in terms of the S/N ratio. The graph above depicts the highest SN ratio at **($X_14X_23X_320$)** for extrusion ratio X1 = 4, ram speed X2 = 3 mm/s, and die length X3 = 20 mm.

II. Analysis of Variance for damage response (cosine)

ANOVA is used to identify key factors influencing aluminum bronze alloy extrusion ratio, ram speed and die length. Abbreviations: DF (degree of freedom), SS (squares), MSS (mean squares), and F (F-ratio).

Table 4-7 Analysis of Variance for damage of aluminum bronze alloy

Source	DF	Seq SS	Adj SS	Adj MS	F	P	Percentage of contribution
X1	2	53.77	53.77	26.887	12.39	0.075	26.33
X2	2	117.05	117.05	58.524	26.98	0.036	57.32
X3	2	29.04	29.04	18.520	8.54	0.105	14.22
Error	2	4.34	4.34	2.169			
Total	8	204.20					

S	R-Sq	R-Sq(adj)
7.6501	97.87%	85.01%

Table 4.7 displays the ANOVA findings for damage. The analysis was carried out with 95% confidence and 5% significance. The table reveals that ram speed (57.32%) is the most significant variable in determining damage, followed by extrusion ratio (26.33%) and die length (14.22%). The ANOVA table displays each factor's importance using F-values and P-values. A parameter's impact on a response variable is considered significant. If the F-value exceeds the tabulated value, Ram speed (P = .036 < .05) greatly affects damage. The regression model fits the data well, as seen by an above-average R-square value of 85.01%.

The below figure 4.6 Shows that by increasing the extrusion ratio of cosine die profile the damage percentage of aluminum bronze alloy has declined in the case of ram speed of 3mm/s. however, for ram speed 1mm/s and 2mm/s damage value is not uniformly increased with extrusion ratio. Damage percentage is highly affected by ram speed as shown in ANOVA table.

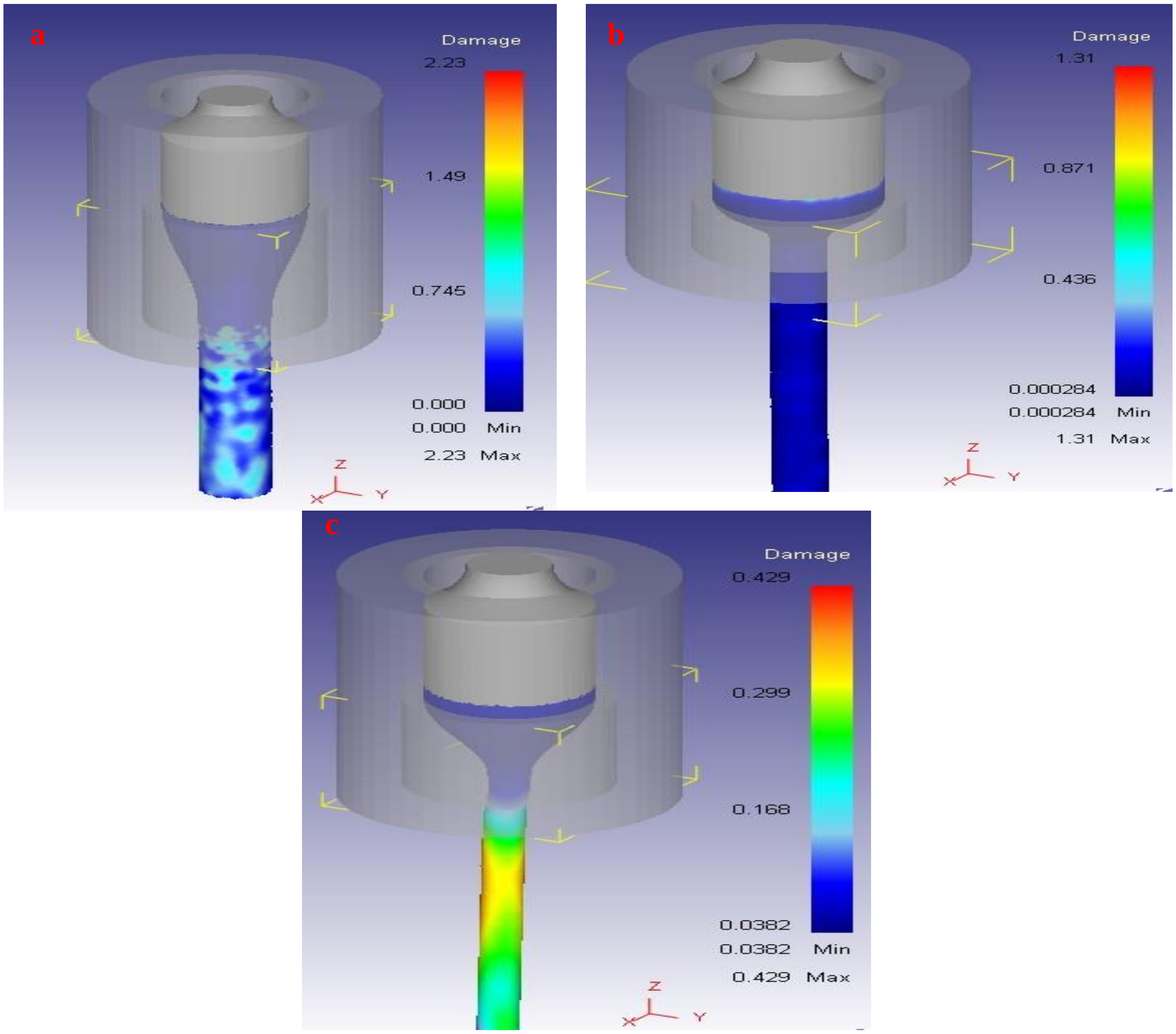

Figure 4-7 Damage distribution over surface of C60800 at ram speed of 3mm/s.(a) extrusion ratio of 2 (b) extrusion ratio of 3 (c) extrusion ratio of 4

4.3.5 Mathematical model for cosine die profile

The regression equation forecasts the relationship between the response (load, effective strain, and damage) and the input factors (extrusion ratio, ram speed, and die length).The equation represented in Equation (4.1), (4.2), (4.3) was obtained from the statistical software Minitab21.

$$\text{Load} = -309.6 + 231.6*X1 - 130.4*X2 + 17.54*X3 - 17.00*X1*X1 + 23.57*X2*X2 - .1951*X3*X3 + 17.40*X1*X2 - 3.909*X1*X3 \quad (4.\ 1)$$

$$\text{Effective strain} = .02817 + .003617*X1 + .02113*X2 - .001730*X3 + .002250*X1*X1 + .001367*X2*X2 - .000006*X3*X3 - .009033*X1*X2 + .000527*X1*X3 \quad (4.\ 2)$$

$$Damage = -0.9823 + .9365*X1 - .5352*X2 + .2863*X3 + .2448*X1*X1 + .3932*X2*X2 - .002932*X3*X3 - .5770*X1*X2 - .06767*X1*X3 \quad (4.3)$$

To confirm the accuracy of the regression model, a verification numerical simulation was performed using different parametric combinations not included in the Taguchi L9 design. The regression model's consistency was tested using two separate and random trial combinations. According to the results of the confirmation experiments in Table 4.8, the load, effective strain, and damage achieved in simulation differed considerably by a tiny margin from those anticipated using the regression model. The regression was validated for the cosine die profile type. All analyses had an error rate of less than 10%, showing that the constructed regression model accurately estimates load, effective strain, and damage for the numerical analysis provided ranges (Vijian & Arunachalam, 2007).

Table 4-8 Verification analysis

Cosine die profile						
S.No	Extrusion ratio	Ram speed	Die length	Regression load	Numerical load	Error
1	2	2	10	86.39	89.1	3.04%
2	3	3	20	247.95	249	0.42%
S.No	Extrusion ratio	Ram speed	Die length	Regression effective strain	Numerical effective strain	Error
1	2	2	10	0.0486	0.0473	2.67%
2	3	3	20	0.0483	0.0502	3.78%
S.No	Extrusion ratio	Ram speed	Die length	Regression damage	Numerical damage	Error
1	2	2	10	1.2807	1.28	0.55%
2	3	3	20	1.2636	1.25	1.0762%

4.4 Analysis of Numerical Simulation and Optimization for Linear Convergent Die Profile

The finite element model of the linear convergent die profile in the C60800 aluminum bronze alloy extrusion process DEFORM 3D forecasts this analysis in terms of load, damage, and effective strain based on process parameters such as extrusion ratio, ram speed, and die length. This process also maintains the same temperature of 800℃ for all L9 Taguchi combinations.

The relevant coefficients are computed using Minitab 21, a static software, and final models are created with these coefficients to estimate extrusion load, damage, and effective strain. Nine experiments are required for the three-factor and three-level L9 Taguchi orthogonal models.

4.4.1 Numerical simulation result for linear convergent die profile

The extrusion load, effective strain and damage was predicted using the DEFORM 3D V11 program. Table 4.9 shows simulation results of extrusion load, effective strain, damage by setting Taguchi's L9 design of the experiment.

Table 4-9 L9 linear convergent simulation result for (load, effective strain, damage)

S.No	Extrusion Ratio (X1)	Ram speed (X2)	Die length (X3)	Load (KN)	Strain effective	Damage
1	2	1	10	204.5	0.0438	1.37
2	2	2	20	304.15	0.0366	1.76
3	2	3	30	122.21	0.0374	2.25
4	3	1	20	285.97	0.0543	2.11
5	3	2	30	282.15	0.0444	1.16
6	3	3	10	163.46	0.12	1.21
7	4	1	30	201.6	0.054	2.57
8	4	2	10	194.13	0.0654	3.34
9	4	3	20	273.47	0.0634	2.18

4.4.2 Analysis of extrusion load

I. Analysis of SN ratio for load (linear convergent)

The statistical rule "smaller the better" has been used to assess and describe extrusion load. To compute the signal-noise ratio, use equation (3.18) Smaller is better.

Table 4-10 Signal to Noise Ratios for the load percentage (smaller the better)

Level	Extrusion ratio (X1)	Ram speed (X2)	Die length (X3)
1	-45.87	-47.14	-45.41
2	-47.47	-48.14	-49.18
3	-46.86	-44.92	-45.61
Delta	1.60	3.23	3.76
Rank	3	2	1

Table 4.10 displays delta statistics for extrusion load, which rank factors influencing responses based on S/N ratios obtained from the Taguchi orthogonal array. The delta statistics were computed by subtracting the highest and lowest average values for each factor. The highest delta value represents the most significant element impacting the die length. The die length has a rank of 1 and a delta value of 3.76, making it the most significant factor impacting the required load of the alloy during hot extrusion. Ram speed and extrusion ratio were placed second (3.23) and third (1.6), respectively.

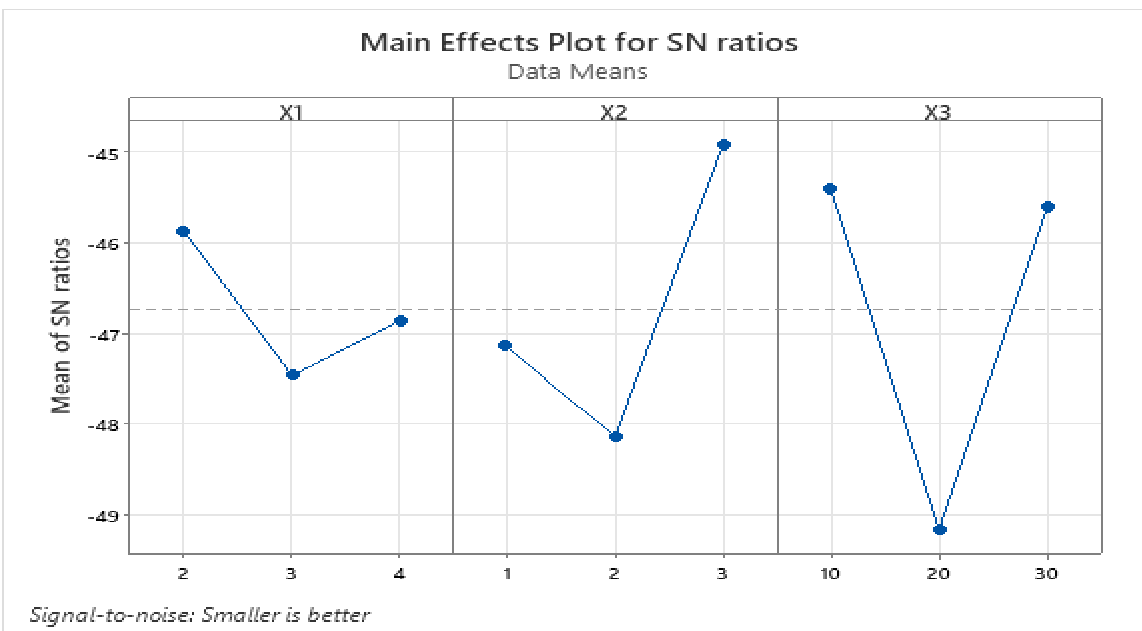

Figure 4-8 Main effect plot of for SN ratio for load

The best combination for extrusion load as shown in the above figure (smaller is better for extrusion load). Due to the fact that a higher SN ratio is preferable, it was chosen for investigation. The optimum possible combination of the variables at that level is shown by the numerical value of the maximum point on each graph in the S/N ratio. The above figure shows the optimum value at (**$X_1$2$X_2$3$X_3$10**) for extrusion ratio X1 at 2, ram speed at X2 at 3mm/s and die length X3 at 10mm.

II. Analysis of Variance extrusion load response (linear convergent)

ANOVA is used to determine key factors influencing aluminum bronze alloy percentage of contribution of extrusion ratio, ram speed and die length. Abbreviations: DF (degree of freedom), SS (squares), MSS (mean squares), and F (F-ratio).

Table 4-11 Analysis of Variance of extrusion load of aluminum bronze alloy

Source	DF	Seq SS	Adj SS	Adj MS	F	P	Percentage of contribution
X1	2	8.975	8.975	4.487	10.06	0.09	15.99
X2	2	16.384	16.384	8.192	18.37	0.052	29.2
X3	2	29.868	29.868	14.934	33.48	0.029	53.22
Error	2	0.893	0.893	0.446			
Total	8	56.120					

S	R-Sq	R-Sq(adj)
2.1184	98.4%	93.64%

Table 4.11 shows the results of the ANOVA findings for load. The analysis was performed with a 95% confidence and 5% significance. The table demonstrates that die length (53.22%) is the most significant factor in determining extrusion load, followed by ram speed (29.2%) and extrusion ratio (15.99%). The ANOVA table displays each factor's importance using F-values and P-values. A parameter's effect on a response variable is regarded as significant if its F-value is greater than the tabulated value. Die length ($P = .029 < .05$) considerably affects extrusion load. The regression model fits the data well, as evidenced by a higher-than-average R-squared value of 93.64%.

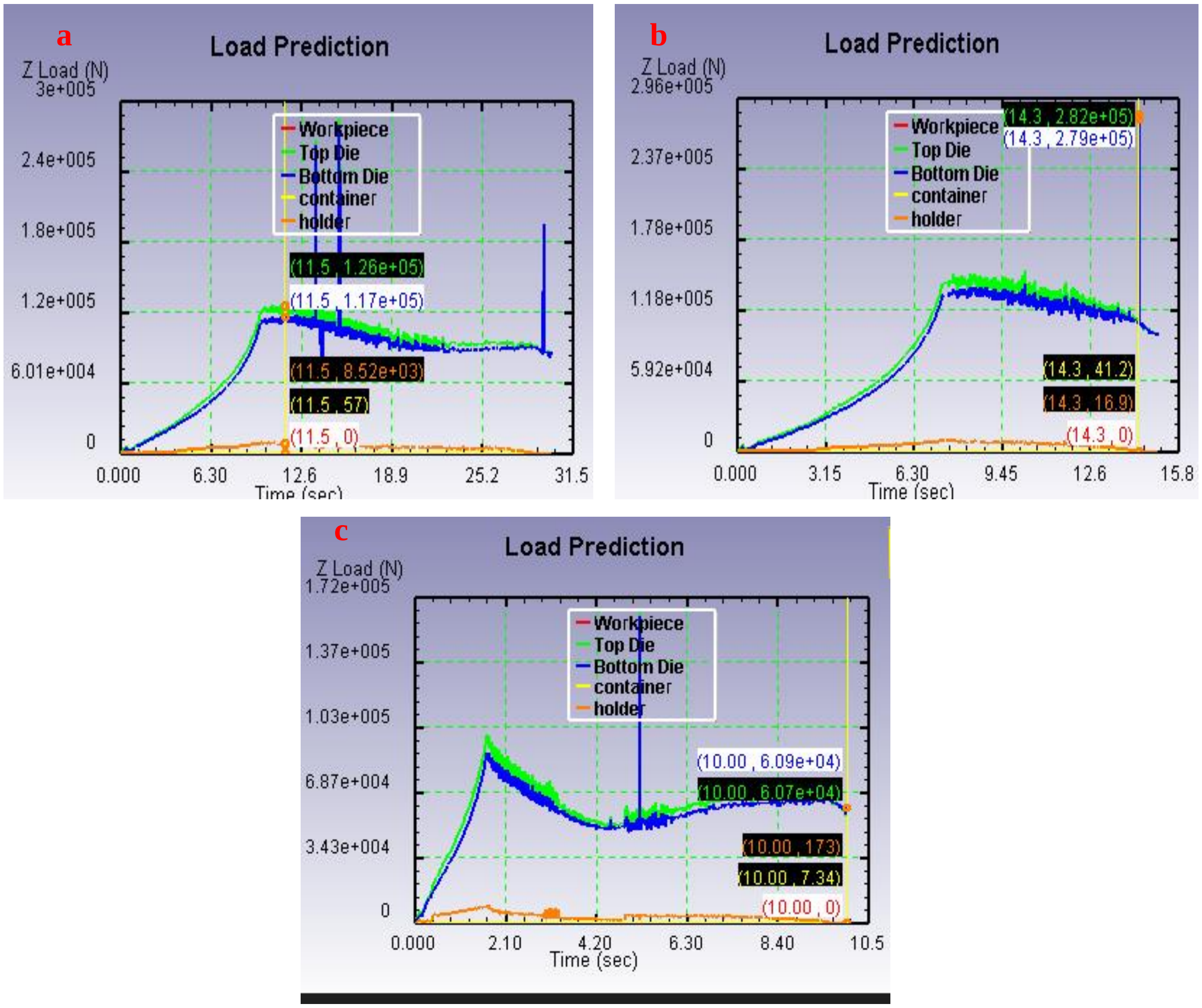

Figure 4-9 Extrusion load distribution over surface of C60800 at extrusion ratio of 3.(a) ram speed 1mm/s (b) ram speed 2mm/s (c) ram speed 3mm/s

The above figure 4.8 Demonstrates that as the ram speed of linear convergent die increases at extrusion ratio 3, the load required to extrude aluminum bronze alloy is minimized. According to ANOVA result as shown in the above table die length the prime impact on extrusion load, when moved to 10mm to 20mm extrusion load is increased but from 20mm to 30mm the extrusion load tends to be minimized.

4.4.3 Analysis of effective strain

I. Analysis of SN ratio for effective strain (linear convergent)

The statistical rule "smaller the better" has been used to assess and describe effective strain. To compute the signal-noise ratio, use equation (3.18) Smaller is better

Table 4-12 Signal to Noise Ratios for the effective strain percentage (smaller the better)

Level	**X1**	**X2**	**X3**
1	28.15	25.94	23.09
2	23.59	26.49	26.00
3	24.33	23.64	26.98
Delta	4.56	2.85	3.89
Rank	1	3	2

The table 4.12 displays the delta statistics of the S/N ratio for effective strain based on the characteristics impacting responses ranked by the Taguchi orthogonal array. Delta values were calculated by comparing the largest and lowest average values for every variable. The factor with the greatest impact on effective strain % has the greatest delta value and is ranked first. The analysis indicates that the extrusion ratio of extruded material, designated a rank 1 with a delta value of (4.56), was the primary factor determining the effective strain percentage of the aluminum bronze alloy. Die length and Ram speed were designated as second (3.89) and third (2.85), respectively.

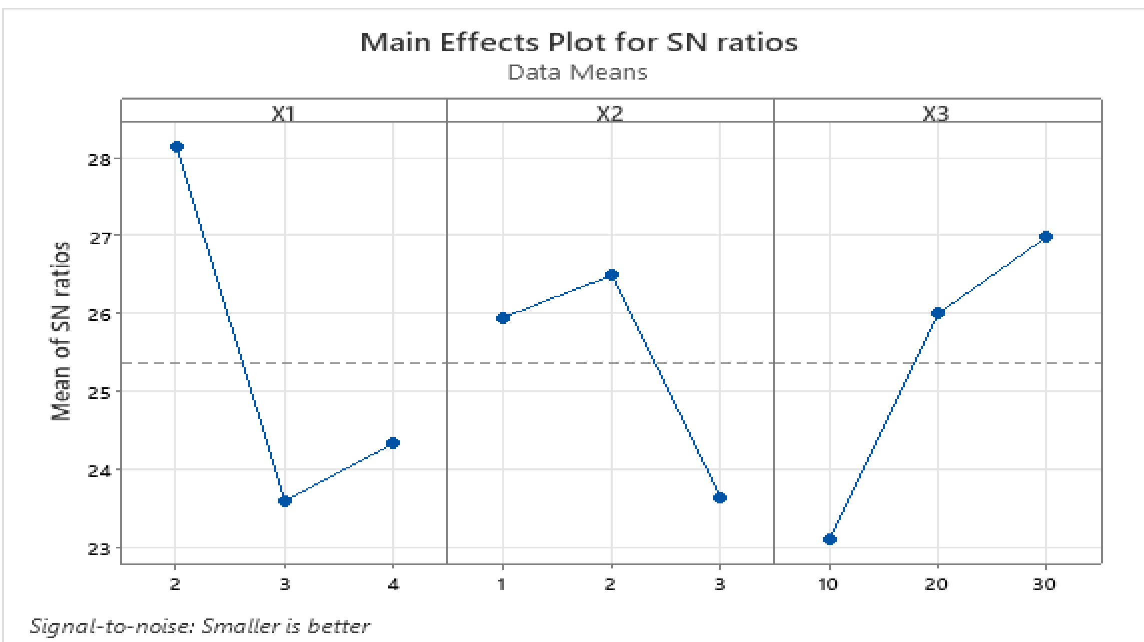

Figure 4-10 Main effect plot of for SN ratio for effective strain

Figure 4.9 indicates the best combination of extrusion parameters for minimal effective strain percentage (the smaller the better). The maximum point on each graph represents the optimal combination of parameters in the S/N ratio. The graph above shows the maximum point of SN ratio **($X_1$2$X_2$2$X_3$30)** for extrusion ratio X1 at 2, ram speed X2 at 2mm/s, and die length X3 at 30mm

II. Analysis of Variance effective strain response (linear convergent)

ANOVA is used to identify the primary variables of die length, ram speed, and extrusion ratio for aluminum bronze alloy. The following are abbreviations: F (F-ratio), DF (degree of freedom), SS (squares), and MSS (mean squares).

Table 4-13 Analysis of Variance effective strain of aluminum bronze alloy

Source	DF	Seq SS	Adj SS	Adj MS	F	P	Percentage of contribution
X1	2	41.869	41.869	20.935	92.63	0.011	51.94
X2	2	13.735	13.735	6.868	30.39	0.032	17.03
X3	2	24.550	24.550	12.275	54.31	0.018	30.46
Error	2	0.452	0.452	0.226			
Total	8	80.606					

S	R-Sq	R-Sq(adj)
1.7961	99.43%	97.76%

Table 4.13 shows the results of the ANOVA findings for effective strain. The analysis was performed with 95% confidence and 5% significance. The table demonstrates that extrusion ratio (51.94%) is the most significant factor in determining effective strain, followed by die length (30.46%) and ram speed (17.03%). The ANOVA table displays each factor's importance using F-values and P-values. A parameter's effect on a response variable is regarded as significant if its F-value is greater than the tabulated value. Extrusion ratio ($P = .011 < .05$) considerably affects the extrusion load. The regression model fits the data well, as evidenced by a higher-than-average R-squared value of 97.76%.

The below figure 4.10 Shows that as the extrusion ratio of linear convergent die profile increased, the effective strain of aluminum bronze alloy also increased. The above ANOVA table 4.13 also shows the extrusion ratio highest percentage of contribution on effective strain.

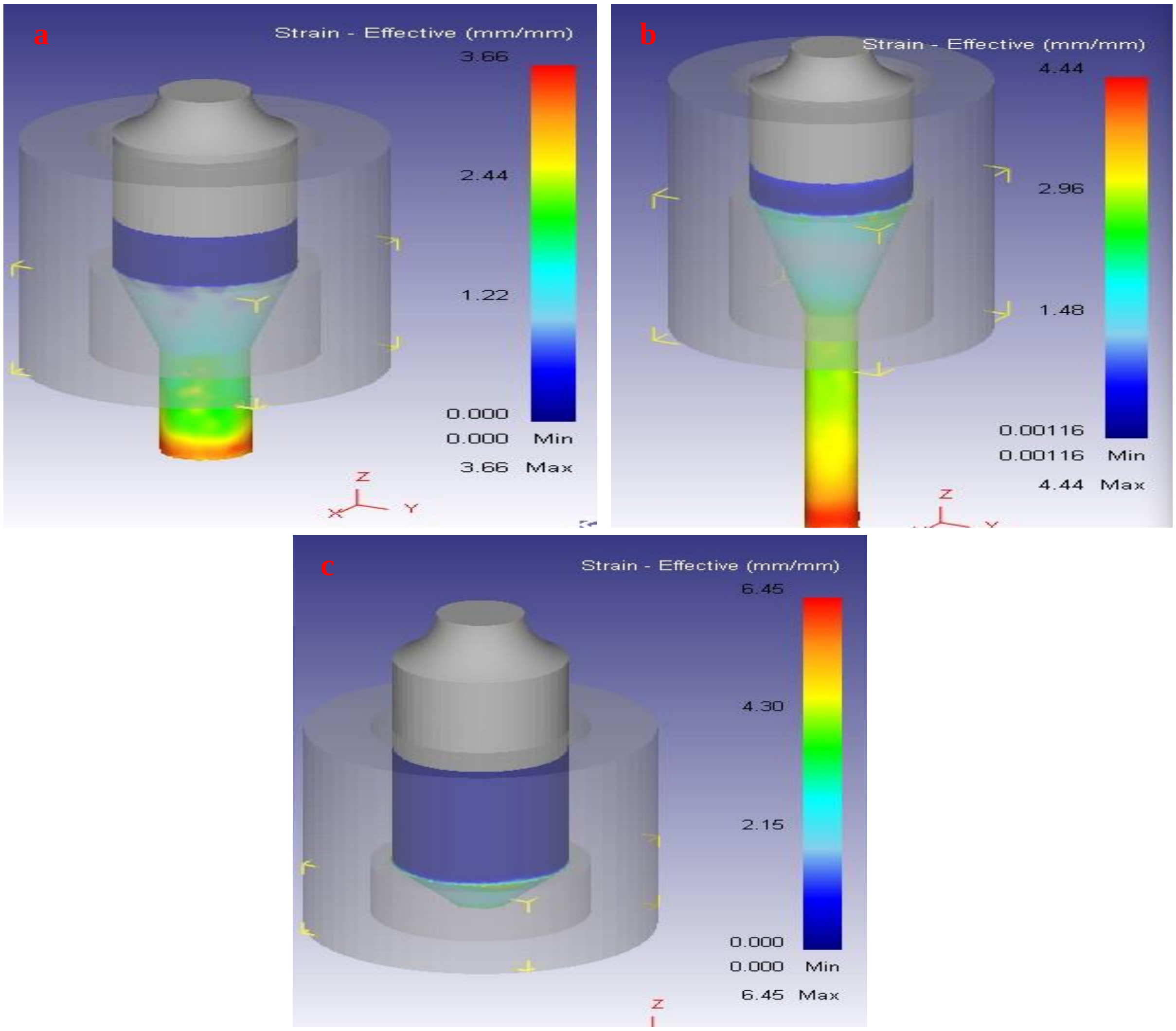

Figure 4-11 Effective strain distribution over surface of C60800 at ram speed of 2mm/s.(a) extrusion ratio of 2 (b) extrusion ratio of 3 (c) extrusion ratio of 4

4.4.4 Analysis of damage

I. Analysis of SN ratio for damage (linear convergent)

The statistical rule "smaller the better" has been used to assess and describe damage. To compute the signal-noise ratio, use equation (3.18). Smaller is better.

The table 4.14 shows the delta statistics of the S/N ratio for damage based on the Taguchi orthogonal array-ranked factors that influence responses. The delta values were obtained by comparing the greatest and lowest average values for every factor. The factor having the greatest impact on damage percentage has the highest delta value and is ranked first.

The research shows that the extrusion ratio of extruded material, classified as rank 1 with a delta value of 5.337, was the key factor determining the damage percentage of the aluminum bronze alloy. Ram speed is the third rank with value of (0.65) and die length were ranked second with value (1.1).

Table 4-14 Signal to Noise Ratios for the damage percentage (smaller the better)

Level	Extrusion ratio (X1)	Ram speed(X2)	Die length (X3)
1	-4.896	-5.806	-4.955
2	-3.144	-5.558	-6.055
3	-8.481	-5.156	-5.510
Delta	5.337	0.650	1.100
Rank	1	3	2

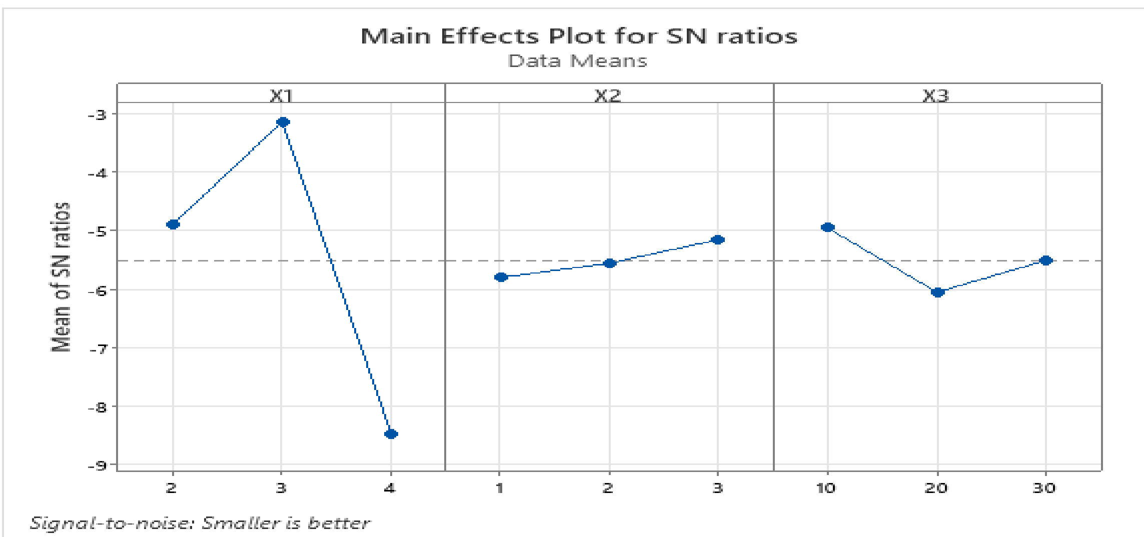

Figure 4-12 Main effect plot of for SN ratio for damage

Figure 4.11 shows the optimal combination of extrusion parameters for the lowest damage percentage (smaller is the better). Each graph's maximum point represents the best parameter combination in terms of the S/N ratio. The graph above depicts the highest SN ratio **($X_1 3 X_2 3 X_3 10$)** for extrusion ratio X1 = 3, ram speed X2 = 3 mm/s, and die length X3 = 10 mm.

II. Analysis of Variance damage response (linear convergent)

ANOVA is used to identify key factors influencing aluminum bronze alloy extrusion ratio, ram speed and die length. Abbreviations: DF (degree of freedom), SS (squares), MSS (mean squares), and F (F-ratio).

Table 4-15 Analysis of Variance for damage of aluminum bronze alloy

Source	DF	Seq SS	Adj SS	Adj MS	F	P	Percentage of contribution
X1	2	44.4103	44.4103	22.2051	68.77	0.014	57.3
X2	2	1.8150	1.8150	0.9075	2.81	0.262	2.34
X3	2	30.6323	30.6323	15.3162	47.43	0.021	39.52
Error	2	0.6457	0.6457	0.3229			
Total	8	77.5034					

S	R-Sq	R-Sq(adj)
3.9136	99.17%	96.67%

Table 4.15 displays the ANOVA findings for damage. The analysis was carried out with 95% confidence and 5% significance. The table demonstrates that the extrusion ratio (57.3%) is the most significant factor in determining the extrusion load, followed by die length (39.52%) and ram speed (2.34%). The ANOVA table displays each factor's importance using F-values and P-values. A parameter's effect on a response variable is regarded as significant if its F-value is greater than the tabulated value. The extrusion ratio (P = .014 < .05) significantly affects the extrusion load. The regression model fits the data well, as evidenced by a higher-than-average R-square value of 96.67%.

The below figure 4.12 Shows that as the extrusion ratio of linear convergent die profile increased, the damage of aluminum bronze alloy also increased at die length of 20mm. but in the case of die lengths of 10mm and 30mm the damage was not uniformly increased with extrusion ratio. The above ANOVA table 4.15 also shown as extrusion ratio is the highest percentage of contribution on damage.

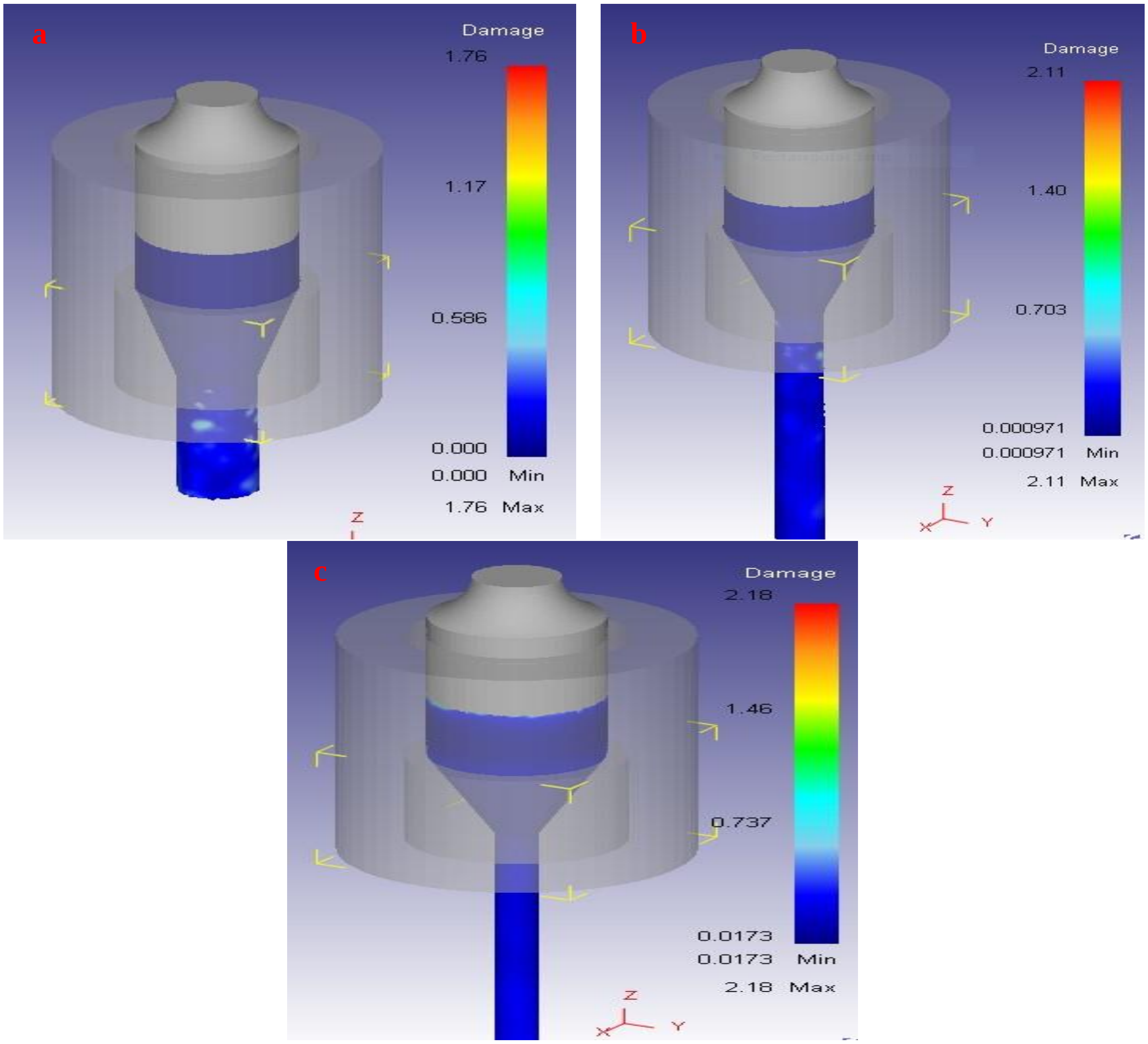

Figure 4-13 Damage distribution over surface of C60800 at die length of 20mm.(a) extrusion ratio of 2 (b) extrusion ratio of 3 (c) extrusion ratio of 4

4.4.5 Mathematical Model for linear convergent die

The regression equation predicts the relationship between the response (load, effective strain, and damage) and the input factors (extrusion ratio, ram speed, and die length). The equation represented in Equation (4.4), (4.5), (4.6), was obtained from the statistical software Minitab21.

$$\text{Load} = -196.6 + 64.28*X1 + 149.1*X2 + 26.77*X3 - 27.18*X1*X1 - 62.76*X2*X2 - .7804*X3*X3 + 30.30*X1*X2 + 2.230*X1*X3 \quad (4.\ 4)$$

$$\text{Effective strain} = .02893 + .01530*X1 - .02903*X2 + .001350*X3 - .000133*X1*X1 + .004433*X2*X2 - .000004*X3*X3 + .003000*X1*X2 - .000483*X1*X3 \quad (4.\ 5)$$

Damage = 2.203 - 2.065*X1 - .4850*X2 + .2718*X3 + .7517*X1*X1 + .2217*X2*X2 - .001717*X3*X3 - .2767*X1*X2 - .07200*X1*X3 (4. 6)

To confirm the accuracy of the developed regression model, a verification numerical simulation was run with many parametric combinations not found in the Taguchi L9 model. The regression model's consistency was assessed using two separate and random trial combinations. According to the results of the confirmation trials in Table 4.16, the load, effective strain, and damage obtained in simulation differed significantly by a small margin from those predicted by the regression model. The regression was confirmed using a linear convergent die. All studies had an error rate of less than 10%, indicating that the built-in regression model accurately predicts load, effective strain, and damage within the numerical analytical limits. (Vijian & Arunachalam, 2007).

Table 4-16 Verification analysis linear convergent die profile

S.No	Extrusion ratio	Ram speed	Die length	Regression load	Numerical load	Error
1	2	2	10	225.86	220.3	2.46%
2	3	3	20	263.82	257.6	2.36%
S.No	Extrusion ratio	Ram speed	Die length	Regression effective strain	Numerical effective strain	Error
1	2	2	10	0.0341	0.0356	4.2%
2	3	3	20	0.0499	0.0481	3.6%
S.No	Extrusion ratio	Ram speed	Die length	Regression damage	Numerical damage	Error
1	2	2	10	0.9961	1.028	3.7%
2	3	3	20	1.2525	1.3	3.6%

4.5 Analysis of Numerical Simulation and Optimization for Streamline Die Profile

The DEFORM 3D finite element model of the streamline die profile in the C60800 aluminum bronze alloy extrusion process estimates this analysis in terms of load, damage, and effective strain using process factors such as extrusion ratio, ram speed, and die length as inputs. For all L9 Taguchi combinations, the procedure maintains a constant temperature of 800℃.

Using Minitab 21, A statical software, the significant coefficients are determined and final models developed incorporating these coefficients to estimate extrusion load, damage and effective strain. For three factor and three level L9 Taguchi orthogonal of nine experiments need to be performed.

4.5.1 Numerical simulation result for streamline die profile

The extrusion load, effective strain and damage was predicted using the DEFORM 3D V11 program. Table 4.17 shows simulation results of extrusion load, effective strain, damage by setting Taguchi's L9 design of the experiment.

Table 4-17 L9 Streamline simulation result for (load, effective strain, damage)

S.No	Extrusion ratio (X1)	Ram speed (X1)	Die length (X2)	Load (KN)	Strain effective	Damage
1	2	1	10	90.512	0.0453	1.84
2	2	2	20	251.96	0.0543	2.29
3	2	3	30	127.37	0.047	2.34
4	3	1	20	137.69	0.0595	2.24
5	3	2	30	381.98	0.0534	1.47
6	3	3	10	457.14	0.0418	1.5
7	4	1	30	173.97	0.0674	1.79
8	4	2	10	188.88	0.0617	2.83
9	4	3	20	312.54	0.0666	2.85

4.5.2 Analysis of extrusion load

I. Analysis of SN ratio for extrusion load (streamline)

The statistical rule "smaller the better" has been used to assess and describe extrusion load. To compute the signal-noise ratio, use equation (3.18) Smaller is better.

Table 4.18 displays delta statistics for extrusion load, which rank factors influencing responses based on S/N ratios obtained from the Taguchi orthogonal array. The delta statistics were calculated by subtracting the largest and lowest average values from each factor. The largest delta value represents the most significant variable influencing the extrusion load.

The ram speed has a rank of 1 and a delta value of (6.16), making it the most significant factor impacting the required extrusion load of the alloy during hot extrusion. Extrusion ratio and die length were placed second (6.12) and third (0.95), respectively.

Table 4-18 Signal to Noise Ratios for the load percentage (smaller the better)

Level	Extrusion ratio (X1)	Ram speed (X2)	Die length (X3)
1	-43.09	-42.24	-45.95
2	-49.21	-48.40	-46.90
3	-46.74	-48.40	-46.18
Delta	6.12	6.16	0.95
Rank	2	1	3

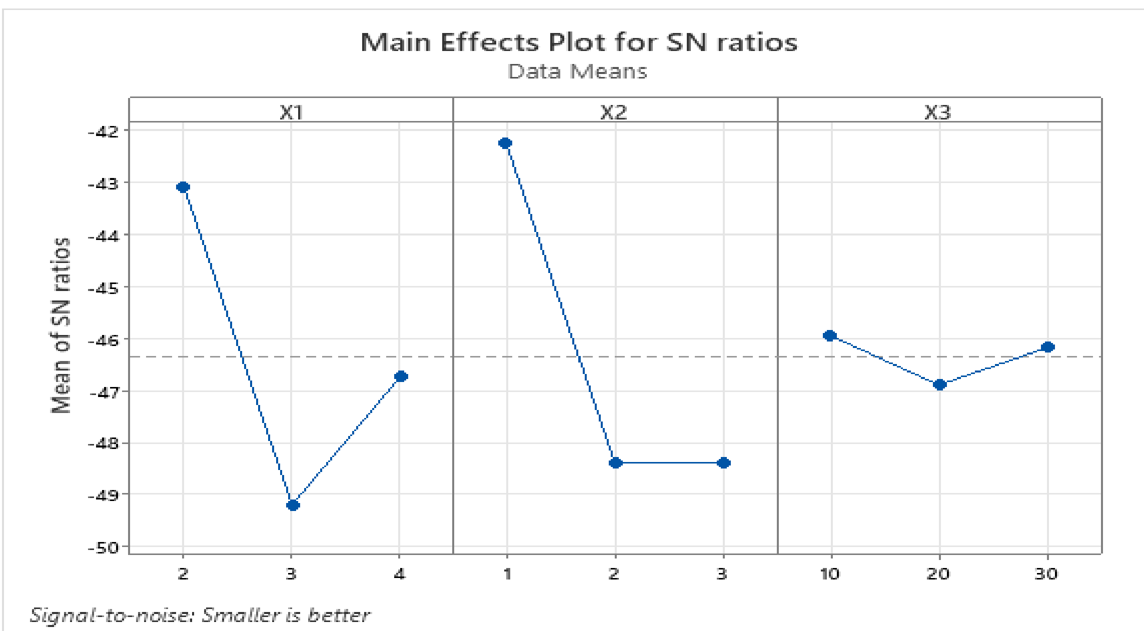

Figure 4-14 Main effect plot of for SN ratio for load

The best combination for extrusion load as shown in the above figure (smaller is better for extrusion load). Due to the fact that a higher SN ratio is preferable, it was chosen for investigation. In the S/N ratio, the numerical value of the maximum point in each graph indicates the best optimal combination of the factors at that level. The above figure shows the optimum value was **($X_1$2$X_2$1$X_3$10)** for extrusion ratio X1 at 2, ram speed at X2 at 1mm/s and die length X3 at 10mm.

II. Analysis of Variance for extrusion load response (streamline)

ANOVA is used to determine key factors influencing aluminum bronze alloy extrusion percentage of contribution extrusion ratio, ram speed and die length. Abbreviations: DF (degree of freedom), SS (squares), MSS (mean squares), and F (F-ratio).

Table 4-19 Analysis of Variance for effective strain response

Source	DF	Seq SS	Adj SS	Adj MS	F	P	Percentage of contribution
X1	2	56.880	56.880	28.4401	38.79	0.025	32.27
X2	2	75.843	75.843	37.9216	51.73	0.019	43.03
X3	2	42.074	42.074	21.0370	28.69	0.034	28.87
Error	2	1.466	1.466	0.7331			
Total	8	176.263					

S	R-Sq	R-Sq(adj)
4.5866	99.16%	96.67%

Table 4.19 shows the ANOVA results of load. The analysis was conducted with 95% confidence and 5% significance. The table shows that the ram speed is the most significant factor (43.03%) in determining the extrusion load, followed by extrusion ratio and die length. The ANOVA table uses F-values and P-values to show the significance of each factor. The regression model fits the data well, as indicated by a higher-than-normal R-square value of 96.67%.

The below figure 4.14 Displayed that at extrusion ratio 2 of streamline die profile as the ram speed increased from 1mm/s to 2mm/s, the load required to extrude aluminum bronze alloy is increased but when the ram speed shift from 2mm/s to 3mm/s the extrusion load is decreased. The above ANOVA table 4.19 is also shown as the ram speed highest significance on load percentage of distribution.

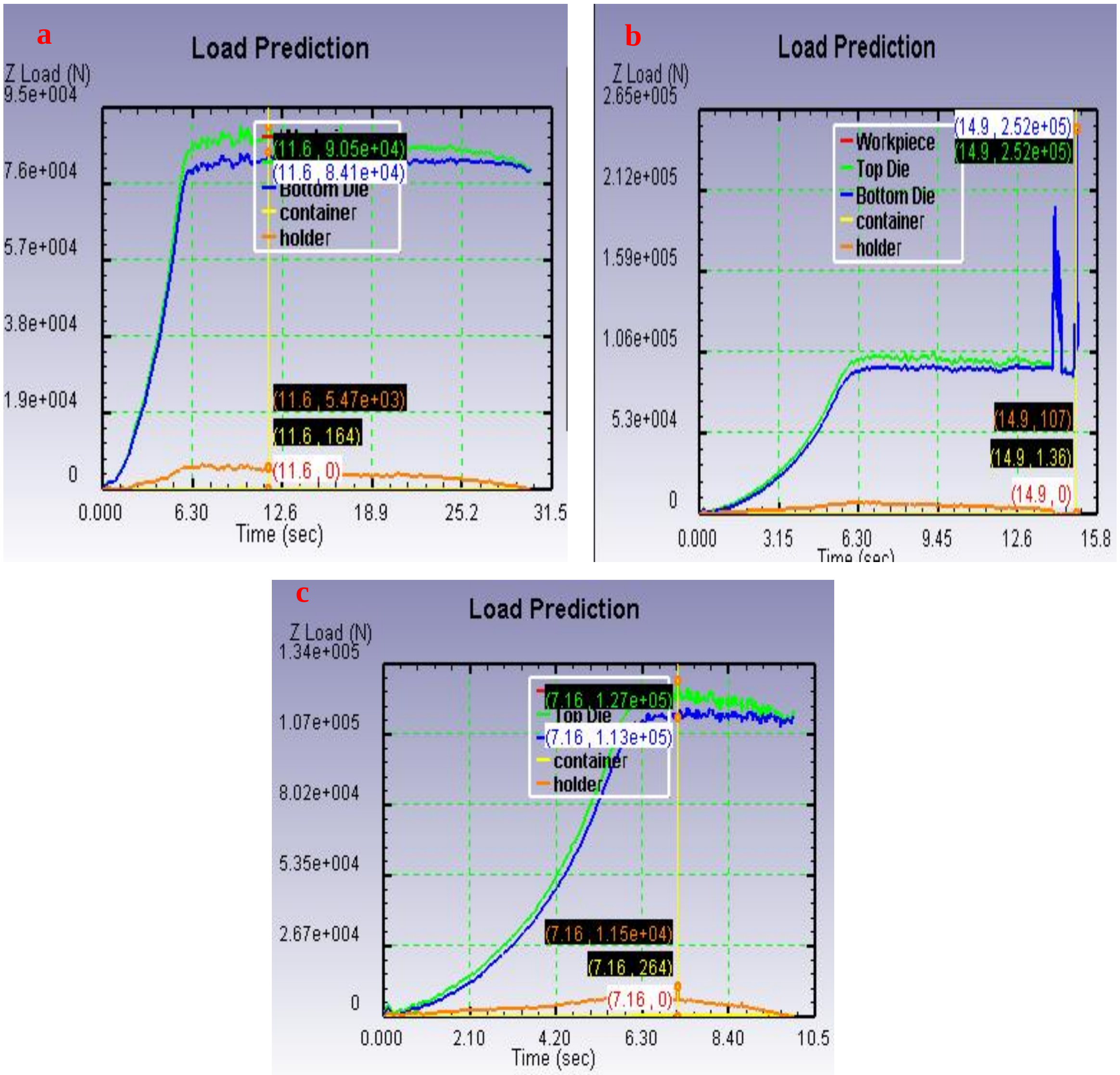

Figure 4-15 Extrusion load distribution over surface of C60800 at extrusion ratio 2. (a) ram speed 1mm/s (b) ram speed 2mm/s (c) ram speed 3mm/s

4.5.3 Analysis of effective strain

I. Analysis of SN ratio for effective strain (streamline)

The statistical rule "smaller the better" has been used to assess and describe effective strain. To compute the signal-noise ratio, use equation (3.18) Smaller is better

The table 4.20 displays the delta statistics of the S/N ratio for effective strain based on the characteristics impacting responses ranked by the Taguchi orthogonal array. Delta data were calculated by comparing the largest and lowest average values for each variable. The factor with the greatest impact on effective strain percentage has the largest delta value and is ranked first. The analysis indicates that the extrusion ratio of extruded material, designated a rank 1 with a delta value of (2.53), was the primary factor determining the effective strain percentage of the aluminum bronze alloy. Die length and Ram speed were designated as second (1.77) and third (0.95), respectively.

Table 4-20 Signal to Noise Ratios for the effective strain percentage (smaller the better)

Level	Extrusion ratio (X1)	Ram speed (X2)	Die length (X3)
1	26.25	24.94	26.22
2	25.85	24.98	24.45
3	23.72	25.89	25.14
Delta	2.53	0.95	1.77
Rank	1	3	2

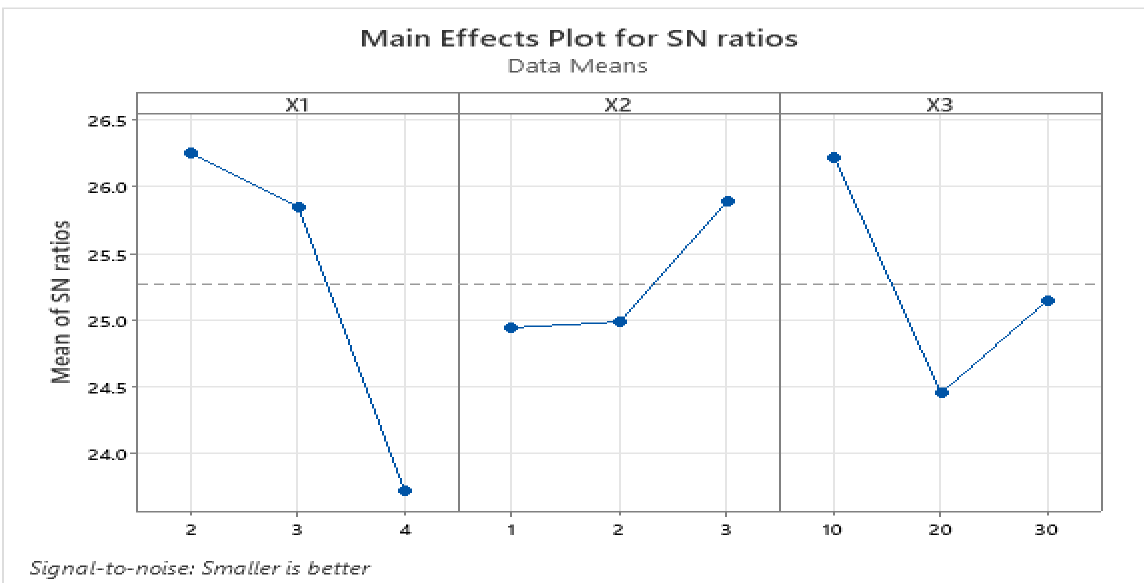

Figure 4-16 Main effect plot of for SN ratio for effective strain

Figure 4.15 indicates the best combination of extrusion parameters for minimal effective strain percentage (the smaller the better). The maximum point on each graph represents the optimal combination of parameters in the S/N ratio. The graph above shows the maximum point of SN ratio **($X_1$2$X_2$3$X_3$10)** at extrusion ratio X1 at 2, ram speed X2 at 3mm/s, and die length X3 at 10mm.

II. Analysis of Variance for effective strain response (streamline)

ANOVA is used to identify key factors influencing aluminum bronze alloy extrusion ratio, ram speed and die length. Abbreviations: DF (degree of freedom), SS (squares), MSS (mean squares), and F (F-ratio).

Table 4-21 Analysis of Variance for effective strain response

Source	DF	Seq SS	Adj SS	Adj MS	F	P	Percentage of contribution
X1	2	11.0875	11.0875	5.54377	60.49	0.016	62.44
X2	2	1.7254	1.7254	0.86269	9.41	0.096	9.72
X3	2	4.7602	4.7602	2.38008	25.97	0.037	26.8
Error	2	0.1833	0.1833	0.09164			
Total	8	17.7564					

S	R-Sq	R-Sq(adj)
0.3027	98.97%	95.87%

Table 4.21 displays the ANOVA findings for the effective strain. The analysis was performed with 95% confidence and 5% significance. The table reveals that the extrusion ratio is the most significant variable (62.44%) in calculating the extrusion load, followed by die length and ram speed. The F-values and P-values in the ANOVA table indicate the significance of each component. A parameter's effect on a response variable is regarded as significant when its F-value exceeds the tabulated value. The extrusion ratio ($P = .016 < .05$) has a substantial impact on effective strain. The regression model fits the data well, with an R-square value of 95.87%, which is higher than normal.

The below figure 4.16 demonstrates that as the extrusion ratio of streamline die profile increases from 2 to 3, the effective strain of aluminum bronze alloy is decreased but when moved from extrusion ratio of 3 to 4 the effective strain is increased. The above ANOVA table 4.21 also shown as extrusion ratio is highest percentage of contribution in effective strain.

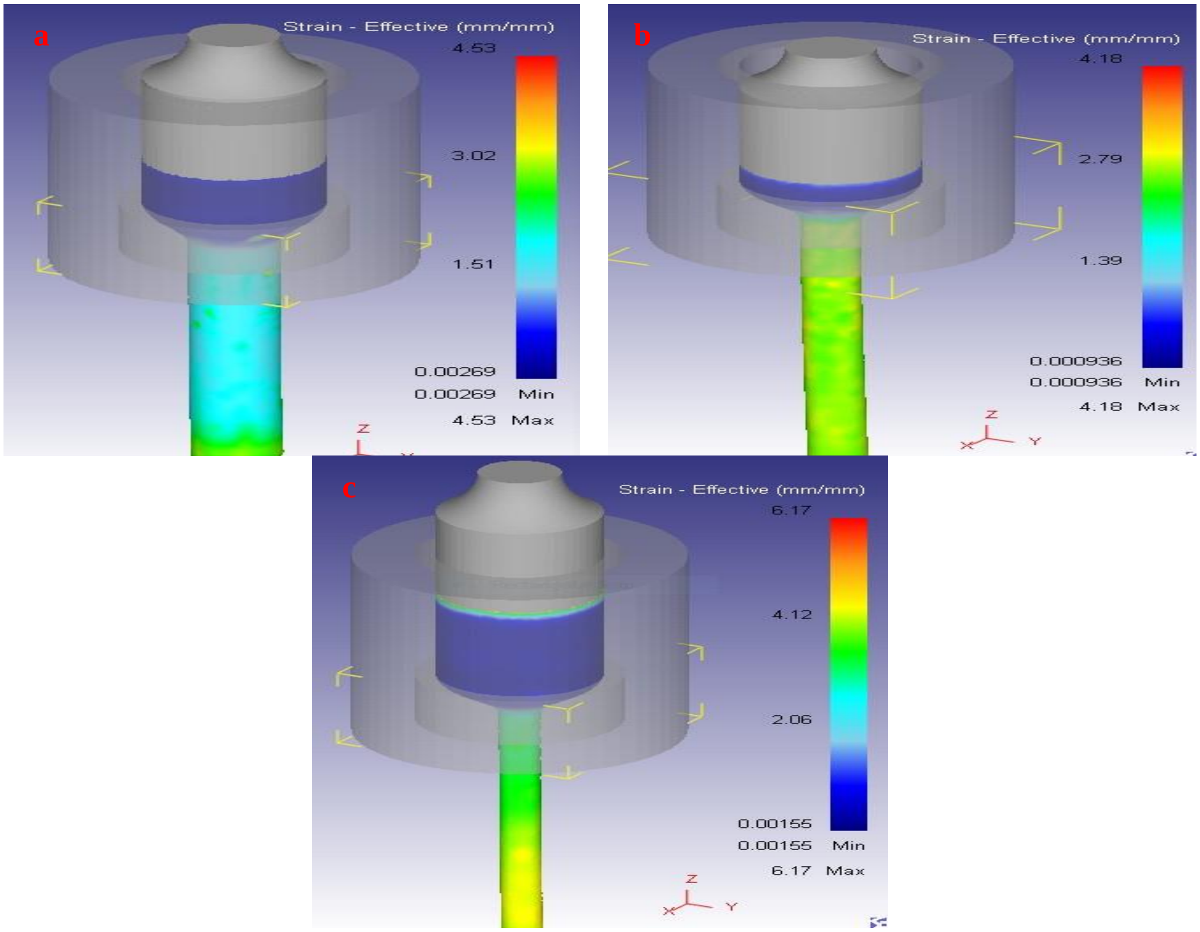

Figure 4-17 Effective strain distribution over surface of C60800 at die length of 10mm.(a) extrusion ratio of 2 (b) extrusion ratio of 3 (c) extrusion ratio of 4

4.5.4 Analysis of damage

I. Analysis of SN ratio for damage (streamline)

The statistical rule "smaller the better" has been used to assess and describe damage. To compute the signal-noise ratio, use equation (3.18). Smaller is better.

Table 4-22 Signal to Noise Ratios for the damage percentage (smaller the better)

Level	Extrusion ratio (X1)	Ram speed (X2)	Die length (X3)
1	-6.626	-5.786	-5.951
2	-4.624	-6.526	-7.766
3	-7.730	-6.668	-5.263
Delta	3.106	0.882	2.504
Rank	1	3	2

The table 4.22 shows the delta statistics of the S/N ratio for damage based on the Taguchi orthogonal array-ranked factors that influence responses. Delta values were obtained by comparing the greatest and lowest average values for each factor. The factor with the highest influence on the damage percentage has the highest delta value and is ranked first. The table shows that the extrusion ratio of extruded material, classified as rank 1 with a delta value of 3.106, was the key factor determining the damage percentage of the aluminum bronze alloy. Ram speed is the third rank with value of .882 and die length was ranked at second (2.504).

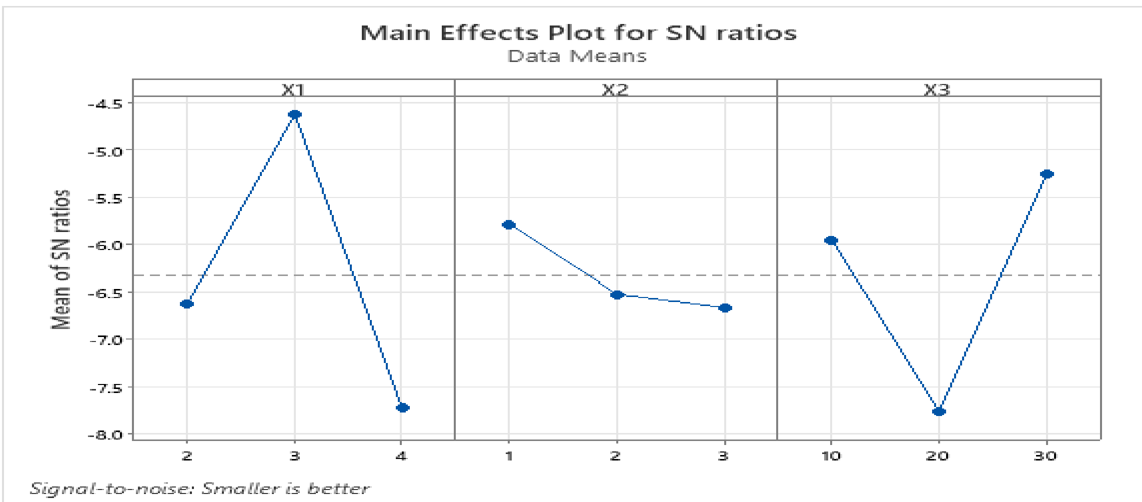

Figure 4-18 Main effect plot of for SN ratio for damage

Figure 4.17 shows the optimal combination of extrusion parameters for the lowest damage percentage (smaller is the better). Each graph's maximum point represents the best parameter combination in terms of the S/N ratio. The graph above depicts the highest SN ratio of optimum value at **($X_1$3$X_2$1$X_3$30)** for extrusion ratio X1 = 3, ram speed X2 = 1 mm/s, and die length X3 = 30 mm in the combination of.

II. Analysis of Variance for damage response (streamline)

ANOVA is used to identify key factors influencing aluminum bronze alloy extrusion ratio, ram speed and die length. Abbreviations: DF (degree of freedom), SS (squares), MSS (mean squares), and F (F-ratio).

Table 4-23 Analysis of Variance for damage response

Source	DF	Seq SS	Adj SS	Adj MS	F	P	Percentage of contribution
X1	2	25.851	25.851	12.925	19.22	0.049	70.3
X2	2	1.036	1.036	0.518	0.77	0.565	.028
X3	2	10.522	10.522	5.2608	7.82	0.113	28.61
Error	2	1.345	1.345	0.6725			
Total	8	36.772					

S	R-Sq	R-Sq(adj)
2.2936	96.34%	85.37%

Table 4.23 shows the ANOVA findings for damage. The analysis was carried out with 95% confidence and 5% significance. The table demonstrates that the extrusion ratio (40.43%) is the most significant factor in determining damage, followed by die length and ram speed. The ANOVA table displays each factor's importance using F-values and P-values. A parameter's effect on a response variable is considered significant if its F-value is greater than the tabulated value. The regression model fits the data well, as evidenced by a higher-than-normal R-square value of 85.37%.

The below figure 4.18 Shown that as the extrusion ratio of streamline die profile increased in 30mm die length from extrusion ratio of 2 to 3, the damage of aluminum bronze alloy decreased. But when it moved from extrusion ratio of 3 to 4 the amount of damage increased with smaller range. The above ANOVA table 4.23 result also demonstrates extrusion ratio highest percentage of contribution on damage.

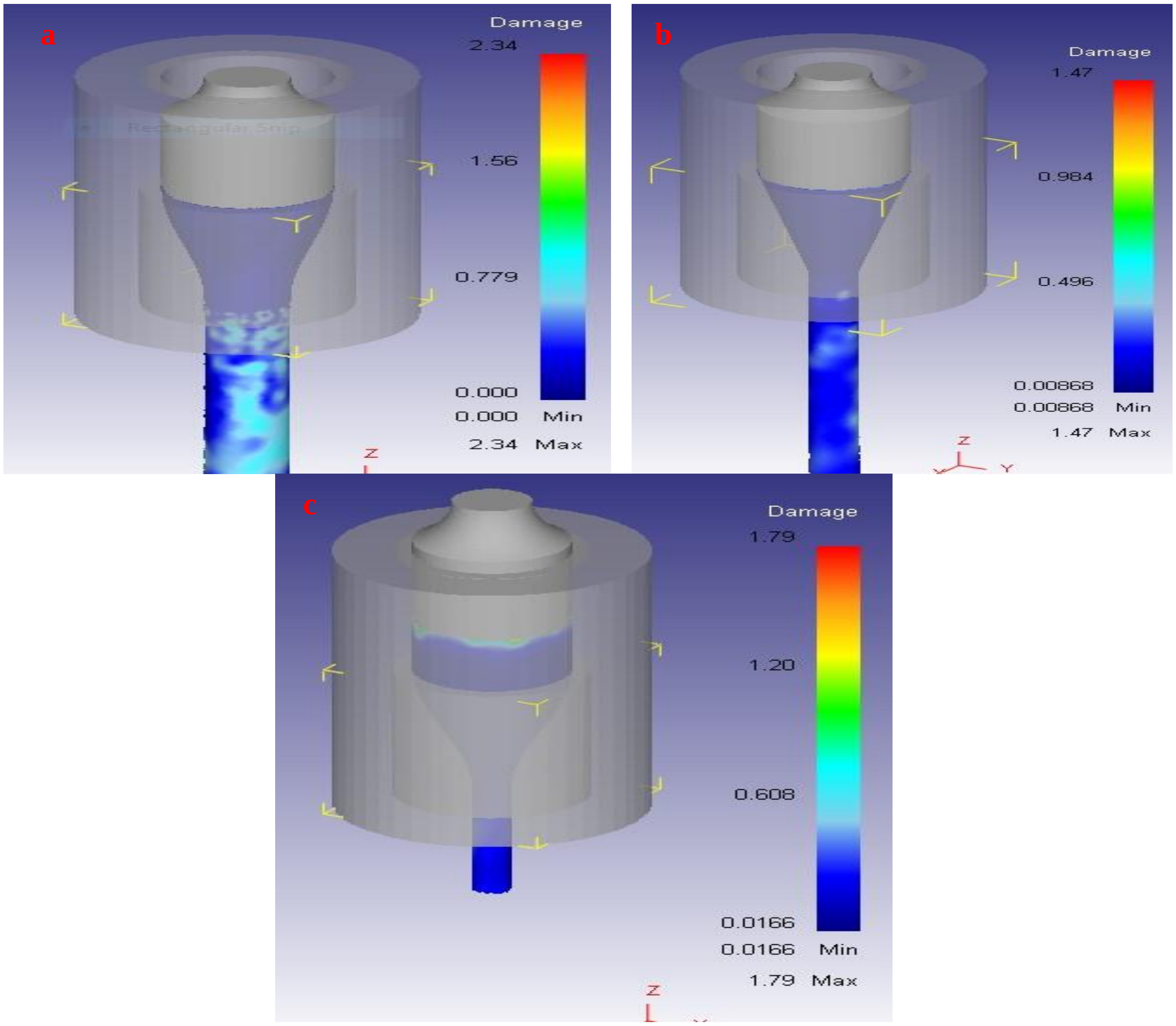

Figure 4-19 Damage distribution over surface of C60800 at die length of 30mm.(a) extrusion ratio of 2 (b) extrusion ratio of 3 (c) extrusion ratio of 4

4.5.5 Mathematical model for streamline die profile

The regression equation predicts the relationship between the input variables (extrusion ratio, ram speed and die length) and response (load, effective strain, damage). The equation represented in Equation (4.7), (4.8), (4.9) was obtained from the statistical software Minitab21.

$$\text{Load} = -832.9 + 403.1*X1 + 692.2*X2 - 24.71*X3 - 82.56*X1*X1 - 148.1*X2*X2 + .05072*X3*X3 + .6540*X1*X2 + 7.204*X1*X3 \quad (4.\,7)$$

$$\text{Effective strain} = .04363 - .02278*X1 - .001050*X2 + .003643*X3 + .005483*X1*X1 - .001083*X2*X2 - .000071*X3*X3 + .000600*X1*X2 - .000157*X1*X3 \quad (4.\,8)$$

$$\text{Damage} = 3.683 - 2.520*X1 - 1.555*X2 + .3438*X3 + .5867*X1*X1 + .2017*X2*X2 - .004017*X3*X3 + .1933*X1*X2 - .06100*X1*X3 \quad (4.9)$$

To confirm the accuracy of the regression model, a verification numerical simulation was performed using different parametric combinations not included in the Taguchi L9 design. The regression model's consistency was tested using two separate and random trial combinations. According to the results of the confirmation experiments in Table 4.24, the load, effective strain, and damage achieved in simulation differed considerably by a tiny margin from those anticipated using the regression model. Regression validity was tested for the streamline die profile. All analyses had an error rate of less than 10%, showing that the constructed regression model accurately estimates load, effective strain, and damage for the numerical analysis provided ranges (Vijian & Arunachalam, 2007).

Table 4-24 Verification analysis of streamline die profile

S.No	Extrusion ratio	Ram speed	Die length	Regression load	Numerical load	Error
1	2	2	10	339.7	323.5	4.7%
2	3	3	20	341.27	333.56	2.27%
S.No	Extrusion ratio	Ram speed	Die length	Regression effective strain	Numerical effective strain	Error
1	2	2	10	0.0422	0.0435	2.98%
2	3	3	20	0.0522	0.052	0.38%
S.No	Extrusion ratio	Ram speed	Die length	Regression damage	Numerical damage	Error
1	2	2	10	1.2761	1.29	1.08%
2	3	3	20	1.9025	1.86	2.23%

4.6 Multi-Response Optimization by Using Taguchi Based GA method

Multi-response optimization issues in complex production systems are difficult to tackle with standard technologies (Singh et al., 2021). This study utilized the Genetic Algorithm (GA), a type of random-based evolutionary algorithm, to determine the optimal input parameter combination for optimal output outcomes. In this optimization, X1 refers to extrusion ratio, X2 is ram speed, and X3 is the die length. Using regression analysis in Minitab 21, three equations were developed to determine extrusion load (1), effective strain (2), and damage (3) for all die profile type as shown in the above equation 4.1-4.9.

These possible combinations were used to determine the common combination of input parameters that resulted in the minimum output, and the genetic algorithm was used as a multi-objective optimization. Equation (4.10-4.12) was utilized to calculate multi-objective optimization using the weight set formula. Multi objective optimization after the combination of w1, w2 and w3 are objective functions with a weighted pattern of w1 + w2 + w3 = 1. The responses produced by numerical analysis (load, effective strain and damage) can be assigned equal value weight (1/3,1/3,1/3). The minimum load is required to reduce die wear, tear and improve surface finish. The minimum effective strain is required to improve fatigue resistance and material properties. A minimum amount of damage is required to improve durability and safety.

For cosine die profile

$$\text{Multi objective } Z_{min} = \mathbf{W_1}*(-309.6 + 231.6*X1 - 130.4*X2 + 17.54*X3 - 17.00*X1*X1 + 23.57*X2*X2 - .1951*X3*X3 + 17.40*X1*X2 - 3.909*X1*X3) + \mathbf{W_2}*(.02817 + .003617*X1 + .02113*X2 - .001730*X3 + .002250*X1*X1 + .001367*X2*X2 - .000006*X3*X3 - .009033*X1*X2 + .000527*X1*X3) + \mathbf{W_3}*(-0.9823 + .9365*X1 - .5352*X2 + .2863*X3 + .2448*X1*X1 + .3932*X2*X2 - .002932*X3*X3 - .5770*X1*X2 - .06767*X1*X3) \quad (4.10)$$

For linear convergent die profile

$$\text{Multi objective } Z_{min} = \mathbf{W_1}*(-196.6 + 64.28*X1 + 149.1*X2 + 26.77*X3 - 27.18*X1*X1 - 62.76*X2*X2 - .7804*X3*X3 + 30.30*X1*X2 + 2.230*X1*X3) + \mathbf{W_2}*(0.02893 + .01530*X1 - .02903*X2 + .001350*X3 - .000133*X1*X1 + .004433*X2*X2 - .000004*X3*X3 + .003000*X1*X2 - .000483*X1*X3) + \mathbf{W_3}*(2.203 - 2.065*X1 - .4850*X2 + .2718*X3 + .7517*X1*X1 + .2217*X2*X2 - .001717*X3*X3 - .2767*X1*X2 - .07200*X1*X3) \quad (4.11)$$

For streamline die profile

Multi objective Z_{min} = **W_1***(-832.9 + 403.1*X1 + 692.2*X2 - 24.71*X3 - 82.56*X1*X1 – 148.1*X2*X2 + .05072*X3*X3 + .6540*X1*X2 + 7.204*X1*X3) + **W_2***(0.04363 - .02278*X1 - .001050*X2 + .003643*X3 + .005483*X1*X1 - .001083*X2*X2 - .000071*X3*X3 + .000600*X1*X2 - .000157*X1*X3) + **W_3***(3.683 - 2.520*X1 - 1.555*X2 + .3438*X3 + .5867*X1*X1 + .2017*X2*X2 - .004017*X3*X3 + .1933*X1*X2 - .06100*X1*X3) (4.12)

The GA was run in MATLAB R2018b to further improve the extrusion load, effective strain and damage result. The population and generation sizes were 50 and 100, respectively. To get the best result, the fitness function was converted into a minimization problem in MATLAB. The upper and lower boundaries were determined using the levels of each process parameter. Demography was chosen as a double-vector type of population. The constraint dependent's creation function has been set.

Table 4-25 GA setting

Parametric function	parametric value
Population size	50
Population type	double vector
Creation function	constraint dependent
Fitness scaling function	Rank
Selection function	Roulette
Reproduction: elite count	default (0.05*population size)
Reproduction: crossover fraction	default: .8
Mutation function	uniform rate: .1
Number generation	100
Function tolerance	$1*10^6$
Constraint tolerance	$1*10^6$
Lower bound	[2, 1, 10]
Upper bound	[4, 3, 30]

4.6.1 GA multi response optimization of cosine die profile

The most precise common combination of input parameters that give minimum output was predicted by a genetic algorithm for cosine die profile multi response optimization. Equation (4.10) was used to find out the multi objective optimization according to the weight set formula. By using equation (4.10) minimum output results have been obtained by using an input parameter combination of 2 (extrusion ratio), 2.045mm/s (ram speed) and 10mm (die length).

The best and mean fitness values were found as 22.5678 and 23.055, as illustrated in figure 4.19.

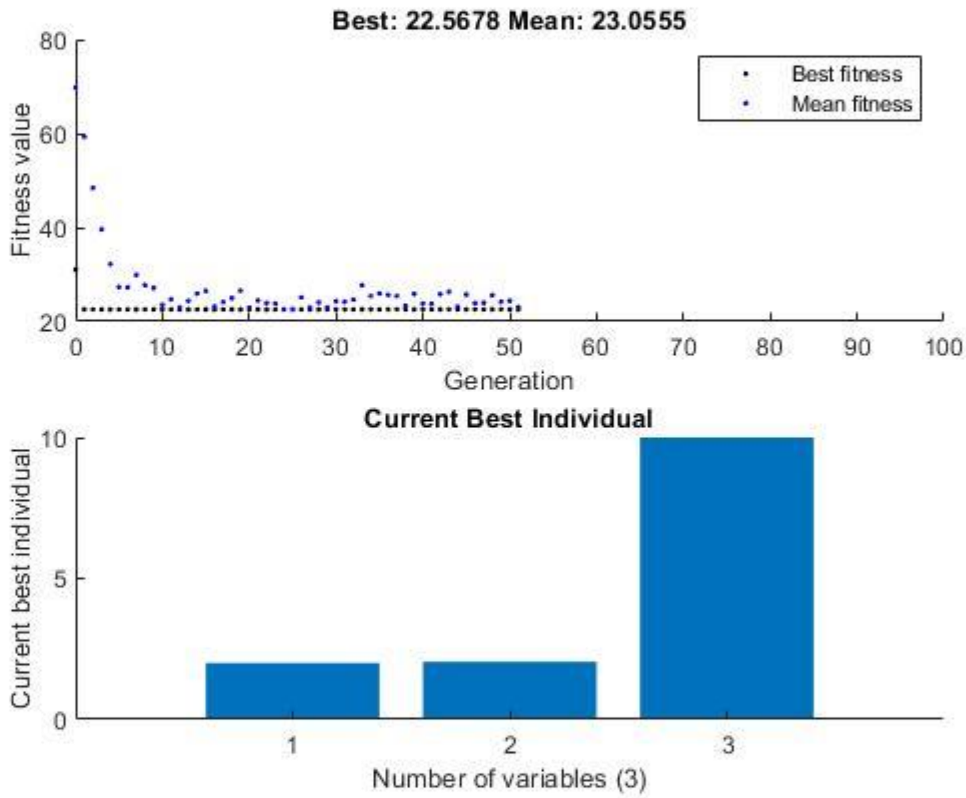

Figure 4-20 GA optimization multi response graph of cosine dies

Table 4-26 GA predicted best individual of multi response optimization results for cosine die

Optimization	Response	Extrusion ratio (X1)	Ram speed (X2)	Die length (X3)	Objective function value
Multi response	Zmin	2	2.045	10	22.5682

4.6.2 Confirmation analysis of GA optimum value for cosine die

The final step is to validate the performance improvement using the optimum parameter values of GA (extrusion ratio, ram speed, and die length at 2, 2.045mm/s and 10mm respectively). Figure 4.20 shows that the numerical simulation result of the multi-response cosine die profile at the optimum value of GA was predicted. The output responses at optimum value (extrusion load, effective strain, and damage of 84 KN, .0438 and .801 respectively). The responses from the simulation result indicate that the GA was obtained to have the lowest value compared to the result performed in the Taguchi design parameter combination.

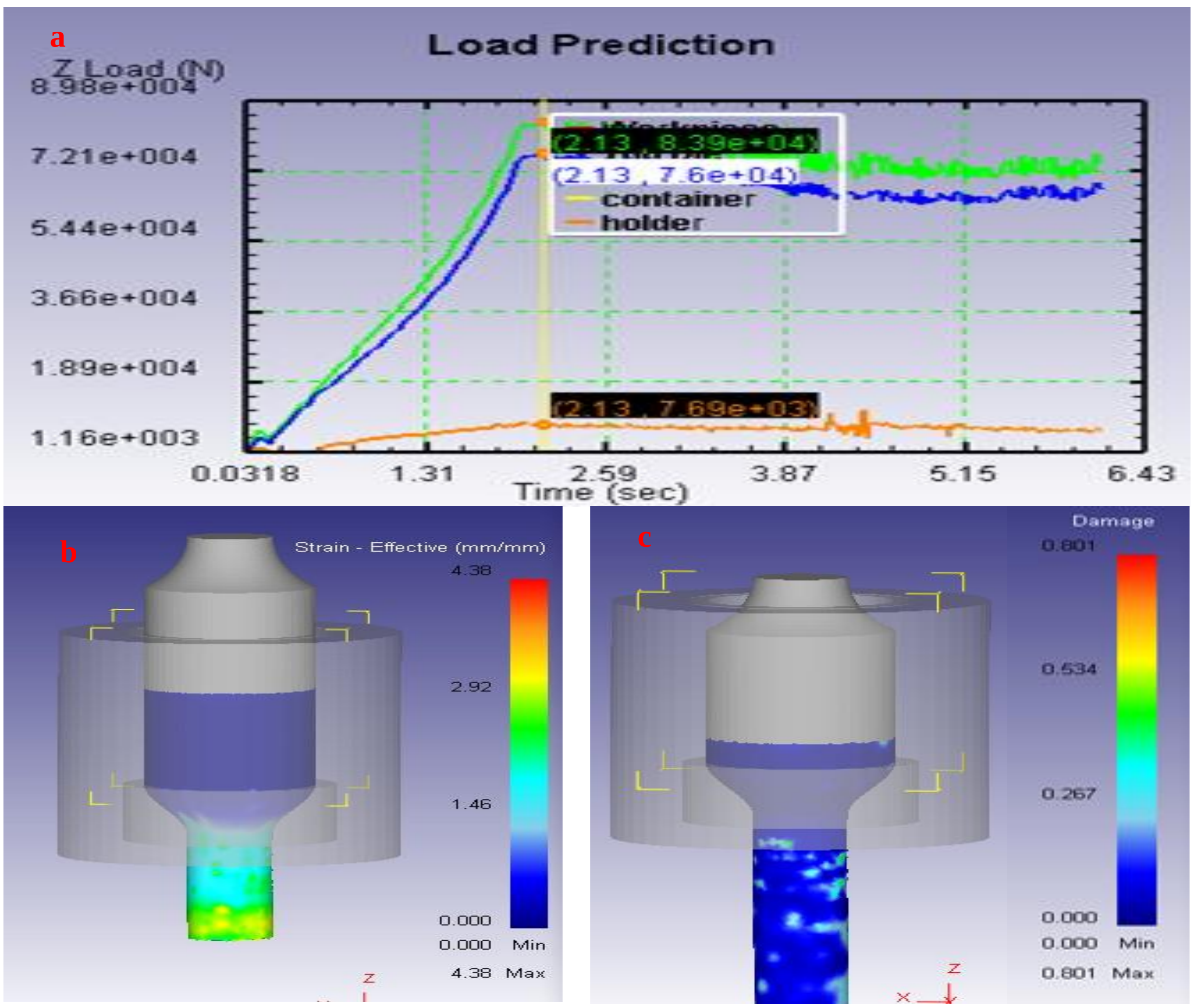

Figure 4-21 GA optimum value cosine die profile response in terms of a) load b) effective strain c) damage

4.6.3 GA multi response optimization of linear convergent die profile

The most precise common combination of input parameters that give minimum output was predicted by a genetic algorithm for linear convergent die profile multi response optimization. Equation (4.11) was utilized to determine the multi-response optimization using the weight set formula. Using equation (4.11), the minimum output values were produced by combining the input parameters 2 (extrusion ratio), 3mm/s (ram speed), and 10mm (die length).

The best and mean fitness values were obtained as 41.5317 and 42.8573, as shown in figure 4.21.

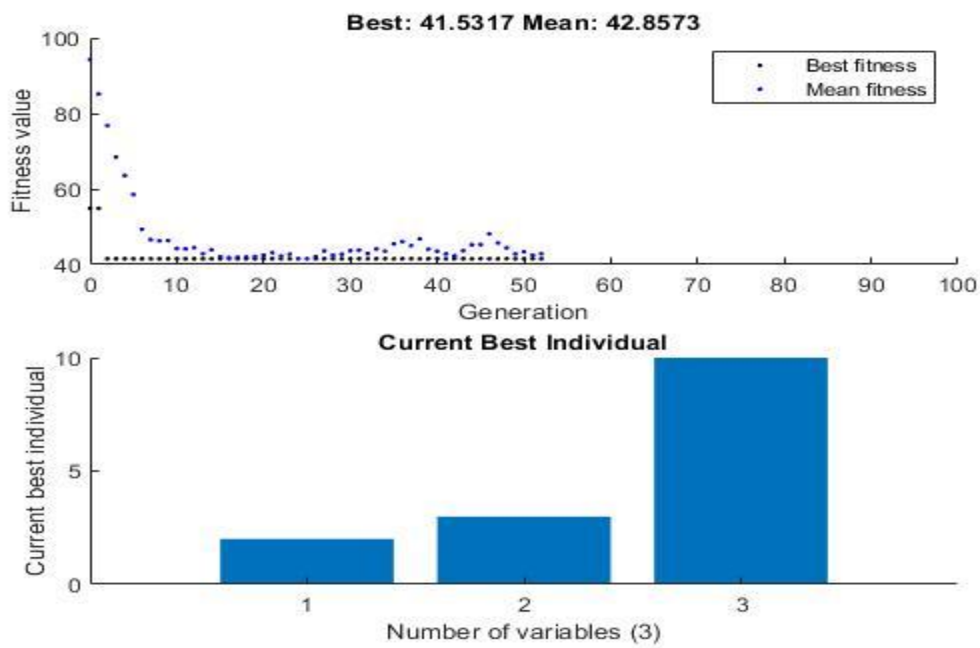

Figure 4-22 GA optimization multi response graph of linear convergent die

Table 4-27 GA predicted best individual of multi response optimization results for linear convergent die

Optimization	Response	Extrusion ratio (X1)	Ram speed (X2)	Die length (X3)	Objective function value
Multi objective	Zmin	2	3	10	41.5317

4.6.4 Confirmation analysis of GA optimum value for linear convergent die

The final stage is to confirm the performance enhancement utilizing the optimum levels of GA design parameters (extrusion ratio, ram speed, and die length at 2, 3 mm/s, and 10mm, respectively). Figure 4.22 depicts the numerical simulation results of a multi-response linear convergent die profile at the optimum GA value (extrusion load, effective strain, and damage of 118KN, .0281, and .984, respectively). The responses from the simulation show that, when compared to the outcome of the Taguchi design parameter combination, the GA was found to have the lowest value.

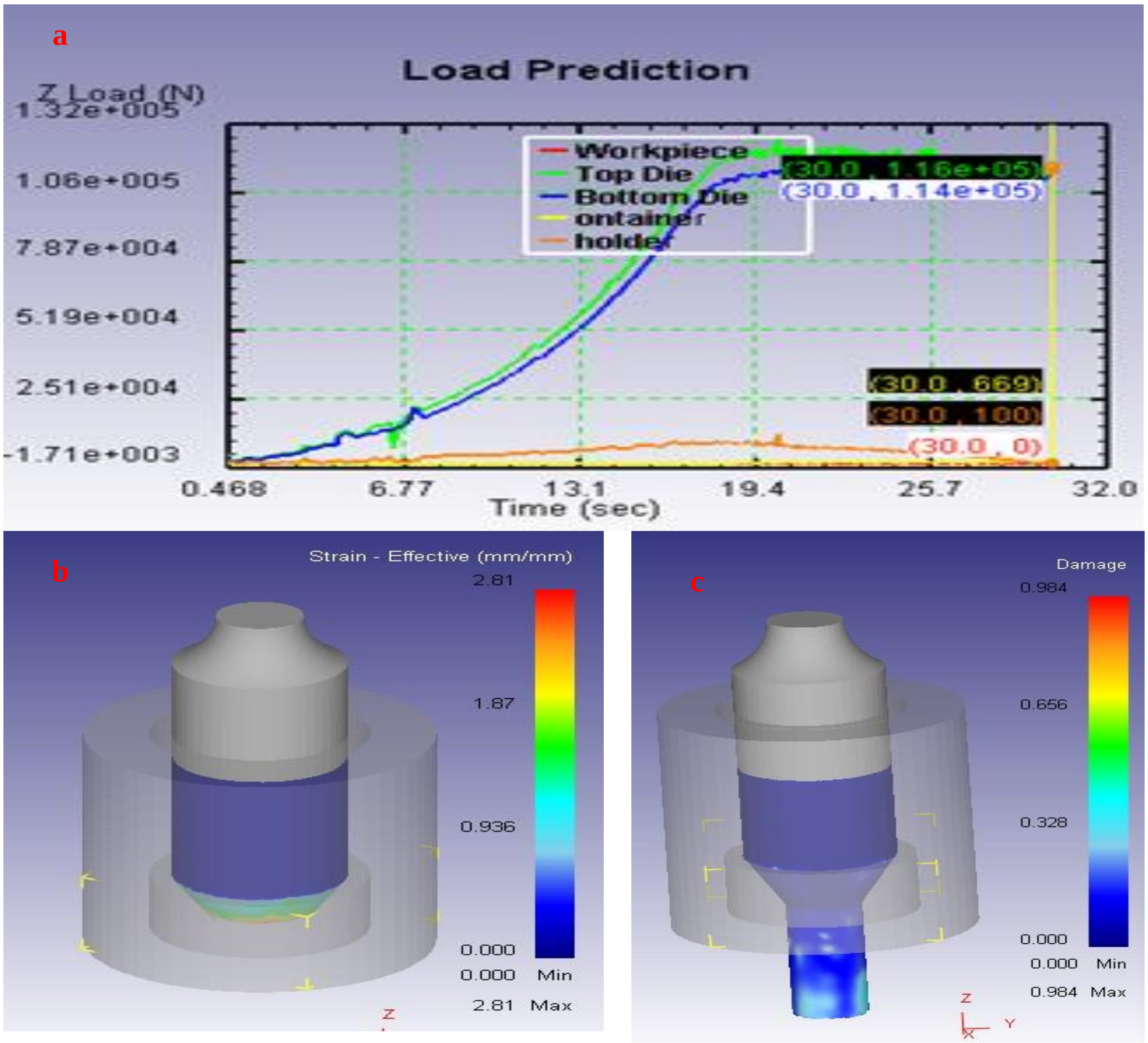

Figure 4-23 GA optimum value linear convergent die profile response in terms of a) load b) effective strain c) damage

4.6.5 GA multi response optimization of streamline die profile

The most precise common combination of input parameters that give minimum output was predicted by a genetic algorithm for streamline die profile multi response optimization. Equation (4.12) was used to calculate multi-objective optimization using the weight set formula. Using equation (4.12), the minimum output values were obtained using the input parameter combination of 2 (extrusion ratio), 1mm/s(ram speed) and 30mm (die length). Figure 4.23 shows the best and mean fitness values of 23.5989 and 23.477, respectively.

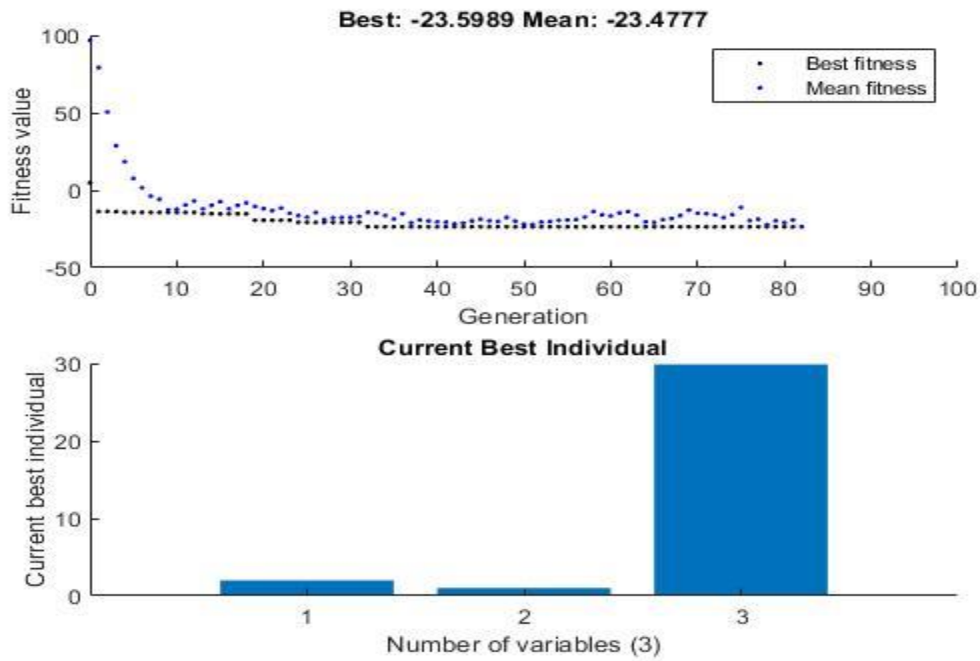

Figure 4-24 GA optimization multi response graph of streamline die

Table 4-28 GA predicted best individual of multi response optimization results for streamline die

Optimization	Response	Extrusion ratio (X1)	Ram speed (X2)	Die length (X3)	Objective function value
Multi response	Zmin	2	1	30	23.5989

4.6.6 Confirmation analysis of GA optimum value for streamline die

The next stage is to confirm the performance enhancement using the optimal GA design parameters (extrusion ratio, ram speed, and die length at 2, 1mm/s, and 30mm, respectively). Figure 4.24 depicts the numerical simulation output result of a multi-response streamline die profile predicted at the optimal GA value (extrusion load, effective strain, and damage of 89KN, .0433, and 1.16, respectively). The responses obtained from the simulation results indicate that the GA anticipated the lowest value as compared to Taguchi's design parameter combination outcomes.

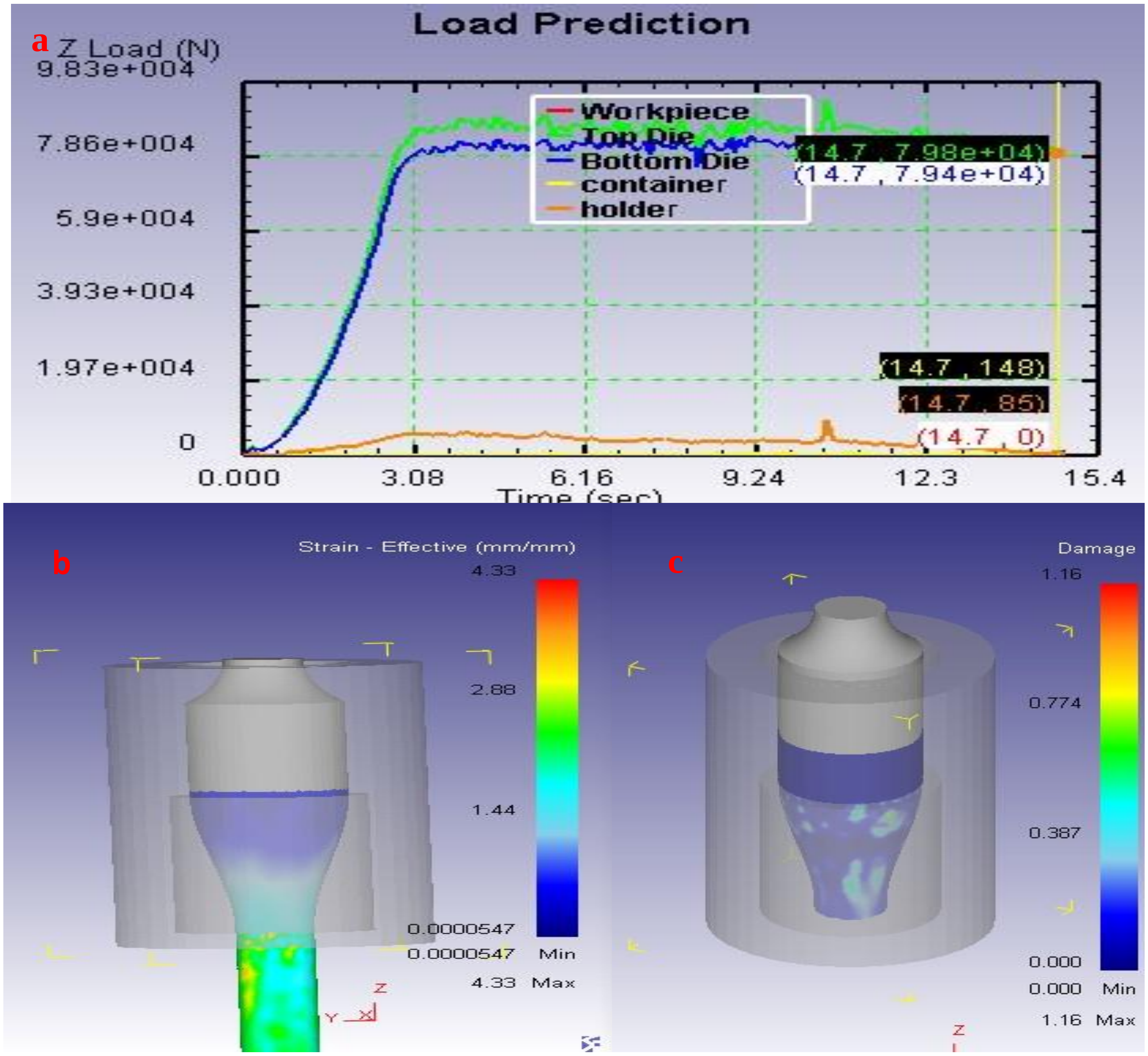

Figure 4-25 GA optimum value streamline die profile response in terms of a) load b) effective strain c) damage

4.7 Experimental Investigation

To validate the FEM results, experimental work was carried out on all types of dies with optimum parameters. The tooling setup for experimentation is manufactured at Kolfe Industrial College. Three experimental runs were chosen based on the simulation and genetic algorithm results for sample preparation. i.e., the optimum condition combination for streamline die profiles is extrusion ratio 2, ram speed of 1mm/s, and die length of 30mm; for linear convergent die extrusion ratio 2, ram speed of 3mm/s, and die length of 10mm; and for cosine die profile, extrusion ratio 2, ram speed of 2.045mm/s, and die length of 10mm. The extrusion process is carried out by pressing the sample after the extrusion components have been arranged in a 50-

ton hydraulic press. During the extrusion process the ram speed was controlled by fixing to the required value and measure the distance moves with the time it takes.

The setup and materials for the extrusion process have been created and chosen. SolidWorks software is used to design and build solid models; Mastercam software is used to develop machining programs for dies; and components are built in accordance with the methods specified.

The billet length was kept at 30mm to avoid additional frictional effort between the billet and other contacts. The billet's diameter is kept slightly smaller than the internal diameter of the holder to account for thermal expansion. The bottom jaw of the hydraulic press is steady, while the top jaw moves at a consistent speed. The detailed list of components is shown in table 4.29

Table 4-29 List of components

S.No	Name of part	Material	Manufacturing process
1	Die	H13	CNC milling, drilling and polishing
2	Ram	H13	CNC turning, polishing
3	Container	H13	Turning, drilling, boring and polishing
4	Holder	H13	Turning, drilling and polishing

4.7.1 Microstructure observation

The optical images of the microstructures of commercially available C60800 aluminum bronze alloy extruded using linear convergent, cosine, and streamline dies are presented in the figure below. The intermetallic complex particles of aluminum bronze alloy are visible under an optical microscope before and after extrusion, which may be due to their small size. When comparing commercial material and after extrusion in linear convergent die, cosine die, and streamline die, the microstructures are noticeably different, showing that the microstructure of after extrusion has a low grain size. The commercial sample contains significant quantities of elongated grains. Furthermore, grain size is not uniform, especially in commercial samples.

Figure 4.25 illustrates that the microstructure of a) commercially raw material of 20mm diameter and deformed with linear convergent, cosine and streamline die 10mm diameter listed in (b),(c),(d). as shown in figure 4.25 the grain size is more refined in cosine and streamline die profile compared to linear convergent die profile.

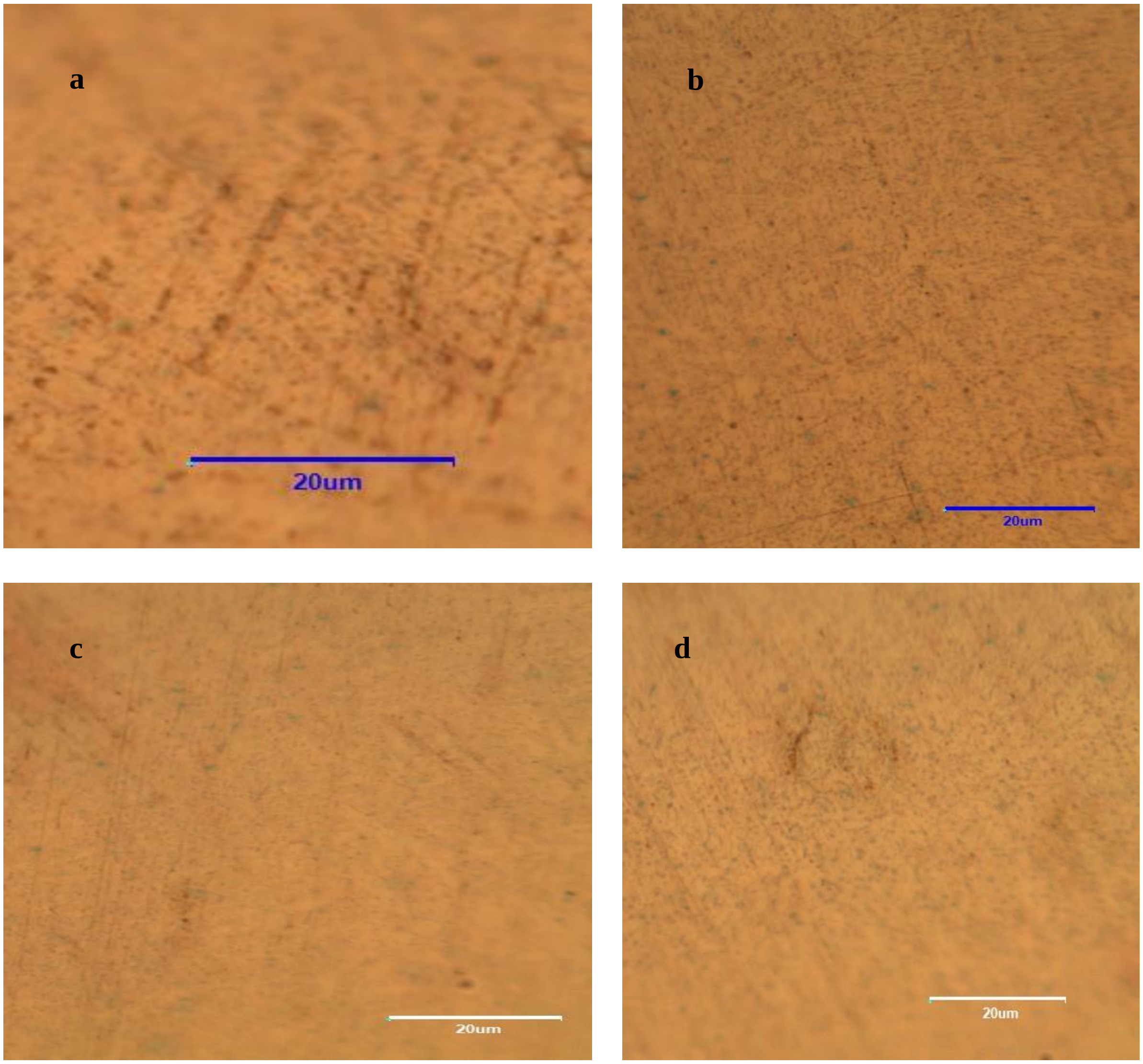

Figure 4-26 Optical microscope image for a) commercial material b) linear convergent die c) cosine die d) streamline die

4.7.2 Hardness test

Vickers hardness tester are performed using diamond indenter in the shape of right pyramid with square base and angle 136 degrees between opposing sides exposed to a force of 10kgf. The results indicate a 18% increase in hardness for cosine die compared to the commercial material of C60800 aluminum bronze alloy before hot extrusion. The linear convergent and streamline die profile also hardness value was improved by 16% and 17.5% respectively. This could be attributed to changes in the material's microstructure caused by high temperature and pressure, notably the grain structure. Hot deformation causes increased dislocation density and dynamic recrystallization, resulting in smaller grain sizes. Smaller grain sizes and increased dislocation density can enhance material strength, hardness, and yield strength. During extrusion, pressure causes grain size particles to disseminate more uniformly throughout the material, leading to a strengthening effect.

Table 4-30 Surface hardness of commercially available C60800 aluminum bronze alloy and deformed in the die

Material	Hardness value			Average hardness value
	Test 1	Test 2	Test 3	
Commercially available	523.2	519.4	517.3	519.97
Cosine die	619.5	634	649.1	634.2
Linear convergent die	623.1	626.7	608.9	619.56
Streamline die	569.1	724.2	598.5	630.6

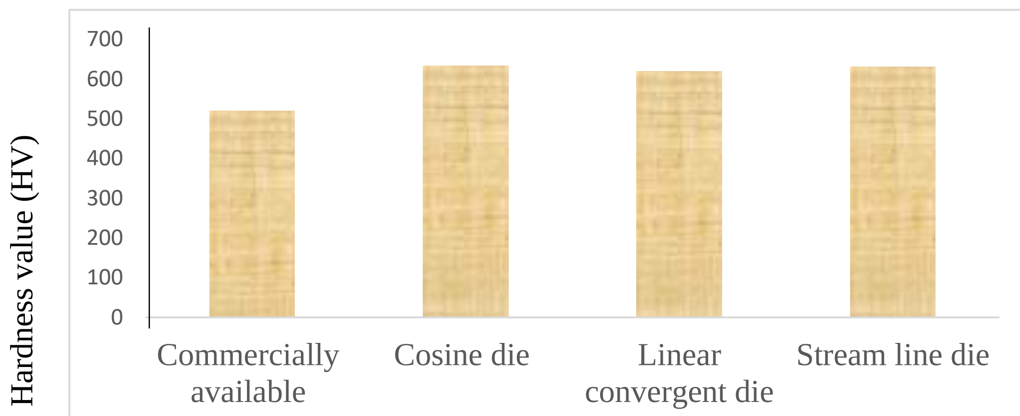

Figure 4-27 Hardness value of commercially available material and deformed in cosine, linear convergent and streamline die profile

As shown in the above figure 4.26 The Vickers hardness test result demonstrates that the deformed product has a higher hardness value when compared to commercially available material. The die profile and process parameter of extrusion also have a significant effect on the hardness value of deformed product. As shown in the above table 4.30 the commercially available specimen has hardness of 519.97HV and the extruded sample of cosine, linear convergent and streamline die profile, the hardness value increase to 634.2HV, 619.56HV and 630.6HV respectively.

4.7.3 Compression test

Extruded and commercially available C60800 aluminum bronze alloys were compressed using universal testing equipment. After hot extrusion in all die profile types, the compression strength of the deformed aluminum bronze alloy was improved by 11%, 9.5%, and 8% for the cosine, streamline, and linear convergent die profiles, respectively. As shown in the compression strength result table 4.31 compression strength after extrusion is increased from 767 MPa to 851 MPa in the cosine die profile, in the linear convergent die from 767 MPa to 828 MPa, and in the streamline die profile also from 767 MPa to 839 MPa. (Wang et al., 2023) also reported that extrusion refined the grain structure and make homogenous microstructure due to that the mechanical property of the alloy is increased.

Table 4-31 Compression strength of commercially available C60800 aluminum bronze alloy and deformed in the die

Sample	Compression strength (MPa)
Commercially available	767
Cosine die	851
Streamline die	839
Linear convergent die	828

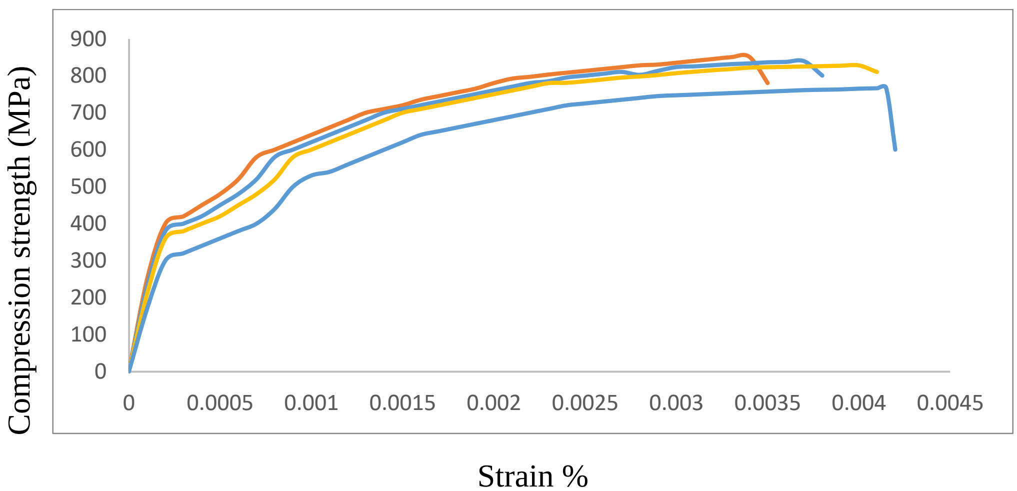

Figure 4-28 Compression strength value of commercially available material and deformed in cosine, linear convergent and streamline die profile

4.7.4 Analysis of corrosion rate

Potentiodynamic polarization curves of extruded and commercial material of aluminum bronze alloys prepared in a 3.5 wt.% NaCl solution indicate that the aluminum bronze alloy has identical polarization and passivity properties. However, corrosion potentials (Ecorr) and corrosion current densities (Icorr) differ significantly between the type of die profile and extruded and commercial aluminum bronze alloy. To assure the material's life span, a minimum corrosion rate value is essential. Several approaches are often employed to provide quantitative estimates of metal corrosion rates. Corrosion experts regard methods of detecting weight loss and thickness loss over time as "accurate" corrosion testing. However, this procedure is time-consuming and thus unsuitable for rapid corrosion screening. Tafel plots are a simple electrochemical approach that can theoretically be used to determine corrosion rates. The corrosion current was determined by the intersection of two slopes of anodic and cathodic Tafel plots.

Table 4-32 Electrochemical corrosion for extruded and commercial alloys specimens in 3.5% NaCl solution

Sample code	Corrosion potential (Ecorr)(V)	Corrosion current (Icorr)(A/cm2)	corrosion rate(mm/year)
Cosine die	-0.198565	2.658	0.00823
Linear convergent die	-0.21323	4.926	0.0115
Streamline die	-0.20906	4.497	0.01055
Commercially available	-0.23993	9.9	0.0232

Table 4.32 depicts the electrochemical corrosion of the prepared specimens as well as the corrosion rate of samples in a 3.5% Nacl solution, depending on the corrosion potential and current density acquired from the Tafel plot upon the test. The extrusion process can refine the grain structure and homogenize the distribution of alloying elements in the aluminum bronze alloy. These microstructural changes can enhance the alloy's corrosion resistance by promoting the formation of a more compact and protective oxide/hydroxide layer on the surface (Ajeel et al., 2019). As seen in table 4.32 the corrosion rate is improved in extruded samples more of them in cosine die compared to other die profiles. The die profile can influence the corrosion

rate after extrusion by influencing aspects such as surface finish, stress distribution, and the production of protective oxide layers. A well-designed die profile can produce a better surface finish, reducing areas prone to corrosion onset. Furthermore, an improved die profile can help distribute stresses more evenly during extrusion, reducing localized stress concentrations that might cause to corrosion. Furthermore, the die profile can influence the production of protective oxide layers on the extruded material, which increases its corrosion resistance (Razooqi et al., 2022).

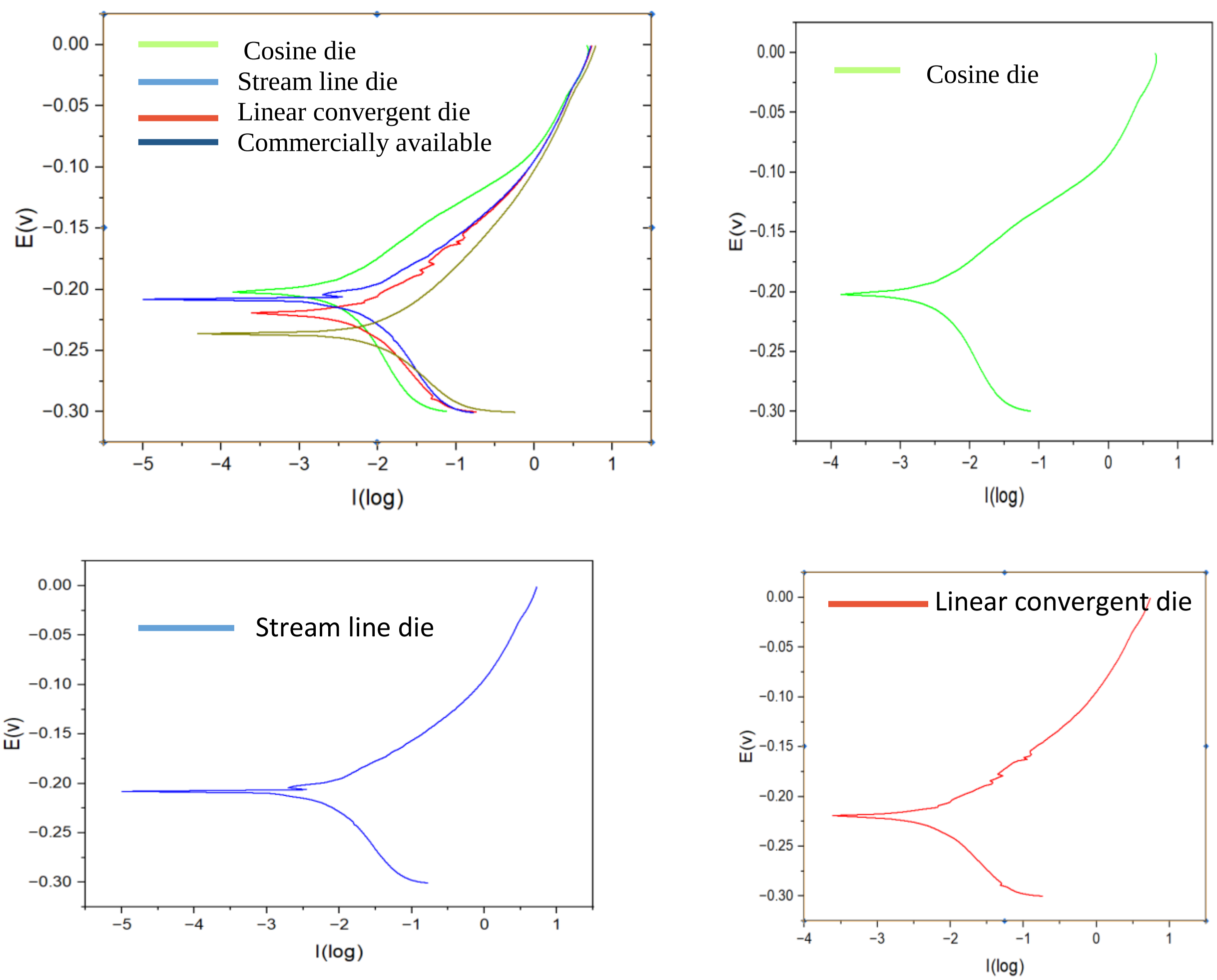

Figure 4-29 Tafel plot of aluminum bronze alloy specimens in 3.5%NaCl solution

4.8 Validation the Result with the Required Application

The force required to extrude the material analytic analysis and simulation result are below 10% range variation. Based on experimental investigation of C60800 aluminum bronze alloy in all types of die, the cosine die profile extruded sample was better hardness, compression strength and minimum corrosion rate compared to linear convergent and streamline die profile. (Mohapatra, 2016) studied aluminum alloy with multi die profile for round-to-square design results in cosine die profile leads to minimal duplicated effort, lower energy usage, fewer product defects and better mechanical property. Corrosion resistance of aluminum bronze is increased after deformation and mechanical property also improved. When comparing the result with the material mostly used in marine shafts of 316 stainless steel (Muhammad et al., 2020), the hardness value is done with HV5. To validate the result, convert it to HV10; the value is in the range of 580–610 HV10. The hardness value (HV10) of the deformed aluminum bronze alloy is also 634.2 in the cosine die, 630.6 in the streamline die, and 619.56 in the linear convergent die. The compression strength of 316 stainless steel is also in the range of 800-1000 MPa. The result of compression strength of a deformed product is also 851MPa in the cosine die, 839MPa in the streamline die and 828MPa in the linear convergent die profile. The corrosion resistant aluminum bronze alloy is higher compared to the type of stainless-steel material, especially in seawater and alkaline environments. In this analysis, extruded C60800 aluminum bronze alloy is suitable for marine shaft applications based on the above properties.

CHAPTER-V

CONCLUSION AND RECOMMENDATION

This study demonstrates the potential of multi-profile die extrusion process enhancement of mechanical property, corrosion behavior and microstructure of C60800 aluminum bronze alloy using various process parameters. The impact of process parameters such as extrusion ratio (2, 3, 4), ram speed (1, 2, 3mm/s) and die length (10, 20, 30mm) on extrusion load, effective strain, and damage was accomplished using the DEFORM 3D simulation software based on FEM. A Taguchi-based genetic algorithm was utilized to optimize process parameters for multiple responses of minimum parametric combination for damage, load, and effective strain percentage. The experimental examination of hot extrusion was conducted using the optimal process parameter acquired from numerical simulation. Testing and characterization were undertaken to investigate the deformation behavior of the C60800 aluminum bronze alloy. The results are as follows:

5.1 Conclusion

- All analytic load and computational load was below 10% range of difference.
- DEFORM 3D was known to be an effective tool for analyzing the consequences of design; therefore, design experiments were implemented, and The Taguchi method was employed to design the experiments. Nine tests are carried out utilizing the Taguchi L9 design, and process parameters for multi-response can be efficiently identified.
- ANOVA and S/N ratio results indicate that extrusion ratio is the most significant extrusion parameter on load and effective strain of the cosine die, whereas ram speed has the greatest impact on damage. The findings of linear convergent and streamline die profile ANOVA and S/N ratio revealed that the extrusion ratio is the most critical extrusion parameter for effective strain and damage. However, for extrusion load, die length is the most critical element on linear convergent die profiles, and ram speed is also a major contributor for streamlines.
- Extrusion load was raised by increasing the extrusion ratio, ram speed, and die length. Effective strain increased with increasing extrusion ratio, whereas It minimized as the ram speed and die length increased. Damage value is not constant with increasing or decreasing extrusion process parameters.

- The optimum condition for cosine die profile multi-response features was obtained using a Taguchi-based genetic algorithm at an extrusion ratio of 2, ram speed of 2.047 mm/s, and die length of 10mm. The output response from the confirmation numerical simulation is load required of 84 KN, effective strain of .0438, and damage of .801.
- The optimal input parameters for a linear convergent die profile are extrusion ratio 2, ram speed 3 mm/s, and die length 10 mm. Output responses are load needed 118 KN, effective strain .0281, and damage .984.
- For streamline die profile, the optimal input parameters combination of extrusion ratio 2, ram speed 1 mm/s, and die length 30mm with output response obtained are extrusion load required of 89 KN, effective strain .0433, and damage 1.16.
- The C60800 aluminum bronze alloy was finally extruded with the optimal parameter combination using an extruder machine, and the hardness of the linear convergent and streamline die profiles was somewhat lower than the cosine die but greater than the commercial material sample.
- The C60800 aluminum bronze alloy enhanced compression strength in all types of dies compared to commercial material, with slightly greater strength in cosine dies over linear convergent and streamline dies.
- Deformed products have a more refined and uniformly distributed microstructure than commercial raw materials.
- Corrosion rates in extruded products are significantly lower than in commercial material products, particularly in cosine dies, which have a lower corrosion rate than linear convergent and streamline die profiles.

5.2 Recommendation

The study concluded with the following recommendations:

- This study focused on round bar extrusion. Complex shapes can be utilized to focus comparable investigations.
- The die profile design for the round bar extrusion process was successful. The design methodology can be extended for the complex shape extrusion.
- This study investigated and characterized a few mechanical properties. Additional tests, like tensile, and impact testing, can be used in similar research.

Reference

Ajeel, S. A., Yaseen, R. S., & Keqal, A. (2019). Improvement the Corrosion Resistance of Aluminum Bronze Alloy (Cu-7.7wt%Al) Reinforced by Al2O3 and TiO2 Nanoparticles. *IOP Conference Series: Materials Science and Engineering*, *518*(3). https://doi.org/10.1088/1757-899X/518/3/032046

Ajiboye, J. S., & Oyinbo, S. T. (2014). Load prediction for the extrusion from circular billet to symmetric and asymmetric polygons using linearly converging die profiles. *Key Engineering Materials*, *622–623*, 119–128. https://doi.org/10.4028/www.scientific.net/KEM.622-623.119

Anantapong, J., Suranuntchai, S., Manonukul, A., & Uthaisangsuk, V. (2014). Investigation of nickel aluminum bronze alloy under hot compression test. *Advanced Materials Research*, *931–932*, 365–369. https://doi.org/10.4028/www.scientific.net/AMR.931-932.365

Ayer, Ö. (2020). Effect of die parameters on the grain size, mechanical properties and fracture mechanism of extruded AZ31 magnesium alloys. *Materials Science and Engineering: A*, *793*(June), 2–10. https://doi.org/10.1016/j.msea.2020.139887

Badashah, S. J. (2012). *S Urface R Oughness P Rediction With D Enoising Using*. *3*(2), 168–177.

Balali, M., Limouei, M. B., & Balali, M. (2018). Study on Optimization of Parameters Affecting Simple Shear Extrusion of Pure Copper to Fabricate Fine Grain Structure. *Transactions of the Indian Institute of Metals*, *71*(3), 605–616. https://doi.org/10.1007/s12666-017-1193-8

Bharath, K., Mandal, A., Karmakar, A., Khanra, A. K., & Davidson, M. J. (2020). Understanding the effect of hot extrusion on the evolution of microstructure and associated mechanical properties in sintered Al-Cu-Mg alloys. *Materials Characterization*, *170*, 110715. https://doi.org/10.1016/j.matchar.2020.110715

Borodin, E. N., Morozova, A., Bratov, V., Belyakov, A., & Jivkov, A. P. (2019). Experimental and numerical analyses of microstructure evolution of Cu-Cr-Zr alloys during severe plastic deformation. *Materials Characterization*, *156*(May), 109849. https://doi.org/10.1016/j.matchar.2019.109849

Cackett, A. J., Lim, J. J. H., Klupś, P., Bushby, A. J., & Hardie, C. D. (2018). Using spherical indentation to measure the strength of copper-chromium-zirconium. *Journal of Nuclear Materials*, *511*, 610–616. https://doi.org/10.1016/j.jnucmat.2018.04.012

Chen, D. C., Syu, S. K., Wu, C. H., & Lin, S. K. (2007). Investigation into cold extrusion of aluminum billets using three-dimensional finite element method. *Journal of Materials Processing Technology*, *192–193*, 188–193. https://doi.org/10.1016/j.jmatprotec.2007.04.067

Chu, W. L., Xie, M. J., Wu, L. W., Guo, Y. S., & Yau, H. T. (2020). The optimization of lathe cutting parameters using a hybrid Taguchi-genetic algorithm. *IEEE Access*, *8*, 169576–169584. https://doi.org/10.1109/ACCESS.2020.3022648

Farzam, M. (2008). *Ar ch ive*. *5*(1).

Francis, R. C. (2020). *Deformation Behavior and Characterization of Copper Alloy*. *6*(January), 74–80.

Gao, L. L., & Cheng, X. H. (2008). *Microstructure and dry sliding wear behavior of Cu – 10 % Al – 4 % Fe alloy produced by equal channel angular extrusion*. *265*, 986–991. https://doi.org/10.1016/j.wear.2008.02.014

Giarmas, E., & Tzetzis, D. (2022). Optimization of die design for extrusion of 6xxx series aluminum alloys through finite element analysis: a critical review. *International Journal of Advanced Manufacturing Technology*, *119*(9–10), 5529–5551. https://doi.org/10.1007/s00170-022-08694-3

Guo, N., Li, D., Yu, H., Xin, R., Zhang, Z., Li, X., Liu, C., Song, B., & Chai, L. (2017). Annealing behavior of gradient structured copper and its effect on mechanical properties. *Materials Science and Engineering A*, *702*(April), 331–342. https://doi.org/10.1016/j.msea.2017.07.023

Hsia, S. Y. (2013). Optimization of microextrusion preforming using taguchi method. *Mathematical Problems in Engineering*, *2013*. https://doi.org/10.1155/2013/305797

Jeyapaul, R., Shahabudeen, P., & Krishnaiah, K. (2006). Simultaneous optimization of multi-response problems in the Taguchi method using genetic algorithm. *International Journal of Advanced Manufacturing Technology*, *30*(9–10), 870–878. https://doi.org/10.1007/s00170-005-0095-9

Kang, C. G., Jung, Y. J., & Kwon, H. C. (2002). Finite element simulation of die design for hot extrusion process of Al/Cu clad composite and its experimental investigation. *Journal of Materials Processing Technology*, *124*(1–2), 49–56. https://doi.org/10.1016/S0924-0136(02)00106-1

Kothasiri, A. F., & Chalamalasetti, S. R. (2022). Investigation of Cold Extrusion of Aluminum AA 2024 Alloy using Finite Element Analysis. *INCAS Bulletin*, *14*(3), 157–171. https://doi.org/10.13111/2066-8201.2022.14.3.14

Lin, Z., Juchen, X., Xinyun, W., & Guoan, H. (2003). Optimization of die profile for improving die life in the hot extrusion process. *Journal of Materials Processing Technology*, *142*(3), 659–664. https://doi.org/10.1016/S0924-0136(03)00686-1

Liu, X., Huang, D., Yan, C., Zhou, Y., & Yan, W. (2020). Multi-directional forging and aging treatment effects on friction and wear characterization of aluminium-bronze alloy. *Materials Characterization*, *167*(July), 110511. https://doi.org/10.1016/j.matchar.2020.110511

M Spittel &thilo spittel. (2006). Advanced Materials and Technologies. In *Materials Science Forum* (Vol. 513). https://doi.org/10.1002/0471221619.ch7

Ma, S., Fu, L., & Shan, A. (2021). Enhancing strength-ductility of the aluminum bronze alloy by generating high-density ultrafine annealing twins. *Materials Characterization*, *177*(800), 111057. https://doi.org/10.1016/j.matchar.2021.111057

Ma YDu ZCui XCheng JLiu GGong TLiu HWang XChen YRusnák JMalega PSvetlík JRudy VŠmajda NProcesses FSethi GMyers NGerman RWorking CStyks JWróbel MFraczek JKnapczyk ADu ZMa YLiu FXu NChen YWang XChen YGong TXu DCheng JLi JYu SDu ZZhang XZhang WGai JWang HSon. (2016). *University of Basrah College of Engineering Mechanical Engineering Department Lecture Notes of MANUFACTURING PROCESSES (ME337)*, *3*. 1–21.

Ma, Z., Zhang, K., Ren, Z., Zhang, D. Z., Tao, G., & Xu, H. (2020). Selective laser melting of Cu–Cr–Zr copper alloy: Parameter optimization, microstructure and mechanical properties. *Journal of Alloys and Compounds*, *828,* 154350. https://doi.org/10.1016/j.jallcom.2020.154350

Majumdar, A., & Ghosh, D. (2015). Genetic Algorithm Parameter Optimization using Taguchi Robust Design for Multi-response Optimization of Experimental and Historical Data. *International Journal of Computer Applications*, *127*(5), 26–32. https://doi.org/10.5120/ijca2015906383

Markforged. (2018). H13 Tool Steel. *Material Datasheet*, 1. http://www.astmsteel.com/product/h13-tool-steel-x40crmov5-1-skd61-hot-work-steel/

Mohapatra, S. K. (2016). *Aluminium Based Material Extrusion through Mathematical Contoured Die : Numerical & Experimental Investigation Certificate of Examination*. *512*.

Muhammad, M. M., Yati, M. S. D., Nik Yusoff, N. H., & Isa, M. C. (2020). Fracture Failure Analysis of a Marine Propeller Shaft. *Defence S and T Technical Bulletin*, *13*(2), 240–246.

Nag, A., Yadav, A., & Pazoki, M. (2020). *Optimization Technique*. *October 2016*, 261–266.

Nwaeju, C. C., Edoziuno, F. O., Adediran, A. A., Nnuka, E. E., Akinlabi, E. T., & Elechi, A. M. (2022). Development of regression models to predict and optimize the composition and the mechanical properties of aluminium bronze alloy. *Advances in Materials and Processing Technologies*, *8*(sup3), 1227–1244. https://doi.org/10.1080/2374068X.2021.1939556

Onuh, S. O., Ekoja, M., & Adeyemi, M. B. (2003). Effects of die geometry and extrusion speed on the cold extrusion of aluminium and lead alloys. *Journal of Materials Processing Technology*, *132*(1–3), 274–285. https://doi.org/10.1016/S0924-0136(02)00941-X

Panwar, V., Kumar, D., Kumar, K. V. P., Jain, A., & Thakar, C. (2021). Materials Today : Proceedings Experimental investigations and optimization of surface roughness in turning of en 36 alloy steel using response surface methodology and genetic algorithm. *Materials Today: Proceedings*, *xxxx*. https://doi.org/10.1016/j.matpr.2021.03.642

Plascencia, G., & Utigard, T. A. (2005). High temperature oxidation mechanism of dilute copper aluminium alloys. *Corrosion Science*, *47*(5), 1149–1163. https://doi.org/10.1016/j.corsci.2004.06.031

Qamar, S. Z., Chekotu, J. C., Al-Maharbi, M., & Alam, K. (2019). Shape Complexity in Metal Extrusion: Definitions, Classification, and Applications. *Arabian Journal for Science and Engineering*, *44*(9), 7371–7384. https://doi.org/10.1007/s13369-019-03886-8

Razooqi, A. I., Abbas, N. M., & Ghazi, S. S. (2022). Influence of Multi Extrusion Die Process on Mechanical and Chemical Behavior of 2024-T3 Alloy. *International Journal of Applied Mechanics and Engineering*, *27*(3), 163–170. https://doi.org/10.2478/ijame-2022-0042

Reinikainen, T., Andersson, K., Kivivuori, S., & Korhonen, A. S. (1992). Finite-element analysis of copper extrusion processes. *Journal of Materials Processing Tech.*, *34*(1–4), 101–108. https://doi.org/10.1016/0924-0136(92)90095-A

Senthilkumar, B., Kannan, T., & Madesh, R. (2017). *Optimization of flux-cored arc welding process parameters by using genetic algorithm*. 35–41. https://doi.org/10.1007/s00170-015-7636-7

Singh, B., Kumar, R., & Chohan, J. S. (2021). Materials Today : Proceedings Multi-objective optimization of 3D Printing process using genetic algorithm for fabrication of copper reinforced ABS parts. *Materials Today: Proceedings*, *xxxx*. https://doi.org/10.1016/j.matpr.2021.06.264

Sommitsch, C., Sievert, R., Wlanis, T., Günther, B., & Wieser, V. (2007). Modelling of creep-fatigue in containers during aluminium and copper extrusion. *Computational Materials Science*, *39*(1 SPEC. ISS.), 55–64. https://doi.org/10.1016/j.commatsci.2006.03.024

Sun, W., & Yang, C. (2023). Simulation of Cross Wedge Rolling and Hot Extrusion-Combined Forming Process for Axle Sleeve. *Metals*, *13*(6), 1–17. https://doi.org/10.3390/met13061017

Tolaminejad, B., & Fakhar, N. (2023). Development of Microstructure Homogeneity and Mechanical Properties After ECA-Extrusion of Copper Alloy C11000. *Transactions of the Indian Institute of Metals*, *76*(1), 259–267. https://doi.org/10.1007/s12666-022-02747-7

Venkatesh, C., & Venkatesan, R. (2014). Design and analysis of streamlined extrusion die for round to hexagon using area mapping technique, upper bound technique and finite element method. *Journal of Mechanical Science and Technology*, *28*(5), 1867–1874. https://doi.org/10.1007/s12206-014-0136-0

Vijian, P., & Arunachalam, V. P. (2007). Modelling and multi objective optimization of LM24 aluminium alloy squeeze cast process parameters using genetic algorithm. *Journal of Materials Processing Technology*, *186*(1–3), 82–86.

https://doi.org/10.1016/j.jmatprotec.2006.12.019

Wang, W., Zhang, W., Liu, Y., Zou, J., Mi, X., Li, D., Li, K., & Huang, G. (2023). Tailoring microstructure of a nickel aluminium bronze by hot extrusion and its impact on mechanical and corrosion behaviour. *Corrosion Science*, *215*, 111049. https://doi.org/10.1016/J.CORSCI.2023.111049

Work, H., & Steel, T. (n.d.). *EXELL H-13*.

Xu, J., Wang, Z., Chen, C., & La, P. (2004). Research into a new high-strength aluminium bronze alloy. *International Journal of Materials and Product Technology*, *21*(5), 443–453. https://doi.org/10.1504/IJMPT.2004.005001

Xu, X., Zhao, H., Hu, Y., Zong, L., Qin, J., Zhang, J., & Shao, J. (2022). Effect of hot compression on the microstructure evolution of aluminium bronze alloy. *Journal of Materials Research and Technology*, *19*, 3760–3776. https://doi.org/10.1016/j.jmrt.2022.06.122

Yadav, R. R., Dewang, Y., & Raghuvanshi, J. (2018). A Study on Metal Extrusion Process. *International Journal of LNCT*, *2*(6), 124–130. https://www.researchgate.net/publication/326210297

Yang, T. S., Hsu, Y. C., Lin, H. S., & Chang, S. Y. (2008). A finite element analysis for the initial blank's shape design of sheet metal in deep drawing process. *Key Engineering Materials*, *364-366 II*, 980–985. https://doi.org/10.4028/www.scientific.net/kem.364-366.980

Zhang, S., Li, R., Kang, H., Chen, Z., Wang, W., Zou, C., Li, T., & Wang, T. (2017). A high strength and high electrical conductivity Cu-Cr-Zr alloy fabricated by cryorolling and intermediate aging treatment. *Materials Science and Engineering A*, *680*(October), 108–114. https://doi.org/10.1016/j.msea.2016.10.087

Appendix I: Micro-Hardness for Deformed Product (From Vickers Hardness)

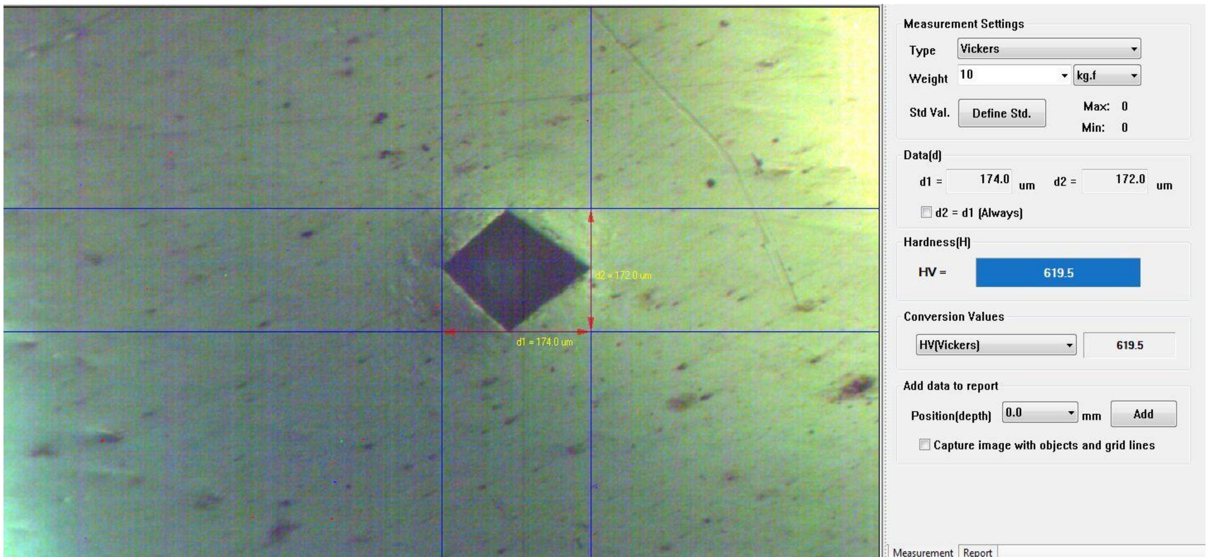

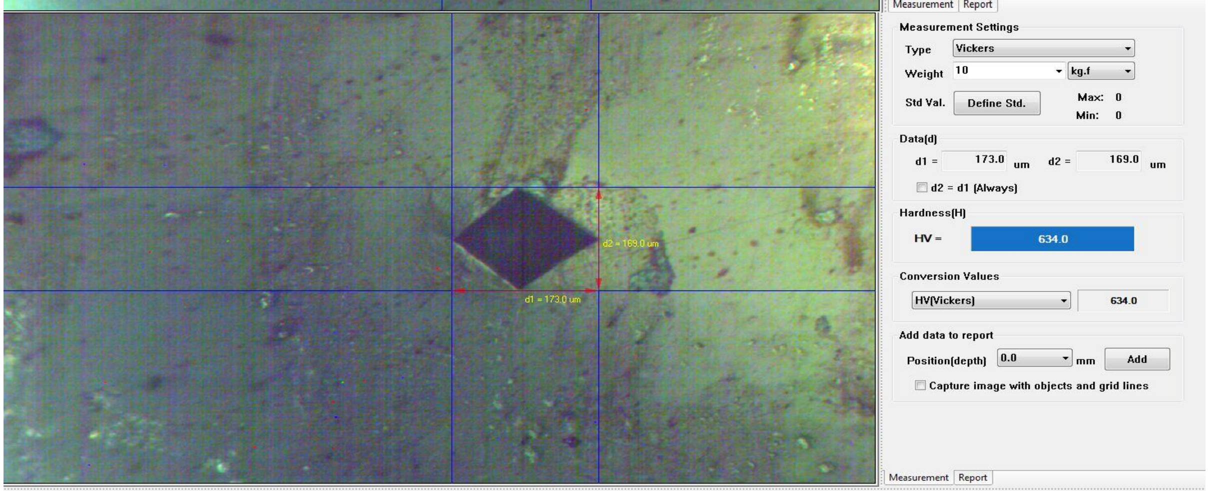

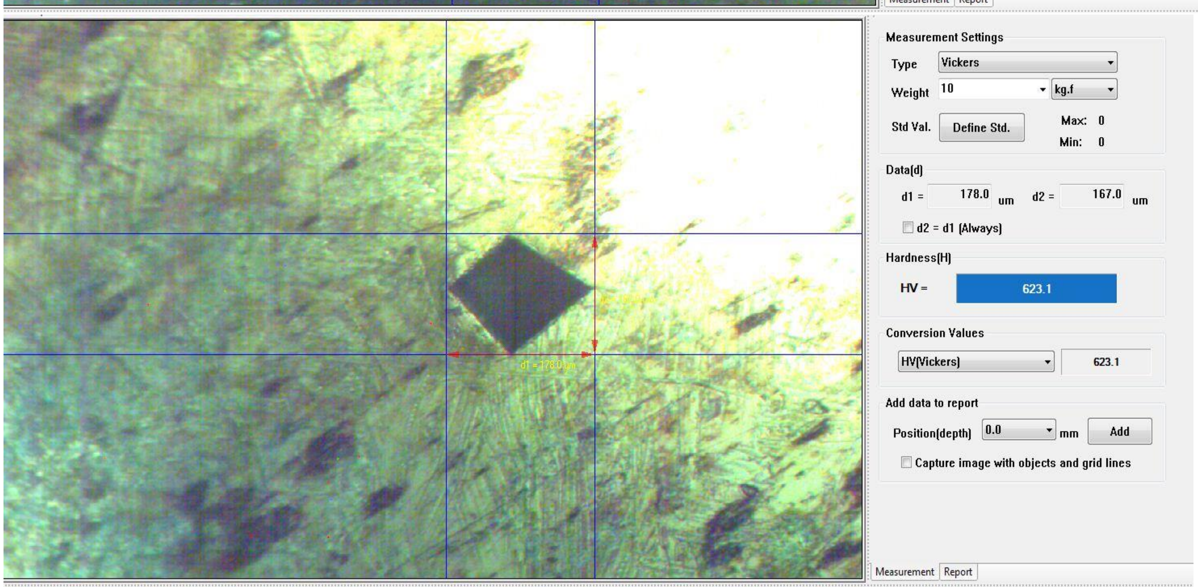

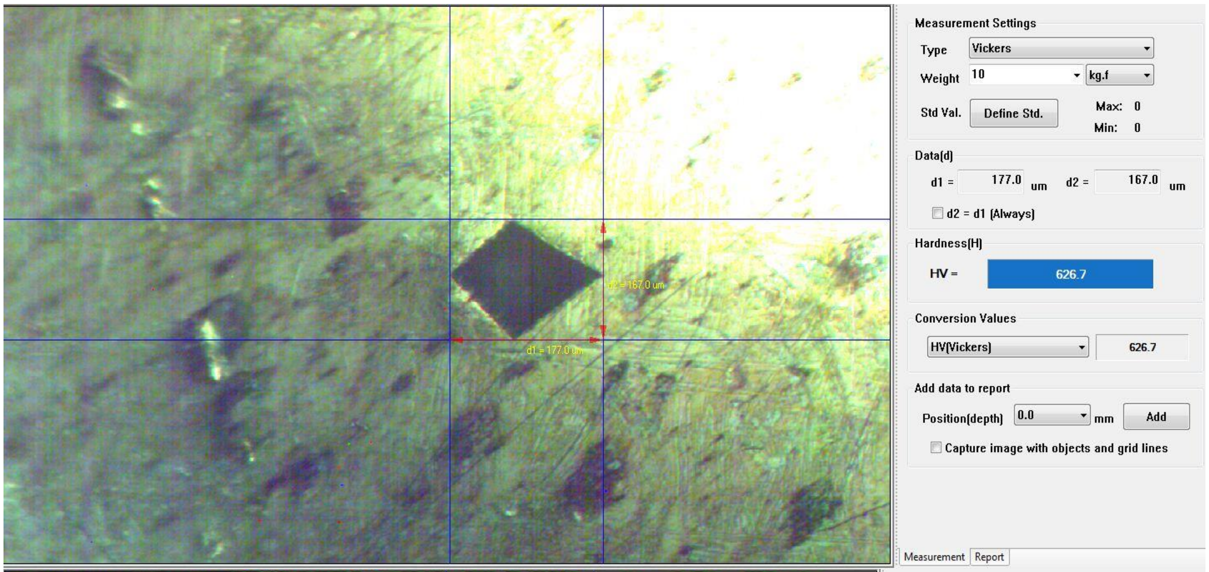
d1 = 177.0 um
Measurement Settings
Type Vickers
Weight 10 kg.f
Std Val. Define Std.
Max: 0
Min: 0
Data(d)
d1 = 177.0 um d2 = 167.0 um
d2 = d1 (Always)
Hardness(H)
HV = 626.7
Conversion Values
HV(Vickers) 626.7
Add data to report
Position(depth) 0.0 mm Add
Capture image with objects and grid lines
Measurement Report

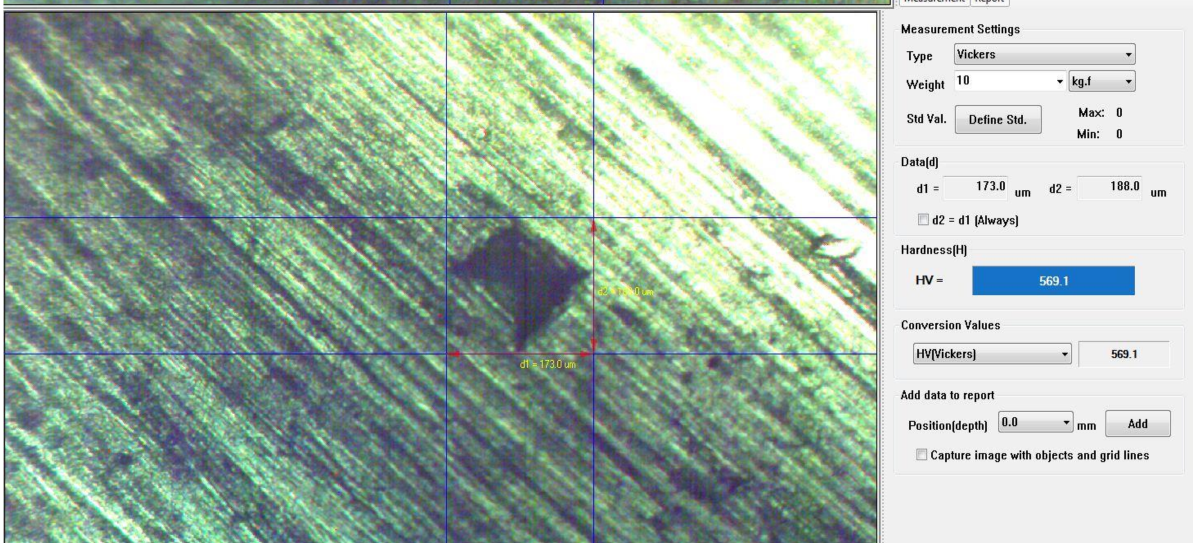
d1 = 173.0 um
Measurement Settings
Type Vickers
Weight 10 kg.f
Std Val. Define Std.
Max: 0
Min: 0
Data(d)
d1 = 173.0 um d2 = 188.0 um
d2 = d1 (Always)
Hardness(H)
HV = 569.1
Conversion Values
HV(Vickers) 569.1
Add data to report
Position(depth) 0.0 mm Add
Capture image with objects and grid lines

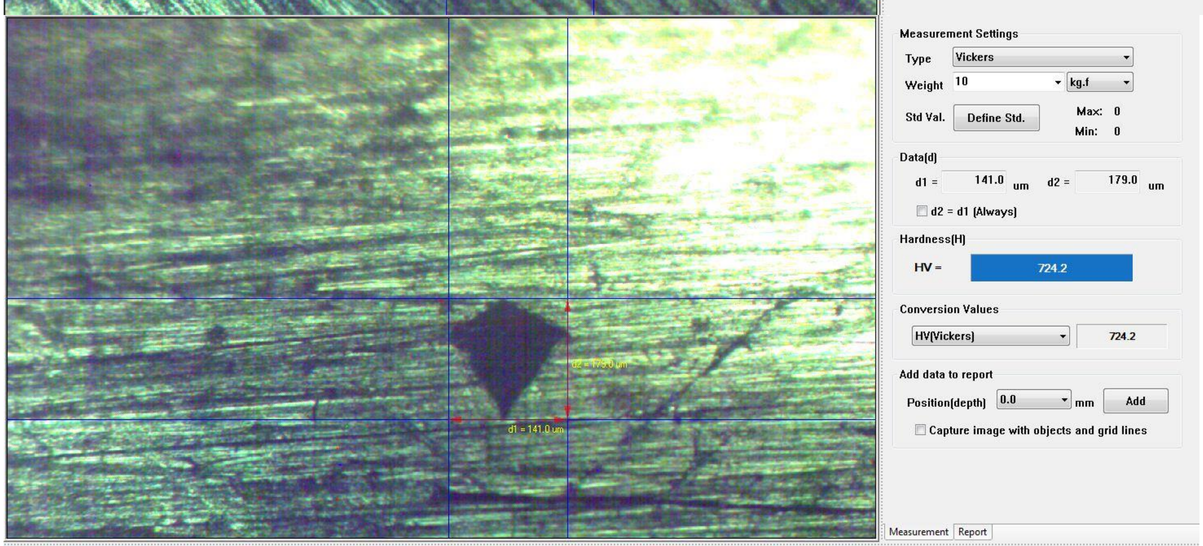
d1 = 141.0 um
Measurement Settings
Type Vickers
Weight 10 kg.f
Std Val. Define Std.
Max: 0
Min: 0
Data(d)
d1 = 141.0 um d2 = 179.0 um
d2 = d1 (Always)
Hardness(H)
HV = 724.2
Conversion Values
HV(Vickers) 724.2
Add data to report
Position(depth) 0.0 mm Add
Capture image with objects and grid lines
Measurement Report

Appendix II: Calculation of Current Density from Tafel Plot

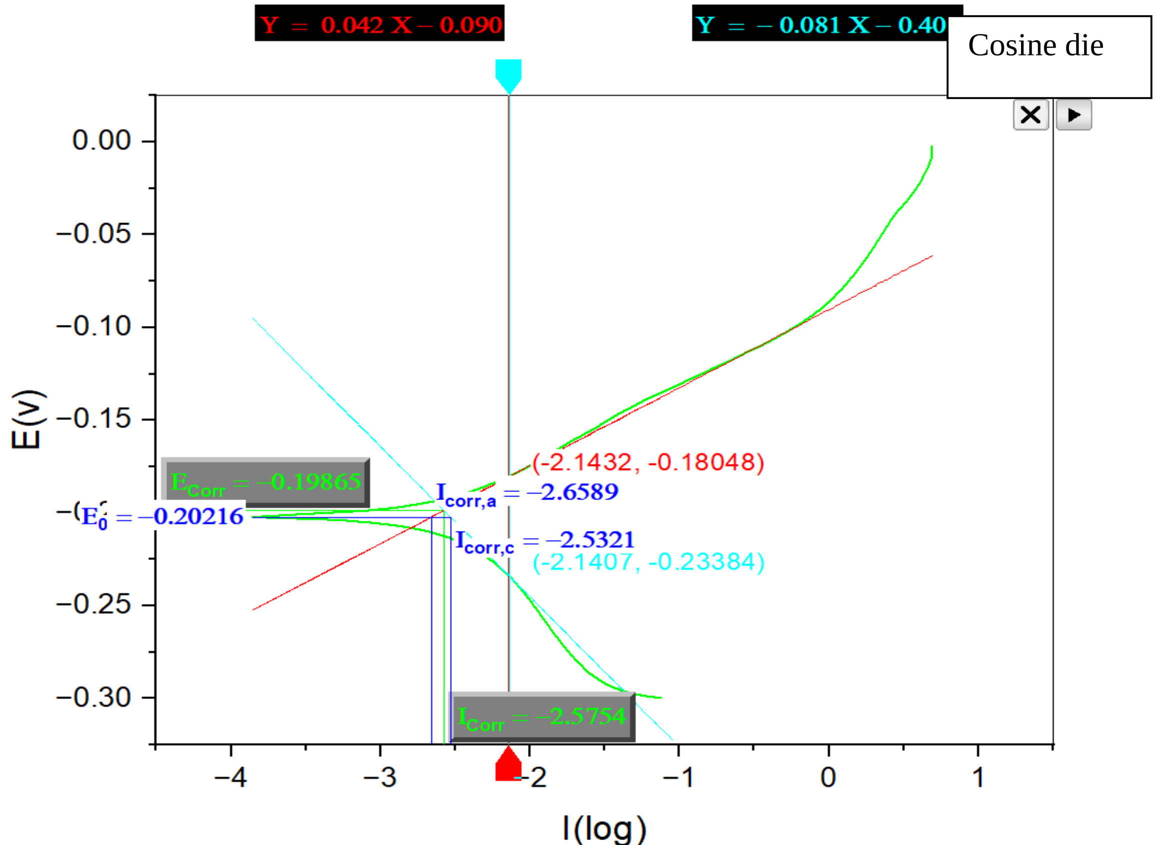

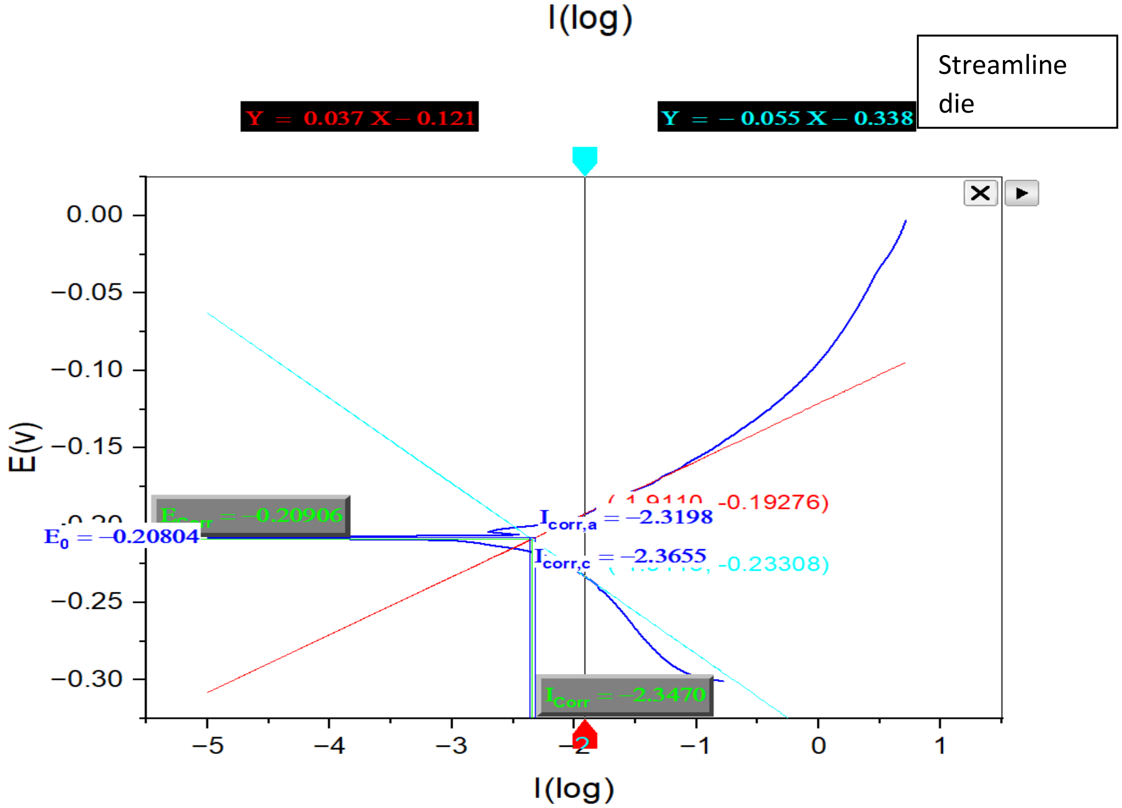

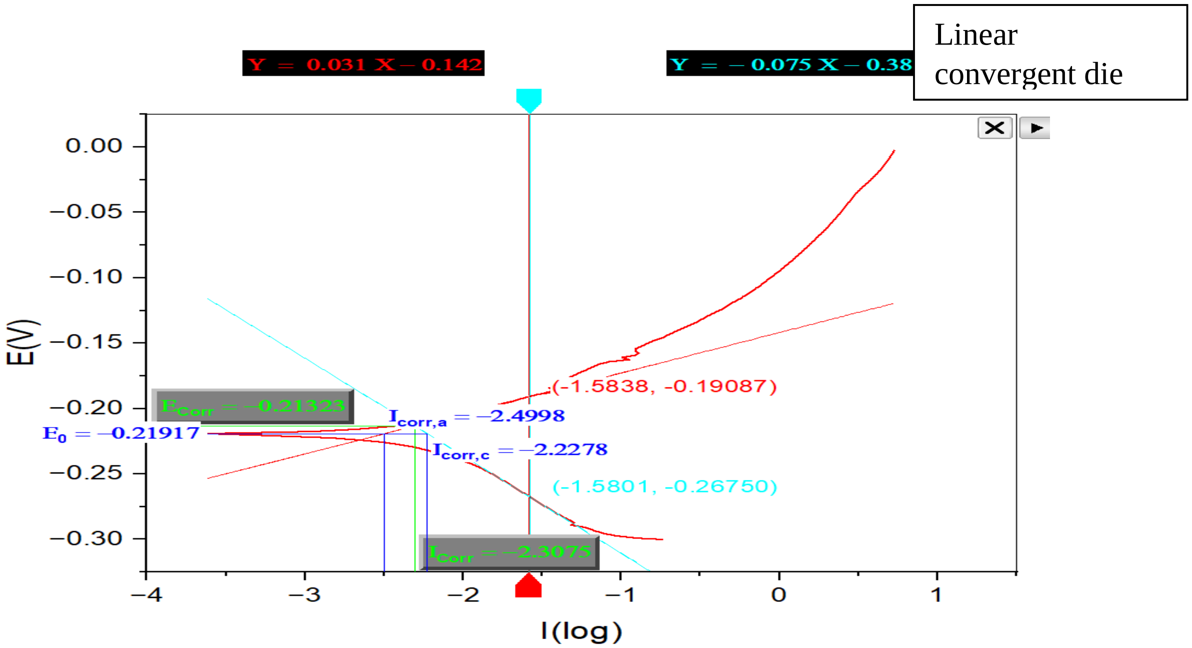

Linear convergent die
Y = 0.031 X – 0.142
Y = – 0.075 X – 0.38
E(V)
I(log)
(-1.5838, -0.19087)
(-1.5801, -0.26750)
$I_{corr,a}$ = –2.4998
$I_{corr,c}$ = –2.2278
E_0 = –0.21917
E_{Corr} = –0.21323
I_{Corr} = –2.3075

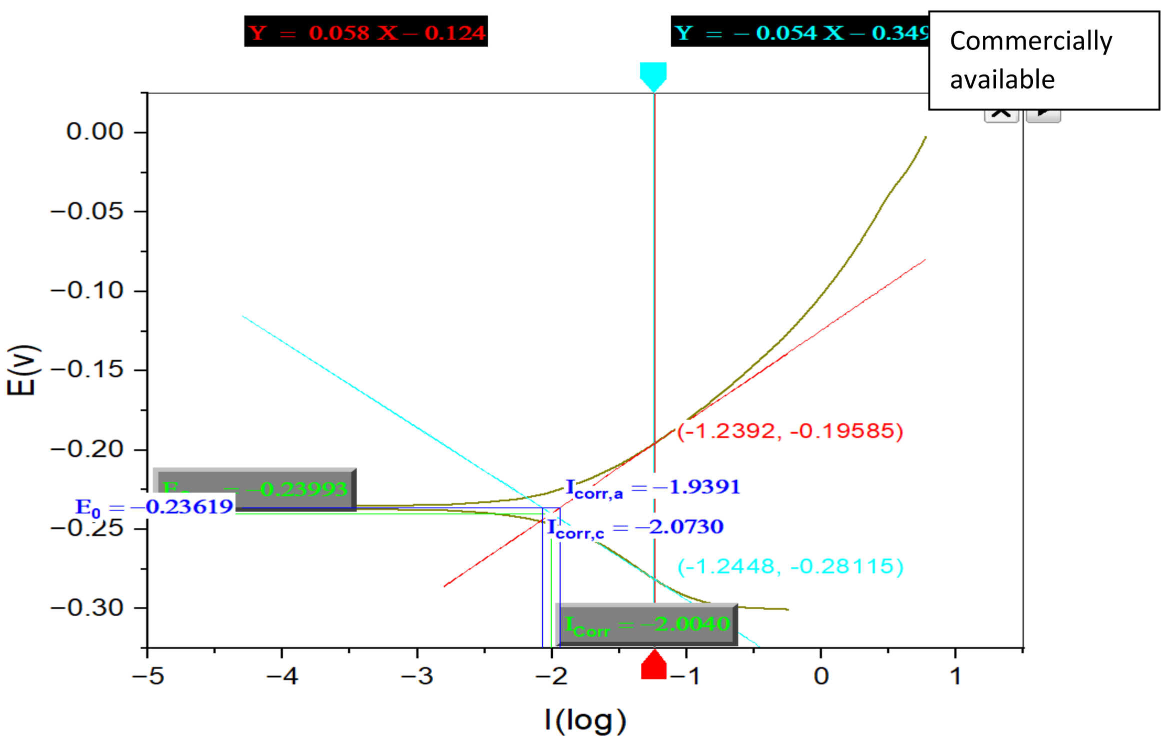

Commercially available
Y = 0.058 X – 0.124
Y = – 0.054 X – 0.349
E(v)
I(log)
(-1.2392, -0.19585)
(-1.2448, -0.28115)
$I_{corr,a}$ = –1.9391
$I_{corr,c}$ = –2.0730
E_0 = –0.23619
–0.23993
I_{Corr} = –2.0040

Appendix III: Spectroscopy Result of C60800 Aluminum Bronze Alloy